DURBAN UNIVERSITY OF TECHNOLOGY

INYUVESI YASETHEKWINI YEZOBUCHWEPHESHE

Synthesis and characterization of humic acid and lignosulphonate based adsorbents for removal of pollutants from textile effluents

Submitted in fulfilment of the requirements for the Degree of Master of Applied Science in Chemistry in the Faculty of Applied Sciences at the Durban University of Technology, Durban, South Africa

Avitha Dass

Supervisor: Professor RM Gengan

Co-Supervisor: Professor GG Redhi

2022

Declaration

I, Avitha Dass, hereby declare that this dissertation titled "***Synthesis and characterization of humic acid and lignosulphonate based adsorbents for removal of pollutants from textile effluents*** ", submitted to the Durban University of Technology, in fulfillment of the requirements for the award of the Degree of Master of Applied Science in the Faculty of Applied Sciences, is the result of my own work and that all sources used or quoted have been indicated and acknowledged by means of complete references.

Signed _____ 10 September 2022

Student: Ms Avitha Dass Date

I hereby approve the final submission of the thesis

Signed 11 September 2022

Supervisor: Prof RM Gengan Date

Signed 11 September 2022

Co-Supervisor: Prof GG Redhi Date

Plagiarism

I declare that this thesis is my own work. I have appropriately referenced this work of other people that I have used. I have not and will not allow anyone to copy my work with the intention of passing it as his or her own work.

____ ____

Avitha Dass

DEDICATION

This dissertation is dedicated to my loving, supportive, and encouraging family. First, my parents, Brummilall and Shruti Dass, raised me with unconditional love and supported and taught me the value of education. Next, my brothers, Shravan and Keshav, have always been there for me and their support. Lastly, my aunt Rehni brings out my inner child. I thank you for the joyfulness you bring to my life. I am grateful to each one of you.

ACKNOWLEDGEMENTS

My sincere appreciation to the following people who contributed immensely to the successful completion of this research project:

First and foremost, I would like to thank God for giving me an excellent opportunity to complete my Master of Applied Sciences Degree within the timeframe allocated for the degree.

My heartfelt thanks to my family, especially my parents and brothers for their full and enduring support in my educational endeavors and upbringing.

My heartfelt thanks to Mr A Maharaj, without his constant support and encouragement, this would not have been possible.

Thanks to The Durban University of Technology, Moses Kotane Institute, and National Research Foundation who funded this research.

My sincere gratitude to Prof Robert M Gengan, Prof G Redhi, and Dr V Arumugam, who provided insight and expertise that greatly assisted the research. Thank you to Prof Gengan for always motivating and inspiring me to climb the academic ladder since my undergraduate studies. My sincere gratitude to him for his relentless encouragement, constructive guidance, and words of motivation throughout this research study and for the inspiration he provided to ensure the completion of this work.

I would also like to thank DUT and UKZN for providing a high-fidelity analytical laboratory to conduct my analyses.

Thank you to my laboratory colleagues: Dr V Arumugam, Dr. M. Arul and Dr. T.R. Makhanya, for their much-appreciated contribution to this research.

My gratitude extends to Mr. S. R. Chetty, Dr. P. Ntola, Dr. M.H. Mabaso, Dr. K. Ramluckan, Mrs. N.P. Cele, Mr. A. Rupee, Mrs. D. Naicker, Prof. N. Deenadayalu, Prof. K.G. Moodley and Mr. S. Mjola for their constant advice and assistance.

Finally, my sincere appreciation and gratitude go to Prof B Sithole, from CSIR, for introducing me to the fascinating world of lignosulphonates.

ABSTRACT

Effluents containing dyes have become a big problem because of the ineffective and uneconomic treatment methods used by industries. There is no single treatment system that is adequate for the degradation of dyes. Currently, several chemical and physical degradation protocols for the remediation of dyes in wastewater are being used. Also, researchers have detected nitro-aromatic compounds in wastewater and these toxic compounds are detrimental to flora and fauna present in water bodies. Our aim was to prepare new materials and assess their potential as adsorbents as well as synthesis of new catalysts for the reduction of selected dyes and nitro-aromatic compounds.

Two new composites were synthesised from starting materials lignosulphonate, humic acid, maleic anhydride and Kraft lignin. The novel nanocomposites were characterized by various spectroscopic techniques such as Fourier-Transform Infra-red Spectroscopy (FTIR), X-Ray Powder Diffraction (XRD), Brunauer-Emmett-Teller (BET), Scanning Electron Microscopy (SEM), Energy Dispersive X-ray Spectroscopy (EDS) and Transmission Electron Microscopy (TEM). Furthermore, the synthesized nanocomposite material was used either as an adsorbent for the dyes such as Reactive Blue 222 (RB), Reactive Red 195 (RR), and Reactive Yellow 145 (RY) or as a heterogeneous catalyst for the reduction of several nitro-anilines and selected dyes. UV-vis spectroscopy was used to assess the potential of the composite as adsorbents or be reductants. Adsorption isotherms, and adsorption kinetics of the new composite were studied. The overall advantage of this investigation is the raw material of the composite is cheap as it is obtained as waste material and is easily available.

Keywords

Humic acid, lignosulphonate, reduction, nitro-aromatics, waste-water treatment, Kraft liquor, catalyst, industrial waste.

Table of Contents **Page number**

LIST OF TABLES **Page**

LIST OF FIGURES **Page**

ABBREVIATIONS

2-NA	2-Nitroaniline
3-NA	3-Nitroaniline
4-NA	4-Nitroaniline
AgNPs	silver nanoparticles
AuNPs	Gold nanoparticles
AIBN	Azoisobutyronitrile
BET	Brunauer-Emmett-Teller
DMSO	Dimethyl sulfoxide
DSC	Differential Scanning Calorimetry
EDX	Energy-dispersive X-ray spectroscopy
FTIR	Fourier-transform infrared spectroscopy
H_2SO_4	Sulphuric acid
HA	Humic acid
HCl	Hydrochloric acid
HLS	Humic lignosulphonate
HRTEM	High-Resolution Transmission Electron Microscopy
HKLC	Humic kraft lignin composite

HKL	Humic kraft Lignin
LS	Lignosulphonate
mL	millilitre
MB	Methylene blue
MHLS	Mealated humic liqnosulphonate
m-NP	Meta nitrophenol
$NaBH_4$	Sodium borohydride
NaOH	Sodium hydroxide
NArs	Nitro Aromatics
NAs	Nitroanilines
NPDA	4-Nitro-o-phenylenediamine
o-NP	Ortho nitrophenol
o-PDA	o-phenylenediamine
PCBs	Polychlorinated biphenyls
p-NP	Para nitrophenol
POPs	Persistent organic pollutants
SEM	Scanning electron microscope
TEM	Transmission Electron Microscopy

TGA	Thermogravimetric analysis
UV-vis	Ultraviolet–visible
RR	Reactive Red 195
RB	Reactive Blue 222
RY	Reactive Yellow 145
XRD	X-ray crystallography
hr	Hour

CHAPTER ONE: INTRODUCTION

1.1.Problem Statement

Several industries, such as textile, pharmaceutical, paper-printing, leather, food, and cosmetics, use synthetic and natural dyes. Because of their mass production and varied applications, dyes have become ubiquitous and have become an environmental concern. Many of these dyes find their way into the environment via wastewater facilities. These compounds retain their color and structural integrity under exposure to sunlight and are persistent in wastewater treatment systems and other water bodies.

Effluents containing dyes have become a big problem because of industries' ineffective and uneconomic treatment methods. There is no single treatment system adequate for degrading the various dye structures. Currently, enterprises use chemical and physical degrading protocols to remediate dyes in wastewater. These methods include chemical oxidation with reagents such as hydrogen peroxide and carbon dioxide. Chemical oxidation is also coupled with UV light to increase color removal. Other techniques involve electrochemical or wet oxidation, activated carbon adsorption, reverse osmosis, or coagulation/flocculation (Edwards, 2000). Furthermore, nitro- aromatic compounds have been detected in wastewater and they are of concern because they are toxic to flora and fauna present in water bodies. One strategy used is to decrease the toxicity of the nitro-aromatic compounds to less toxic compounds such as the amines via oxidation/reduction reactions.

The conversion of discarded biomass to value-added chemicals and products is a topical because of the monetary and environmental rewards. Hence more extensive investigations are being made into waste materials. In the last decade, valuable materials from lignin biomass have been produced. Currently, sodium lignosulphonate and calcium lignosulphonate are vital lignin

derivatives produced from black liquor is a by-product of the cooking process in the paper industry. The lignin obtained from black liquor shows different structures due to the origin and the industrial process from which it is received; for instance, specific industries produce different qualities and grades of black liquor. For example, industries that produce black liquor with a pH range 8-10 are considered kraft lignin, whereas black liquor with an acidic pH is referred to as lignosulphonate (LS). This lignosulphonate is a waste liquor and can be obtained cheaply in large quantities. Currently, many industries use lignosulphonate is as a dispersant to reduce viscosity in slurries, generate electricity in plants, and produce fine chemicals. Its structure consists of different functional groups, including the hydrophilic and hydrophobic groups, and is used in various applications.

Minimal studies have focused on using lignosulphonate as a raw material to synthesize a new high valued material with other readily available organic compounds. Furthermore, these new composites have not been adequately investigated for their use as an adsorbent to remove textile dyes or reduce nitro-aromatic compounds.

1.2 The Scope of Research

Worldwide, a million tons of waste and pollutants from households, industries, transport, mining, and agriculture are discarded into the aquatic surroundings. These wastes are produced frequently with no adequate treatment. The ever-increasing industrial activities have caused the discharge of large amounts of inorganic and organic pollutants into aqueous systems. Therefore, polluted water bodies not only pose health risks to human and animals, they are also an ecological threat. Pollution of water sources is an environmental dilemma because many substances are not biodegradable, and most are highly toxic. In addition to aquatic life, human and terrestrial animals that depend on water bodies are at risk because of pollutants such as textile dyes and nitro-anilines (NAs), which

are highly carcinogenic and are becoming ubiquitous. Hence there is a need to develop simple and effective processes for the removal of these pollutants. The present work involves the study of adsorption of textile dyes and the reduction of nitro-aromatics using various adsorbent materials derived from Kraft lignin, lignosulphonate and humic acid. These low-cost industrial waste materials can be converted into adsorbents that are effective and efficient for the removal of dyes and nitro-aromatic compounds from laboratory simulated wastewater.

1.2.1 Aims and Objectives

This study aims to synthesize and characterize the new composites from humic acid, lignosulphonate, maleic anhydride and kraft liquor, and evaluate their potential to adsorb textile dyes and reduce nitro-aromatic compounds.

The objectives of this study were to synthesize and characterize:

- humic-lignosulphonate composite
- humic acid-lignosulphonate-maleic anhydride composite
- humic-based kraft composite

  and
- evaluate the composites for the adsorption and reduction of nitro-anilines and textile dyes

1.3 Structure of the Thesis

This thesis consists of three chapters; each chapter presents different aspects of the study as given below:

Chapter One: This chapter exposes the problem, scope, aims, and objectives of the study. Also, a summary of each chapter is enunciated.

Chapter Two: This chapter presents a detailed literature review. Topics such as types of dyes, nitro-compounds, different methodologies used for pollutant removal from wastewater, and the reduction of aromatic compounds are discussed. We also focus on adsorption, the various isotherms, and the oxidation-reduction process. Finally, an extensive literature search is presented on the synthesis of humic acid and derivatives of lignosulphonates and their utility in chemical fields.

Chapter Three: The materials and instruments used in this study are presented.

Also, the experimental procedures for synthesizing the three composites, viz., humic lignosulphonate, maleated humic lignosulphonate, and humic kraft lignin, are detailed. Finally, the protocols used for adsorption studies and the reduction of nitro-aromatics, and the kinetic evaluations are presented.

Chapter Four: This chapter is divided into two parts.

The first part comprises the adsorption studies using the humic acid-lignosulphonate-maleic anhydride composite. Herein, the synthesis and characterization of the composite is discussed. Thereafter, the data gathered for the adsorption and kinetics are interpreted and discussed.

In the second part, the humic acid-based kraft lignin composite is characterized, and the reduction of 4 nitro-aromatic compounds and 5 dyes is discussed. Also, a plausible mechanism for the reduction reaction is described. Finally, the conclusion is drawn, and a recommendation is made for further investigation.

Chapter Two: Literature Review

2.1 Types Of Pollutants and their Impact on the Environment

The survival of humanity depends on some critical sources such as clean and adequate water, fertile land, air with the correct proportion of gases. Unfortunately, presence of pollutants in the environment: air, water, land adversely affects the health of humans and organisms that resides in habitats. Some industries responsible for generating pollutants include textile, mining, agriculture, refinery, chemical, and pharmaceutical industries. When these industries produce and discharge toxic gases and untreated or poorly treated effluents, human and animals are exposed to harmful compounds with chronic toxicity (Rieger et al., 2002). Some pollutants also exhibit an unpleasant color and offensive odor, while others display biochemical and physiological properties that can cause tissue and organ damage to animal and plants. Thus, the continuous disposal of municipal, industrial, and agricultural effluents into the environment can caused a substantial increase in toxic pollutants, which are dangerous to all life forms.

2.1.1Types of Water Pollutants

Water is an essential resource to plants and animals and hence needs to be safeguarded. Water pollution is one of the most severe problems affecting the world today as it results in the reduction of freshwater supplies. Water pollution can arise from an increase in the population, depletion of natural habitat, and development of industrialization. It is, therefore, imperative to treat effluents and wastewater with low-cost and efficient techniques to remove both organic and inorganic compounds. Over the years, many scientists have conducted extensive research to highlight and investigate the effects of different pollutants and how to reduce them in the environment(Yu et al., 2019, Aguilar et al., 1999, Bilal et al., 2018, Subramaniam et al., 2019, Crini, 2006, Gupta and Suhas, 2009, Pan et al., 2009, Kowsari, 2014, Gangadhar et al., 2012)

Water pollutants can be placed into various categories such as organic contaminants (Nie et al., 2019), pathogens (Strokal et al., 2019), nutrients and agricultural runoff (Nsenga Kumwimba et al., 2018), suspended solids and sediments (organic and inorganic) (Rügner et al., 2019), inorganic and metals (Hlongwane et al., 2019), and radioactive materials (Mahmoud et al., 2019). However, the most common types of pollutants in the environment are persistent organic pollutants (POPs) such as polychlorinated biphenyls (PCBs) (Ontiveros-Cuadras et al., 2019), industrial dyes (Bilal et al., 2018) and nitro-aromatics (NArs). Persistent organic pollutants pose a health hazard because of their mutagenic and carcinogenic nature (Yazdi et al., 2009; Khalid et al., 2009; Sun et al., 2007; Singh et al., 2019).

Industrial dyes and toxic NArs are the most common pollutants among the several classes of organic pollutants. These organic compounds are produced by many industries, including paper and pulp, textile, plastic, leather, cosmetics, pesticides, pharmaceuticals, and allied food industries. In addition, several pollutants are stable compounds and illustrate low biodegradability with cumulative effects (Gu et al., 2018; Khalid et al., 2009; Crini, 2006). The growing concerns over the harmful effects of dyes in aquatic surroundings caused researchers to find new ways to remove them from the marine surroundings. It includes chemical, physical and biological techniques, photocatalytic degradation, and adsorption.

2.1.2 Impact of Wastewater Effluent Contaminants

Over the century, the massive increase in organic chemicals has inevitably caused an upsurge of organic pollutants in aquatic bodies. Organic contaminants can become accumulative in marine mammals, body fat of humans, and other animals that come into contact with them. Also, they can easily be moved to different regions and transported by wind or water bodies, and they can be passed from mother to fetus. Even in small dosages, organic pollutants can cause the following:

- Damage to human and animal tissues
- Trigger nervous system damage
- Severe physiological or neurological damage to the human body
- The disease of the immune system and cancer
- Reproductive disorders
- Damage to the liver and cause hemolytic anaemia

2.1.3 Lignin

Lignin is the second most abundant organic compound present in the world. The annual production of lignin is estimated to be 36 x 108 tons (Gellerstedt and Henriksson, 2008, Bajwa et al., 2016, Bajwa et al., 2019, Dessbesell et al., 2020). The enzymatic polymerization of the monomers p-coumaryl alcohol, coniferyl, and sinapyl creates the amorphous polyphenolic structure in the lignin (Maziero et al., 2012; Fratini et al., 2006; Yadav et al., 2018; Santos et al., 2014; Dos Santos et al., 2014). Lignin is a polyaromatic macromolecule made up of 70% carbon content and contains functional groups such as phenolic, aliphatic hydroxyls, and carboxyls (Fig 1). In addition, lignin can be used as a neutralizer or inhibitor in oxidation processes, thus stabilizing reactions induced by oxygen radicals and their derived species (Dos Santos et al., 2014, García et al., 2010). The pulp, paper, and biofuel industries are the primary lignin producers. In the Pulp and Paper industries, it is treated as a waste liquor and burnt off for steam or electricity generation.

The partial chemical structure of lignin is shown in Fig. 1. Lignosulphonate can be used to produce different phenolic products such as resins and chelating agents. The transformation of lignin into profitable products is one way to show lignin's potential (Fierro et al., 2008, Fierro et al., 2006, Guo and Rockstraw, 2006, Shu et al., 2020, Shi et al., 2013, Faba et al., 2015). Lignin can also be used as an alternative to non-renewable coal resources. Due to the high carbon content, lignin can

be used as an alternative to commercial activated carbon. Lignin could be transformed into activated carbon either by chemical or physical activation methods. Chemical activation is preferable since it requires a lower activation temperature and produces higher product yields. Also, lignin-derived from chemical pulping processes is a renewable alternative to many chemicals derived from petroleum refining. Both Kraft lignin and lignosulphonate (LS) are valued by-products of pulp industry. LS is one of the significant by-products of the pulp and paper processing industry.

Generally, sulfite pulping produces L.S. as a by-product of de-lignification of Wood (Sjostrom, 1993). Lignosulphonate are water-soluble anionic polyelectrolytes which contains sulfonate group. The degree of sulfonation occurs at approximately 0.5 per phenylpropane unit (Sjostrom, 1993). Lignosulphonate has a comparatively high molecular weight with a wide distribution and relatively high ash content (Vishtal and Kraslawski, 2011). Therefore, it is usually obtained as dry solids (Hu, 2002, Hu and Hsieh, 2016). Lignosulphonate is produced commercially by many industries; Borregaard LignoTech is one of the largest producers with more than a million tons per annum (Vishtal and Kraslawski, 2011). The carbon gained from biomass components is cheap, primarily spherical, micron-size, contains a sp^2 hybrid carbon skeleton, and contains many oxygen-containing functional groups.

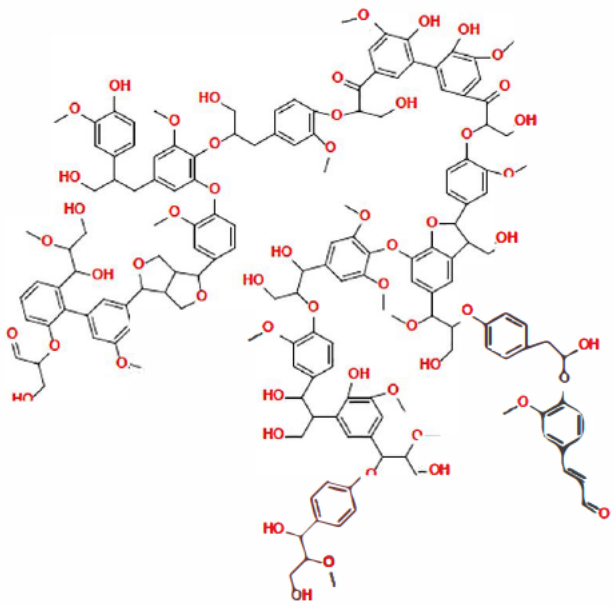

Figure 1. The partial structure of lignin

Owing to its low cost, biodegradability, and non-toxicity, L.S. is a good material for various industries. Hence, a new method of synthesis of L.S. was developed to improve its quality and production quantity (Hao et al., 2016, Tan et al., 2012, Won and Borden, 2016, Hao et al., 2017). It is used in the degradation of explosives in soil, to enhance the performance of zinc batteries, as a composite superabsorbent polymer, a water reducer, and dispersant for gypsum paste (Matsushita and Yasuda, 2005, Tan et al., 2012, Hao et al., 2016, Won and Borden, 2016). However, although L.S. has been used as an adsorbent, it has not been adequately utilized as a carbon adsorbent.

2.1.4 Humic Acid

Humic acid (HA) is a natural macromolecular structured material found abundantly on the earth's surface. It has formed from the decaying of organic matter and can be easily obtained from the environment (Zhang et al., 2013). It constitutes a significant component of humic substances that originate from the organic matter of soil, peat, and coal. HA is an amorphous powdered material that enhances its reactivity and allows for a broad framework of polycyclic aromatic hydrocarbons

(Fig. 2) within the structure (Huang et al., 1996; Yang et al., 2005). It contains aliphatic and aromatic units (Fig 2) crossed linked by different types of oxygen comprising functional groups (Xing et al., 2017).

Furthermore, HA contains predominantly a large amount of surface functional groups in its structure, namely hydroxyl, carboxyl, and phenolic groups. These groups are the main coordination sites for bentonite, metal ions, and organic matter (Catrouillet et al., 2014). HA strongly likes hydrophobic organic compounds, but unfortunately, removing them from water systems is quite troublesome. It was reported that the combination of HA and iron oxide with magnetic separation could improve the removal of contaminants from water (Liu et al., 2008). In addition, Liu reported that HA coated with a Fe_3O_4 effectively removed the heavy metals present in contaminated waters (Liu et al., 2008).

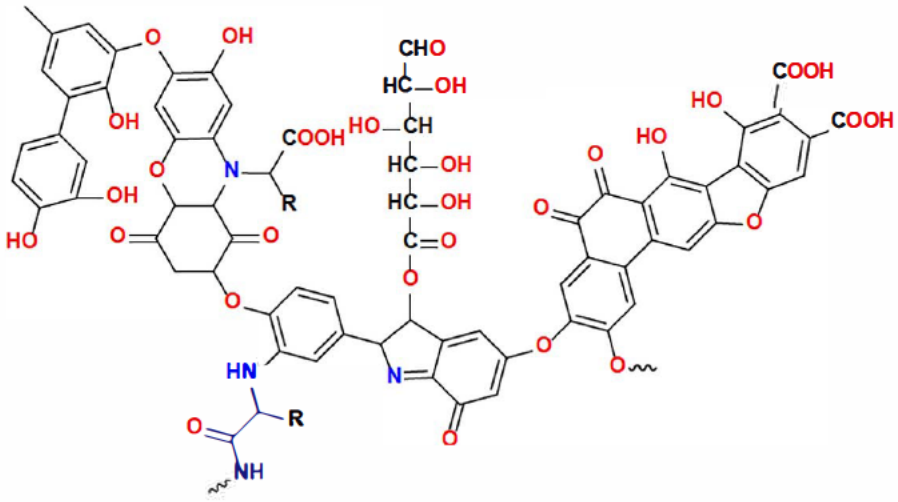

Figure 2. The Partial Structure of Humic acid

HA is well known for binding a large variety of metalloids, metals, and toxic elements (Thanabalasingam and Pickering, 1986). In addition, HA acts as a regulator of metal mobility and influences its bioavailability in the environment (Sposito and Weber, 1986). The binding ability is due to the oxygen-containing functional groups. High reactivity would possibly cause different types of contamination in water. Also, HA can freely bind with metal ion species and organic compounds, thereby contributing to their movement within water bodies (Deng and Bai, 2004). HA also harms the environment by changing watercolour and taste. It can also promote bacterial growth in water. Carcinogenic compounds arise when HA undergoes chlorination (Deng and Bai, 2004). However, HA is a green, inexpensive, renewable biomass material and a natural polymer and could be used for various essential applications; hence more extensive research is encouraged.

2.1.5 History of Dyes

Historically, many ancient civilizations used natural dyes, such as the Indians, Chinese, Mesopotamians, Egyptians, Greeks, and the Aztecs. In early culture, most dyes were obtained by physically crushing and grinding roots, leaves, and barks of plants and fungi (Adrosko, 2012), and these molecules were classified as natural dyes. The oldest dye recorded in history was Indigo,

whereas red colors were used for over fifteen thousand years at burial sites. The practice of dyeing material cloths began around 3000BC in China (Har Bhajan and Bharati, 2014). However, the dyes obtained by crushing selected plant organs were of low yield, and it was a time-consuming task. As industrialization developed, it resulted in a higher demand for dyes for various plastic, textile, leather, and paper applications. Hence dyes were synthesized: they are categorized as disperse, azoic, direct, vat, acidic, basic, and reactive.

2.1.6 Types of Dyes

There are several categories of dyes. The classification is based on chemical structure and color index (Benkhaya et al., 2020). They are ionizing, aromatic, colored compounds. The color comes from groups that can absorb specific wavelengths of visible light and diffuse other wavelengths. These groups are called chromophores and auxochromes (Benkhaya et al., 2020). The chromophores are made up of delocalized electron systems with conjugated double bonds. The function of the chromophores is their ability to impact color. The auxochromes consist of electron-withdrawing or electron-donating substituents. The auxochromes are functional groups attached to the chromophore. It alters the capacity of the chromophore to absorb light (Vankar, 2000; Benkhaya et al., 2020). Chromophores are carbonyl, azo, nitro, quinoid, carbon-nitrogen groups while the $–NH_3$, -COOH, $-HSO_3$, -O.H., -NHR and $-NR_2$ groups are auxochromes. For the classification of dyes, the auxochromes are very important.

The different classes of dyes are further grouped based on their color, such as black, blue, red, yellow, brown, orange, green, and violet (Vankar, 2000). According to the chemical classification of dyes, they are grouped based on the chromogen group, for instance, azo dyes (-N=N- azo structure), nitro dyes (2 nitro functional group), and thiamin dyes (derivatives of thiamin)(El Harfi and El Harfi, 2017, Benkhaya et al., 2020).

2.1.6.1 The Azoic Dyes

These dyes are produced by reacting coupling compounds with either di-azo, diazo base, or diazo salts (Panda, 2013). These dyes have excellent coloring properties, mainly from the red to yellow range. They do not degrade upon oxidation and are considered stable in a range of pH values. Certain azo dyes can release aromatic amines; this occurs by breaking down the azo dyes under reductive conditions (Zhang and Ma, 2013; Zhang et al., 2013). The aromatic amines are carcinogenic, toxic, and mutagenic and affect the cellular response in humans (Zhang and Ma, 2013, Leo et al., 2018). Their presence can significantly affect water bodies and surrounding environments. The following Fig. 3 shows the two important dyes in the azo dyes family:

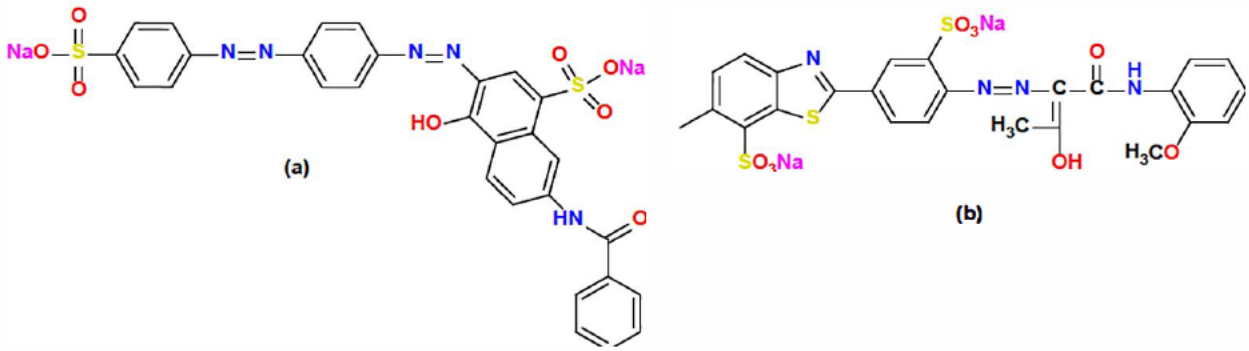

Figure 3. The structure of azoic dyes a). Congo Red b). Allura Red

2.1.6.2 The Direct Dyes

Direct dyes have been widely used for the dyeing of textiles (Koh, 2011). Direct dyes interact with cellulose under an alkaline medium to form covalent bonds with the fiber (Hawkyard, 2006). Direct dyes are made up of four parts: the chromogen is the reactive system that allows the dye to interact with the substrate. This linking system provides for the formation of a link for the reactive system to the chromogen part. Also, a solubilizing group is present that aids water solubility (Chattopadhyay, 2011). Direct dyes come in a wide variety of shades, allow for easy application,

and can be easily removed by bleaching. During bleaching, the azo moieties can stop or slow down this process. They are water-soluble anionic dyes and can be applied directly to cellulose fibers without a mordant. However, saline dye wastewater is produced in this process, adversely affecting aquatic life, water potability, and agriculture (Sekar, 2011; Lefebvre and Moletta, 2006).

2.1.6.3 Reactive dyes

Reactive dyes were synthesized in 1950. These dyes have a much simpler chemical structure than direct dyes. The series of dyes and their applications as shown in Table 1. Reactive dyes also have more good absorption bands in their absorption spectra and reflect a brighter colour during dyeing. Reactive dyes are anionic; they can occur in different forms such as granules, and solutions and are also water-soluble dyes. The dyeing process can happen in a single step, and they have lower dyeing temperatures:1000° C. The following are examples of reactive dyes: Remazol Black B, (Fig. 4) Remazol Red (Fig. 5) and Remazol Golden Yellow (2) (Jahan Ara et al., 2013, Norsita et al., 2016, Chattopadhyay, 2011).

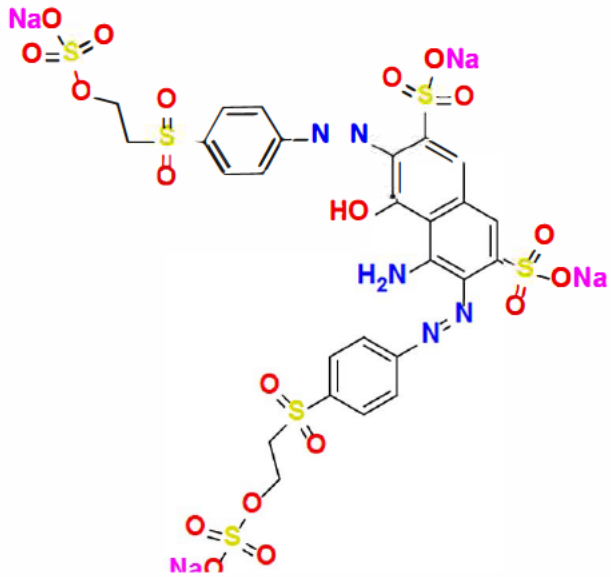

Figure 4. The structure of Remazol Black B dye

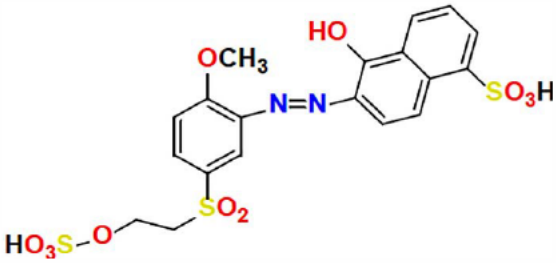

Figure 5. The structure of Remazol Red

2.1.6.4 Sulphur Dyes

Sulfur dyes contain sulfur linkages. They are non-ionic, reasonably cheap, and insoluble in water (Chakraborty, 2011). The dyeing process requires high temperature and excess salts for the color to penetrate the fiber. Also, oxidation must occur either by chemicals or air is required after the dyeing process (Chakraborty, 2011). (Fig. 6)

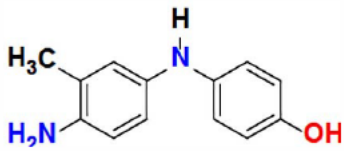

Figure 6. Sulphur Blue 7 structure

2.1.6.5 Vat Dyes

Vat dyes are water-insoluble and are applied to cellulosic fibers. These dyes contain the carbonyl group with a co-planar aromatic skeleton (Fig. 7). The aromatic rings are responsible for the Van Der Waal forces between the substrate and the molecule. These dyes are used in soluble form to infuse the fibers.

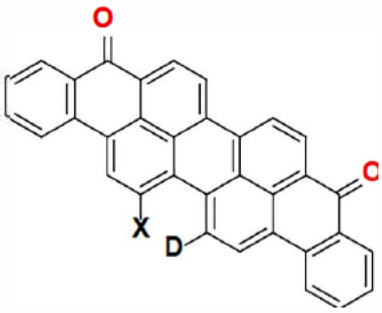

Figure 7. The structure of Vat Black 7

2.1.6.6 Cationic or Basic Dyes

They are used for dyeing acrylic fiber but were initially used in silk dyeing when the brightness of the color was more important. In an aqueous solution, basic dyes form positively charged ions that interact with the negatively charged groups in the fiber to produce a salt. Some of the ionic dyes, as shown in Fig. 8.

Methylene Blue (C.I. Basic Blue 9)

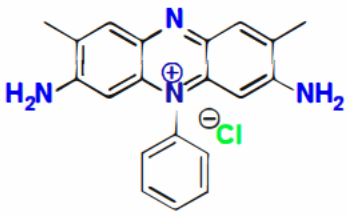

Safranine O (C.I. Basic Red 2)

Thioflavin T (C.I. Basic Yellow 1)

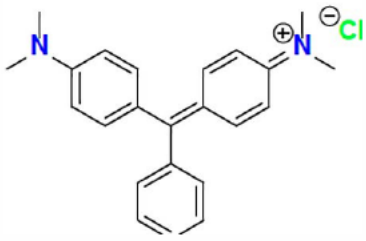

Malachite Green (C.I. Basic Green 4)

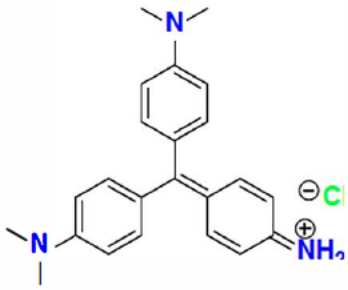

Crystal Violet (C.I. Basic Violet 3)

Figure 8. The structure of selected basic or cationic dyes

2.1.6.7 Classification of dyes and their use

Table 1 presents a summary of the classification of dyes and their use

Type of dye	**Type of dye applied material**	**Applications of the dyes**	**Name of the chemical moiety present**
Vat	Cotton, wool, leather, and rayon	Water-insoluble and solubilized by reducing with sodium hydrogen sulfide	Anthraquinone and Indigoids
Reactive	Cotton, wool, silk, and nylon	The reactive site on the dye responds to the functional group on the fiber molecule to link the dye covalently	Basic, azo, oxazine, phthalocyanine and anthraquinone
Sulfur	Cotton	Aromatic substrate vatted with chemicals and further re-oxidized to form insoluble sulfur-containing products on the material.	Unspecified structures
Azoic	Cotton, rayon, cellulose and polyester	Material infused with coupling element and reacted with a stabilized salt	Azo
Basic	Paper, polyacrylonitrile, nylon and inks	Added into dyebaths	Azo, azine, xanthene, acridine and anthraquinones, cyanine, hemicyanine and diazahemicyanine.

Direct	Cotton, paper, and leather	Added from solutions containing excess electrolyte	Azo, phthalocyanine and Stilbene

2.2 Introduction to Nitroaromatics

The release of organic effluent water into water bodies poses grave risks to marine life and human beings and produces a carbolic scent in the water. One of the notorious organic pollutants is nitro compounds, which are well known for their carcinogenic properties and dangerous nature (Wan et al., 2019). The nitro compounds that are commonly found in effluent wastewater are aniline, phenol, p-nitroaniline (p-NA), o-nitroaniline (o-NA), m-nitroaniline (m-NA), o-nitrophenol (o-NP), m-nitrophenol (m-NP), p-nitrophenol (p-NP). Nitroaniline, although with high toxicity, is used in preparing other organic compounds that are used as pharmaceuticals, antioxidants, azo dyes, pesticides, corrosion inhibitors, and fuel additives (Orelup, 1980, Wood et al., 2008, Arumugam, 2018, R. Rajesh and Venkatesan, 2012, Chen et al., 1997, VanVliet et al., 2005).

In many first world and developing countries, N.A.s are considered priority pollutants (Bakhsh et al., 2019). The United States Environmental Protection declared 2-NA as a priority harmful pollutant and toxic waste product (Dong et al., 2015; Dong et al., 2014b). The nitro anilines are soluble in water, causing them to permeate throughout soil into surrounding water bodies freely. Therefore, it is vital to find effective methods and techniques to remove and dispose of N.A.s from wastewater and other water sources. Different researchers reported various techniques for the removal of N.A.s. Technologies such as catalytic reduction, electrochemical degradation, biological degradation, photocatalysis, adsorption, and modification can be found in the literature. The reduction method is the best-opted technique as catalytic reduction converts N.A.s into o-

phenylenediamine (o-PDA) (Naseem et al., 2017) which can be helpful in many different types of applications such as antiseptic agents, dyes, in chicken products (Dayan et al., 2015, Liu et al., 2014). However, better protocols are required to convert the N.A.s to less toxic and more valuable products. One such methodology is to use catalysts that could be used in ambient reaction conditions and preferably in an aqueous solution (Bakhsh et al., 2019). Such a method is based on reducing N.A.s to their corresponding amine derivatives (Santhosh et al., 2016, Wang et al., 2013, Baran, 2018). There are many derivatives of N.A.s, but aniline and N.A. isomers that the focus of this thesis are shown in Fig.9.

2.2.1 2-Nitroaniline

2-Nitroaniline (2-NA) is currently used in anthropogenic activities, pharmaceuticals, and explosives (Bano et al., 2017). However, 2-NA is regarded as an environmental pollutant. Even a low concentration of 2-NA is detrimental to marine, animals and human life since it is carcinogenic, toxic, and mutagenic (Abay et al., 2017; Wang et al., 2012; Singh et al., 2014). The best method to produce 2-NA is by reacting ortho nitro chlorobenzene with ammonia, but multiple other reactions can produce 2- nitroaniline.

2.2.2 3-Nitroaniline

The toxic effect of 3-NA damage (Bakhsh et al., 2019; Abay et al., 2017; Wang et al., 2012) on mammals are many, some of which include: liver damage, anaemia and convulsions, seizure, damage to respiration organs, mutations and DNA alterations.

2.2.3 4- Nitroaniline

4- nitroaniline (4-NA) is currently used as an intermediate in the synthesis of dyes in manufacturing drugs, gasoline, medication for livestock, and corrosion inhibitors (Booth, 2000,

Williamson and Masters, 2010). 4-NA can be highly toxic in ways that include inhalation, adsorption, and ingestion (Emmrich, 1999; Bradley and Chapelle, 1995). In addition, research has shown that 4-NA is exceptionally harmful to aquatic animals, and lab-based studies have shown that it can be detrimental to rats (Maté et al., 1967; Degawa et al., 1998, Espinosa-Aguirre et al., 1991, Emmrich, 1999).

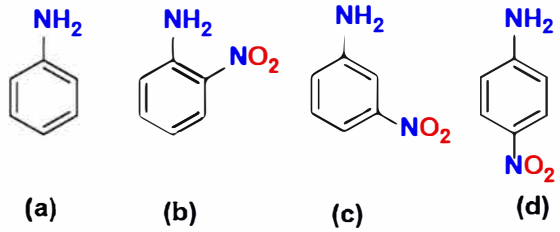

Figure 9. The structure of a) Aniline b) 2-nitroaniline c) 3-nitroaniline and d) 4-nitroaniline

2.3.1 Catalytic Methods for the Reduction of Nitroaniline

Nitro aniline is usually reduced to less harmful compounds in the presence of a mild reducing agent. The reduction process is slow and not kinetically feasible. Hence, there is a search for new materials or catalysts to speed up the entire process. These are grouped into supporting systems and nanoparticles containing a metal.

2.3.2 Supporting systems

Graphene is a versatile material used in many different applications. Graphene is a carbon structure made up of multiple functional groups such as hydroxyl, carbonyl and carboxylic groups that are found on its surface and thus contribute to its hydrophilic characteristics and adhesive properties (Naseem et al., 2017, Khoa et al., 2014). The graphene compound demonstrates unique features such as light in weight, electronic, magnetic, excellent electron mobility, and large surface area (Schwierz, 2010). Nanotechnology generally uses different forms of graphene due to its stability.

The high surface area and electronic structure make graphene a good support material for harnessing and enhancing catalytic propertiesof metal nanoparticles (Khoa et al., 2014; Salam, 2015; Ersan et al., 2017; Tang et al., 2018, Kyzas et al., 2018, Huang et al., 2010).

Silica has the following desirable properties: high surface area, low density, and thermal and chemical stability (Naseem et al., 2017). They also show good catalytic activity. Nanoporous silica material excellent supporting material for metal nanoparticles. Silica nanoparticles are synthesized using various reagents (Gade et al., 2018, Kyzas et al., 2018, Fernandes and Jonas, 2018, Dong et al., 2014, Le et al., 2014). One of the disadvantages of using silica as a supporting system is the small pore size which can restrict access to metal nanoparticles that are inside pores due to size exclusion of large substrates

A hydrogel has a 3-dimensional network frame of hydrophilic polymer units for secure attachment. A hydrogel contains multiple functional groups; these include alcohols, carboxyl's, and sulphonic acid, which contribute to its hydrophilic properties and make it easy to absorb water (Sanyang et al., 2013). Hydrogel has numerous applications - extraction of precious metals, removal of solvents, and chemical catalysts (Mathur et al., 1996). Hydrogels are used as a supporting system in a catalytic reduction of poly(acrylamide)-chicken biochar's hydrogel composites for the removal of phenol (Sanyang et al., 2013), biochar embedded with hydrogel for removal of 4-nitrophenol (Sahiner et al., 2013) and silver nanoparticles-fabricated hybrid microgels for reduction of 2-nitroaniline (Farooqi et al., 2015).

2.3.2 Nanoparticles Containing a Metal Ion

Gold nanoparticles (AuNPs) have been extensively used in catalysis (Corma et al., 2007; Gu et al., 2013; Shi et al., 2012). They have desirable electronic, optical, and excellent surface properties.

Another commonly used catalyst is silver nanoparticles (AgNPs), which had been used to reduce 2-nitroaniline (Gnanaprakasam and Selvaraju, 2014; Dong et al., 2014; Zeng et al., 2012). Silver is a cheaper noble metal compared to Pt and Au (Farooqi et al., 2016). Furthermore, AgNPs are easy to prepare and the particle size can be controlled. In addition, AgNPs possess excellent stability in the presence of an appropriate stabilizing agent. These factors make it a suitable candidate for use as a catalyst (Naseem et al., 2017; Gnanaprakasam and Selvaraju, 2014).

2.3.3 Polymeric Compounds for Wastewater Treatment

The first macro reticular polymeric adsorbent was produced in the 1970s (Kunin, 1977). They displayed excellent physical properties, making them an eligible candidate for adsorption and filtration techniques (Pan et al., 2009). They were initially used in gel permeation chromatography. It is currently used to remove both organic and inorganic pollutants from effluent wastewaters. Some of the various organic contaminants adsorbed are phenolic compounds, organic acids, aromatic or polyaromatic hydrocarbons, alkanes, and their derivatives. These polymers were modified and functionalized to intensify and increase their adsorption toward selected contaminants (Pan et al., 2009). Polymeric adsorbents can undergo efficient regeneration under mild conditions using diverse desorption reagents depending on the adsorbed pollutants (Ferrari, 2014; Pan et al., 2007; Pan et al., 2005). The key polymeric adsorbents currently used for wastewater treatment are polyacrylic ester or polystyrene matrixes. They are used in their pristine or modified form, and their preparation is intensively discussed in the literature (Pan et al., 2009). Some examples of the type of organic molecules that were removed with a polystyrene matrix are phenol, p-chlorophenol, amino acids, salicylic acid, p-hydroxybenzoic acid, 1-naphthol, 2-naphthol, 1-naphthylamine, 2-naphthylamine, 4-nitrophenol, aniline, and dyes (Yang et al., 2003, Abburi, 2003, Deosarkar and Pangarkar, 2004, Zhaoyi et al., 1997, Pan et al., 2007, Azanova and

Hradil, 1999, Zhang et al., 2006, Pan et al., 2009, Ferrari, 2014). Hybrid polymeric adsorbents are currently attracting attention for the removal of pollutants. They are made by infusing fine non-toxic natural particles that can be either inorganic or metal and organic particles on the support of larger particles (Ferrari, 2014). The main reason for developing these hybrid adsorbents depends on the fine particles, as they show a strong affinity for the specific pollutants in the effluent (Ferrari, 2014). Therefore, they had to be infused into porous supports of bigger particle sizes to overcome this issue. Due to the modifiable chemical-physical properties, natural polymeric compounds appeared to look very promising compared to activated carbon, cellulose, and sand.

2.3.4 Adsorption Technique Used for Remediation of Pollutants

Since the first industrial revolution, fast expansions in industrialization and population growth have greatly accelerated with the pollution of the environment. As a result, different technologies have been developed to regulate pollution levels (Wang et al., 2013). The adsorption technique is seriously used by the available technology and is known for being a simple process to remove various pollutants efficiently. Furthermore, adsorption ensures no further pollution from the production of harmful substances during its technique(Wang et al., 2013). The adsorption capacity of an adsorbent is a function of its porosity and surface area. Nowadays, various porous materials have been on the market; these include activated carbon, clay, and polymers, illustrating various abilities to remove pollutants from water.

Adsorption is the method where dissolved particles are adhered to the exterior of an adsorbent due to either physical or chemical influence. Adsorption is a well-established process for the treatment and action of industrial effluent water containing toxic organic and inorganic impurities (Foo and Hameed, 2009). An adsorbent substance can be obtained from synthetic materials or freely

available agriculture wastes. Agriculture wastes such as sawdust, nutshell, macadamia nuts, coconut shell, walnut shells, char, camphor wood, and palm shell can be made into activated carbons (Kassim et al., 2004, Wongcharee et al., 2019, Li et al., 2009, Benedetti et al., 2018, El-Shahat and Shehata, 2014, Dong et al., 2019, Di Natale et al., 2013, Hajialigol and Masoum, 2019). The following are adsorbent materials: inorganic oxides, eggshells, silica, and bentonite (Banat et al., 2000; Banat et al., 2003; Rauf and Malik, 2001, Huang et al., 2017, Zulfikar et al., 2012). In addition, humic acid cryogel based monolithic adsorbent, nanographene, hyper-cross-linked polymeric adsorbent, and amine-epoxy based polymers are also used (Raghunath et al., 2016, Huang et al., 2009, Narimani and Mansour Lakouraj, 2015, Wang et al., 2018, Salam, 2015, Senlik et al., 2017). These adsorbents are currently used to remove and recover organic and metal pollutants from wastewater sewage (Rajasulochana and Preethy, 2016). The process involved in the adsorption technique comprises selecting an ideal adsorbent based on the surface area, porosity, and particle size. However, this technique has problems that include the inability to have complete removal, low adsorption capacity, high material costs, lack of the availability of material, regeneration of the adsorbent material, and problems arising from discarding of the adsorbent after its use.

2.4.1 The Process of Adsorption

Of all the wastewater treatment processes, adsorption is regarded as the superior process, considering that it is a very efficient and affordable method for treating industrial effluent water containing dyes and nitroaromatic compounds. Adsorption can be classified as chemisorption and physisorption. The two types occur when the molecules are in a liquid phase and are then attached to the adsorbent surface, which is the solid phase. Attractive forces on the adsorbent's surface overpower the adsorbate particles' kinetic energy.

In physisorption, the adsorption is due to weak Van Der Waal forces. As a result, the adsorbate molecules become physically fastened to the surface of the adsorbent. Physisorption permits single or multiple adsorbate layers on the adsorbent surface, and the process is characterized by low enthalpy of adsorption. In chemisorption, the process occurs when a chemical reaction takes place between the adsorbed molecule and the adsorbent, resulting in the formation of a chemical bond. It is characterized by a high enthalpy of adsorption (Dargo Beyene, 2014).

2.4.2. Adsorbent for the Removal of Dyes and Nitroaromatics

Practically all solids have the potential to adsorb the sorbate. However, the efficiency of a specific solid in the effluent's treatment process is a function of its structure, porosity, degree of polarity, and specific surface area. The nature of the adsorbate can either be inorganic or organic; but, the most common adsorbents are activated carbon, organic polymers, and silica-based compounds (Muhi Mohammed, 2011). Among the adsorbent materials studied previously, activated carbon is the most commonly used to remove pollutants from wastewater. Its utility is its porous texture, structural characteristic, and large available surface area (Khattri and Singh, 2000). However, activated carbon poses some disadvantages, including high cost, non-selective, and poor removal of disperse and vat dyes removal. Another disadvantage is the loss of adsorbent during the regeneration process. Hence there is an urgent need to use an alternative, environmental surplus, low-cost materials with excellent adsorption capacity to answer the environmental issues experienced over the past few decades (Khoo and Ong, 2011). This study seeks to convert waste into materials that are suitable for use as an adsorbent.

2.5.1 Adsorption isotherm

Absorption isotherm provides mathematical relationship to determine the amount of solute that would be adsorbed by a material (Steve et al., 1998). The adsorption isotherm is interpreted as a graphical depiction illustrating the association between the amount adsorbed and the amount of absorbate in the solution at equilibrium. It represents the dispersal of an adsorbable solute with different phases, such as liquid and solid, at different equilibrium concentrations (Ng et al., 2002). The most used isotherms are the Freundlich, Langmuir, and BET adsorption isotherm (Desta, 2013).

2.5.2 The Freundlich Isotherm

It is a model that defines the relationships between the concentration of adsorbates and the amount adsorbed. The Freundlich isotherm is represented by

$$X = K_F C^{1/n} \qquad (1)$$

X- the amount of adsorbate adsorbed per mass of adsorbent (μg/g) K.F.- Freundlich constant C- is the concentration of adsorbate in the solution at equilibrium (M or mg/L)

2.5.3 The Langmuir isotherm

The Langmuir isotherm assumes that all sorption sites on the surface are the same, indicating the same adsorption strength for a given solute molecule. Also, a significant assumption is that not more than a monolayer of adsorbate onto the surface is allowed. The Langmuir isotherm is determined by using

$$X = X_{max} \frac{K_L C}{1+K_L C} \quad (2)$$

Where X- the mass of adsorbate adsorbed per mass of adsorbent (µg/g). X_{max} - maximum adsorption capacity (empirical constant) K.L. -the binding constant related to the energy of adsorption (L/µg) C -concentration of adsorbate in the solution after adsorption at equilibrium (M or mg/L)

The Langmuir isotherm takes an L-shaped curve and is characterized by a decreasing slope as the concentration increases. This adsorption characteristic is due to the high affinity of the adsorbent at a low concentration, which then decreases as the concentration increases. This isotherm suggests strong adsorbate-adsorptive interaction, which includes inner-sphere complexes. The Langmuir isotherm resembles an S-shaped isotherm. Here the slope firstly increases with adsorptive concentration as time progresses. It eventually decreases and becomes zero since the empty, vacant adsorbent sites are occupied. This isotherm occurs when the surface contains a low affinity at a low concentration and increases when the concentration gets higher (Sparks, 2003). The final C-type isotherm (Fig. 10) suggests a separating mechanism where adsorptive molecules are separated amongst the interfacial and bulk solution phases. There is no specific bonding between the adsorbent and adsorbate.

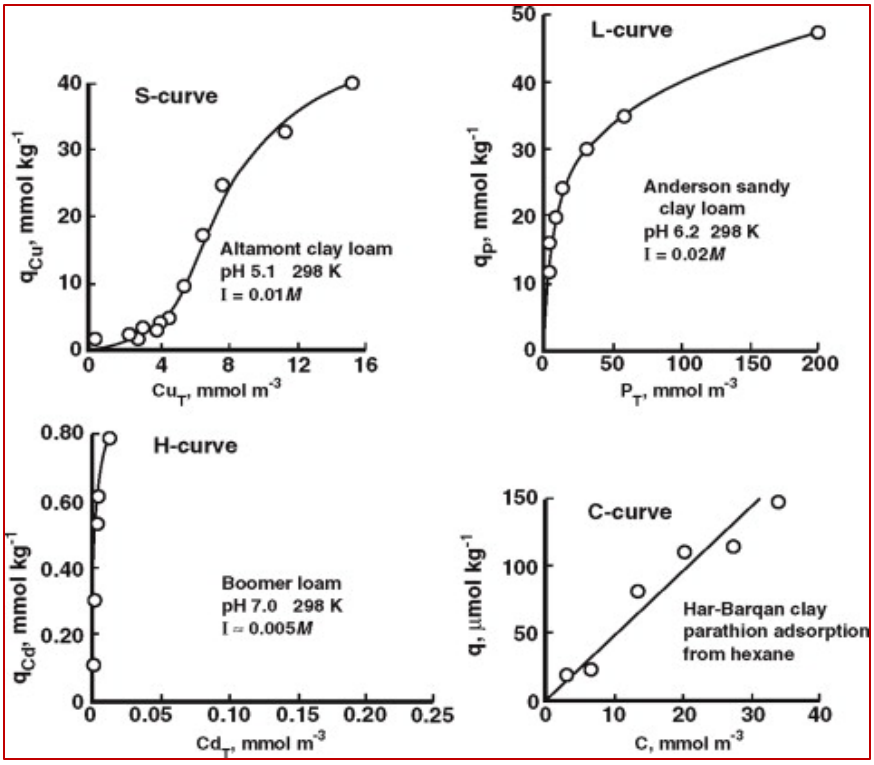

Figure 10. The four overall classes of adsorption isotherms.

2.5.4 The BET isotherm

The BET isotherm describes and characterizes the pore area of material with N_2 adsorption at pressure 77K. The two distinctive traits of porous materials are surface area and pore volume. An inert material such as nitrogen is used since it is high purity and found as cryogenic fluid, which allows it to be a perfect candidate for physically examining these two material traits. Furthermore, nitrogen's boiling point is 77.3K and determined at atmospheric pressure (P/Po) < 1), thus accommodating the vapor-liquid equilibrium on the surface. The BET technique contains five assumptions; these are as follows.

- A single molecule can adsorb on individual distinct adsorption sites, which creates an entire monolayer

- The adsorbed molecule can behave as an adsorption site for further molecules to join as added layers
- The highest layer will act as a liquid phase and shall be in equilibrium with the vapor phase
- The amount of heat that is needed for the adsorption/desorption process is determined using the Arrhenius-type rate equations. The desorption energy of a molecule within the layer at the solid surface is equal and represented as E_1. All further layers are equal $E_2 = E_3 = E_n = E_L$, the heat of liquefaction
- The number of layers reaches infinity as P/Po reaches unity.

$$\frac{\frac{p}{p_o}}{v\left(1-\left(\frac{p}{p_o}\right)\right)} = \left(c - \frac{1}{v_m c}\right)\left(\frac{p}{p_o}\right) + \frac{1}{v_m c} \quad (3)$$

where,

$c = \exp(E_1 - E_L / RT)$

and v -volume, vm -monolayer volume, P/Po- relative pressure, c -the BET constant, R -ideal gas constant and T- absolute temperature

2.5.5 The Linear Isotherm

The linear isotherm is the easiest adsorption isotherm and is employed when the graph C_s plotted against C_w has a linear form.

$$C_s = K_D C_W \quad (4)$$

where K_D-the adsorption coefficient (L/m2) and the slope of the trendline, C.W.- concentration of adsorbate in the solution after adsorption at equilibrium (M or mg/L).

2.6 Raw Agricultural Solid Waste

The agricultural waste materials such as sawdust, black liquor, and bark from paper, pulp mills, and forestry industries can be potentially used as adsorbents. These agricultural wastes are available in large quantities and have possible use as sorbents considering that they are cheap and possess suitable physicochemical characteristics. Moreover, they are of little or no value and their disposal is often a problem. In some cases, the waste material is burnt off to generate electricity for the plant, so finding suitable applications for the waste materials will add value to them and constitute wealth exercise. (Khoo and Ong, 2011). There are some reports on using waste materials such as mangrove wood, wheat straw, orange peel, and rice husk to remove dyes from aqueous media at varying conditions (Bharathi and Ramesh, 2013, Tan et al., 2010, Wong et al., 2014). Scientists have studied the appropriateness of multiple waste by-products to remove pollutants. The waste materials included diverse groups of synthetic dye.

2.7. Composites

A composite comprises two or more compounds with different functions that merge to form a material. Together, each compound's physical and chemical properties become more recognizable in the new material. The cooperation of the two materials contributes to enhancing the properties compared to the individual compounds. In 3400 B.C., composites were used in the production of plywood. It involved physically gluing together Wood at different angles. These civilizations also combined mud and straw to produce stable dwelling structures (Todd, 2018). In the 1940s, composites were used to reinforce the strength of materials and reduce their brittleness by forming fiberglass-enforced polymers. The composite was made by incorporating a polymer fiber into a lightweight material to produce a more durable material previously used in an airplane wing. The

polymer fiber itself is very fragile but, with the addition of the lightweight material, results in stronger interfacial bonds. Table 4 shows some of the current composites used for pollutant removal and the variety of uses of lignin-derived composites.

Table 2. Some Current composites and their uses in the removal of selected dyes and contaminants

Composite	Uses	Reference
Ag_2CO_3-halloysite	Removal of water-soluble dyes	(Nyankson et al., 2019)
The membrane of sepiolite with coated polysulfone	Removal of textile dyes and inorganic salts	(Zhu et al., 2020)
The thin-film composite membrane containing a high perm-selectivity	Removal of anionic dyes (methyl blue, reactive red and Congo red) and the enhanced anti-dye-deposition	(Wu et al., 2020)
Aerogel polymer composite that also had exhibited magnetic properties	Removal of organic dye (Reactive Black 5)	(Bober et al., 2020)
The composite containing chitosan/mg	Removal reactive blue in an aqueous medium	(Nga et al., 2020)
Mesoporous silicate/carbon composites produced using palygorskite clay waste	Removal of organic contaminants	(Wang et al., 2019)
Polyvinyl-alcohol/melamine-formaldehyde composite	Removal of Congo red dye	(Bhat et al., 2020)
Lignin	As biocatalysts for the generation of renewable chemicals from biomass	(Bugg et al., 2020)
Lignin catalyst	Application in green synthesis	(Zhu et al., 2019)
Lignin activated carbon	Application for supercapacitor electrode	(Zeng et al., 2019)
Lignin material	Wound healing application	(Ravishankar et al., 2019)
Graphene oxide adsorbent composite	Adsorption of cationic dyes (Methylene blue and crystal violet)	(Abd-Elhamid et al., 2019)
Novel lignin-based phenolic composites	Demonstrated excellent catalytic performance and good reusability	(Chen et al., 2020)

Adsorbent containing lignin-cellulose nanocrystal	Removal of cationic organic dyes	(Ma et al., 2019)
Composite made up of alginate and sugarcane bagasse biochar	Removal of methylene blue dye in an aqueous medium	(Biswas et al., 2020)
Graphene oxide/lignosulphonate thin film	Humidity sensor	(Chen et al., 2018)
Lignin	Reduction of iron oxide	(Wei et al., 2020)
Hydroxypropyl sulfonated lignin	For the preparation and in the mechanism of Nano disperse dye	(Qin et al., 2020)
Lignin	For the preparation of light-resistant azo-lignin colorant for coating use	(Pandian et al., 2020)
Pd nps@Fe_3O_4 lignin	For the reduction of Cr (VI) and Suzuki-Miyaura reaction in an eco-friendly method	(Nasrollahzadeh et al., 2020)
Thin films of celery nanocellulose and lignin/hemicellulose	Dye removal	(Luo et al., 2020)
Lignin-hydrogels	Developing the absorption capacity	(Morales et al., 2020)

References

Abay, A. K., Kuo, D.-H., Chen, X. & Saragih, A. D. 2017. A new V-doped $Bi_2(O,S)_3$ oxysulfide catalyst for highly efficient catalytic reduction of 2-nitroaniline and organic dyes. *Chemosphere,* 189**,** 21-31.

Abburi, K. 2003. Adsorption of phenol and p-chlorophenol from their single and bisolute aqueous solutions on Amberlite XAD-16 resin. *Journal of Hazardous Materials,* 105**,** 143-156.

ABD-Elhamid, A. I., Kamoun, E. A., EL-Shanshory, A. A., Soliman, H. M. A. & ALY, H. F. 2019. Evaluation of graphene oxide-activated carbon as effective composite adsorbent toward the removal of cationic dyes: Composite preparation, characterization and adsorption parameters. *Journal of Molecular Liquids,* 279**,** 530-539.

Adrosko, R. J. 2012. *Natural dyes and home dyeing*, Courier Corporation.

Aguilar, A., Borrell, A. & Pastor, T. 1999. Biological factors affecting variability of persistent pollutant levels in cetaceans.

Ali Zulfikar, M., Mariske, E.D. and Djajanti, S.D., 2012. Adsorption of lignosulfonate compounds using powdered eggshell. Songklanakarin Journal of Science & Technology, 34(3).

Azanova, V. & Hradil, J. 1999. Sorption properties of macroporous and hypercrosslinked copolymers. *Reactive and Functional Polymers,* 41**,** 163-175.

Bajwa, D. S., Pourhashem, G., Ullah, A. H. & Bajwa, S. G. 2019. A concise review of current lignin production, applications, products and their environmental impact. *Industrial Crops and Products,* 139**,** 111526.

Bajwa, D. S., Wang, X., Sitz, E., Loll, T. & Bhattacharjee, S. 2016. Application of bioethanol derived lignin for improving physico-mechanical properties of thermoset biocomposites. *International Journal of Biological Macromolecules,* 89**,** 265-272.

Bakhsh, E. M., Ali, F., Khan, S. B., Marwani, H. M., Danish, E. Y. & Asiri, A. M. 2019. Copper nanoparticles embedded chitosan for efficient detection and reduction of nitroaniline. *International Journal of Biological Macromolecules,* 131**,** 666-675.

Banat, F., AL-Asheh, S. & AL-Makhadmeh, L. 2003. Evaluation of the use of raw and activated date pits as potential adsorbents for dye containing waters. *Process Biochemistry,* 39**,** 193-202.

Banat, F. A., AL-Bashir, B., AL-Asheh, S. & Hayajneh, O. 2000. Adsorption of phenol by bentonite. *Environmental Pollution,* 107**,** 391-398.

Bano, M., Ahirwar, D., Thomas, M., Sheikh, M. U. D. & Khan, F. 2017. Hierarchical porous silver metal using Pluronic F-127 and graphene oxide as reinforcing agents for the reduction of o-nitroaniline to 1, 2-benzenediamine. *Journal of Solid State Chemistry,* 248**,** 40-50.

Benedetti, V., Patuzzi, F. & Baratieri, M. 2018. Characterization of char from biomass gasification and its similarities with activated carbon in adsorption applications. *Applied Energy,* 227**,** 92-99.

Benkhaya, S., M' Rabet, S. & EL Harfi, A. 2020. A review on classifications, recent synthesis and applications of textile dyes. *Inorganic Chemistry Communications,* 115**,** 107891.

Bharathi, K. S. & Ramesh, S. T. 2013. Removal of dyes using agricultural waste as low-cost adsorbents: a review. *Applied Water Science,* 3**,** 773-790.

Bhat, S. A., Zafar, F., Mondal, A. H., Mirza, A. U., Rizwanul Haq, Q. M. & Nishat, N. 2020. Efficient removal of Congo red dye from aqueous solution by adsorbent films of polyvinyl alcohol/melamine-formaldehyde composite and bactericidal effects. *Journal of Cleaner Production,* 255**,** 120062.

Bilal, M., Rasheed, T., Iqbal, H. M. N. & Yan, Y. 2018. Peroxidases-assisted removal of environmentally-related hazardous pollutants with reference to the reaction mechanisms of industrial dyes. *Science of The Total Environment,* 644**,** 1-13.

Biswas, S., Mohapatra, S. S., Kumari, U., Meikap, B. C. & Sen, T. K. 2020. Batch and continuous closed circuit semi-fluidized bed operation: Removal of MB dye using sugarcane bagasse biochar and alginate composite adsorbents. *Journal of Environmental Chemical Engineering,* 8**,** 103637.

Bober, P., Minisy, I. M., Acharya, U., Pfleger, J., Babayan, V., Kazantseva, N., Hodan, J. & Stejskal, J. 2020. Conducting polymer composite aerogel with magnetic properties for organic dye removal. *Synthetic Metals,* 260**,** 116266.

Booth, G. 2000. Nitro compounds, aromatic. *Ullmann's Encyclopedia of Industrial Chemistry*.

Bradley, P. M. & Chapelle, F. H. 1995. Factors affecting microbial 2, 4, 6-trinitrotoluene mineralization in contaminated soil. *Environmental science & technology,* 29**,** 802-806.

Bugg, T. D. H., Williamson, J. J. & Rashid, G. M. M. 2020. Bacterial enzymes for lignin depolymerisation: new biocatalysts for generation of renewable chemicals from biomass. *Current Opinion in Chemical Biology,* 55**,** 26-33.

Chakraborty, J. N. 2011. 14 - Sulphur dyes. *In:* CLARK, M. (ed.) *Handbook of Textile and Industrial Dyeing.* Woodhead Publishing.

Chattopadhyay, D. P. 2011. 4 - Chemistry of dyeing. *In:* CLARK, M. (ed.) *Handbook of Textile and Industrial Dyeing.* Woodhead Publishing.

Chen, C., Wang, X., Li, M., Fan, Y. & Sun, R. 2018. Humidity sensor based on reduced graphene oxide/lignosulfonate composite thin-film. *Sensors and Actuators B: Chemical,* 255**,** 1569-1576.

Chen, S., Wang, G., Sui, W., Parvez, A. M., Dai, L. & Si, C. 2020. Novel lignin-based phenolic nanosphere supported palladium nanoparticles with highly efficient catalytic performance and good reusability. *Industrial Crops and Products,* 145**,** 112164.

Corma, A., Concepción, P. & Serna, P. 2007. A Different Reaction Pathway for the Reduction of Aromatic Nitro Compounds on Gold Catalysts. *Angewandte Chemie International Edition,* 46**,** 7266-7269.

Crini, G. 2006. Non-conventional low-cost adsorbents for dye removal: A review. *Bioresource Technology,* 97**,** 1061-1085.

Beyene, H. D. 2014. The potential of dyes removal from textile wastewater by using different treatment technology. A review. *International Journal of Environmental Monitoring and Analysis,* 2(6), 347-353.

Degawa, M., Nakayama, M., Konno, Y., Masubuchi, K. & Yamazoe, Y. 1998. 2-Methoxy-4-nitroaniline and its isomers induce cytochrome P4501A (CYP1A) enzymes with different selectivities in the rat liver. *Biochimica et Biophysica Acta (BBA) - General Subjects,* 1379**,** 391-398.

Deosarkar, S. & Pangarkar, V. 2004. Adsorptive separation and recovery of organics from PHBA and SA plant effluents. *Separation and purification technology,* 38**,** 241-254.

Dessbesell, L., Paleologou, M., Leitch, M., Pulkki, R. & Xu, C. 2020. Global lignin supply overview and kraft lignin potential as an alternative for petroleum-based polymers. *Renewable and Sustainable Energy Reviews,* 123**,** 109768.

Desta, M. B. 2013. Batch sorption experiments: Langmuir and Freundlich isotherm studies for the adsorption of textile metal ions onto teff straw (Eragrostis tef) agricultural waste. *Journal of thermodynamics,* 2013.

DI Natale, F., Erto, A. & Lancia, A. 2013. Desorption of arsenic from exhaust activated carbons used for water purification. *Journal of Hazardous Materials,* 260**,** 451-458.

Dong, X., Wang, Y., Jia, M., Niu, Z., Cai, J., Yu, X., Ke, X., Yao, J. & Zhang, X. 2019. Sustainable and scalable in-situ synthesis of hydrochar-wrapped Ti_3AlC_2-derived nanofibers as adsorbents to remove heavy metals. *Bioresource Technology,* 282**,** 222-227.

Dong, Z., Le, X., Li, X., Zhang, W., Dong, C. and Ma, J., 2014. Silver nanoparticles immobilized on fibrous nano-silica as highly efficient and recyclable heterogeneous catalyst for reduction of 4-nitrophenol and 2-nitroaniline. *Applied Catalysis B: Environmental,* 158, 129-135.

EL-Shahat, M. & Shehata, A. 2014. Extraction of p-nitroaniline from aqueous solutions onto activated carbon prepared from treated camphor wood. *Int. J. Emerging Technol. Adv. Eng,* 4**,** 423-4430.

EL Harfi, S. & EL Harfi, A. 2017. Classifications, properties and applications of textile dyes: A review. *Applied Journal of Environmental Engineering Science,* 3, 311-320.

Emmrich, M. 1999. Kinetics of the alkaline hydrolysis of 2, 4, 6-trinitrotoluene in aqueous solution and highly contaminated soils. *Environmental science & technology,* 33**,** 3802-3805.

Ersan, G., Apul, O. G., Perreault, F. & Karanfil, T. 2017. Adsorption of organic contaminants by graphene nanosheets: A review. *Water Research,* 126**,** 385-398.

Espinosa-Aguirre, J. J., Reyes, R. E. & Cortinas DE Nava, C. 1991. Mutagenic activity of 2-chloro-4-nitroaniline and 5-chlorosalicylic acid in Salmonella typhimurium: two possible metabolites of niclosamide. *Mutation Research Letters,* 264**,** 139-145.

Farooqi, Z. H., Naseem, K., Begum, R. & Ijaz, A. 2015. Catalytic reduction of 2-nitroaniline in aqueous medium using silver nanoparticles functionalized polymer microgels. *Journal of Inorganic and Organometallic Polymers and Materials,* 25**,** 1554-1568.

Farooqi, Z. H., Naseem, K., Ijaz, A. & Begum, R. 2016. Engineering of silver nanoparticle fabricated poly (N-isopropylacrylamide-co-acrylic acid) microgels for rapid catalytic reduction of nitrobenzene. *Journal of Polymer Engineering,* 36**,** 87-96.

Fernandes, A.E. and Jonas, A.M., 2019. Design and engineering of multifunctional silica-supported cooperative catalysts. *Catalysis Today,* 334, 173-186.

Ferrari, E. 2014. Polymeric materials for the quantitative and reversible absorption of organic and inorganic water contaminants.

Foo, K. Y. & Hameed, B. H. 2009. An overview of landfill leachate treatment via activated carbon adsorption process. *Journal of Hazardous Materials,* 171**,** 54-60.

Gade, R., Ahemed, J., Yanapu, K. L., Abate, S. Y., Tao, Y.-T. & Pola, S. 2018. Photodegradation of organic dyes and industrial wastewater in the presence of layer-type perovskite materials under visible light irradiation. *Journal of Environmental Chemical Engineering,* 6**,** 4504-4513.

Gangadhar, G., Maheshwari, U. & Gupta, S. 2012. Application of nanomaterials for the removal of pollutants from effluent streams. *Nanoscience & Nanotechnology-Asia,* 2**,** 140-150.

Gnanaprakasam, P. & Selvaraju, T. 2014. Green synthesis of self assembled silver nanowire decorated reduced graphene oxide for efficient nitroarene reduction. *RSC Advances,* 4**,** 24518-24525.

González-lópez, M. E., Robledo-ortíz, J. R., Rodrigue, D. & Pérez-fonseca, A. A. 2020. Highly porous lignin composites for dye removal in batch and continuous-flow systems. *Materials Letters,* 263**,** 127289.

Gu, H., Wang, J., Ji, Y., Wang, Z., Chen, W. & Xue, G. 2013. Facile and controllable fabrication of gold nanoparticles-immobilized hollow silica particles and their high catalytic activity. *Journal of Materials Chemistry A,* 1**,** 12471-12477.

Gupta, V. K. & Suhas 2009. Application of low-cost adsorbents for dye removal – A review. *Journal of Environmental Management,* 90**,** 2313-2342.

Hajialigol, S. & Masoum, S. 2019. Promising electrochemical hydrogen storage properties of nano biomass derived from walnut shell. *International Journal of Hydrogen Energy,* 44**,** 10713-10721.

Har bhajan, S. & Bharati, K. A. 2014. 2 - History of natural dyes. *In:* Har Bhajan, S. & Bharati, K. A. (eds.) *Handbook of Natural Dyes and Pigments.* Woodhead Publishing India.

Hawkyard, C. 2006. 12 - Substrate preparation for ink-jet printing. *In:* UJIIE, H. (ed.) *Digital Printing of Textiles.* Woodhead Publishing.

Huang, J., Wang, X. & Huang, K. 2009. Adsorption of p-nitroaniline by phenolic hydroxyl groups modified hyper-cross-linked polymeric adsorbent and XAD-4: A comparative study. *Chemical Engineering Journal,* 155**,** 722-727.

Huang, J., Zhang, L., Chen, B., Ji, N., Chen, F., Zhang, Y. & Zhang, Z. 2010. Nanocomposites of size-controlled gold nanoparticles and graphene oxide: Formation and applications in SERS and catalysis. *Nanoscale,* 2**,** 2733-2738.

Huang, Z., Li, Y., Chen, W., Shi, J., Zhang, N., Wang, X., Li, Z., Gao, L. & Zhang, Y. 2017. Modified bentonite adsorption of organic pollutants of dye wastewater. *Materials Chemistry and Physics,* 202**,** 266-276.

Ara, N. J., Hasan, M. A., Rahman, M. A., Salam, M. A., Salam, A. and Alam, A. S. 2013. Removal of remazol red from textile waste water using treated sawdust-an effective way of effluent treatment. *Bangladesh Pharmaceutical Journal,* 16(1), 93-98.

Kassim, A., Joseph, C.G., Zainal, Z., Zobir hussein, M., Jelas Haron, M.D. and Abdullah, A.H. 2004. Activated carbons prepared from oil palm shells: application for column separation of heavy metals. *Journal of the Indian Chemical Society,* 81(11), 946-949.

Khattri, S. & Singh, M. 2000. Colour removal from synthetic dye wastewater using a bioadsorbent. *Water, Air, and Soil Pollution,* 120**,** 283-294.

Khoa, N. T., Kim, S. W., Yoo, D.-H., Kim, E. J. & Hahn, S. H. 2014. Size-dependent work function and catalytic performance of gold nanoparticles decorated graphene oxide sheets. *Applied Catalysis A: General,* 469**,** 159-164.

Khoo, E.-C. & ONG, S.-T. Utilization of Agricultural Waste as a Biosorbent for the Removal of Dyes from Aqueous Solution. 1st World Sustain. Forum, 2011. MDPI.

Koh, J. 2011. 3 - Dyeing of cellulosic fibres. *In:* CLARK, M. (ed.) *Handbook of Textile and Industrial Dyeing.* Woodhead Publishing.

Kowsari, M., 2014. Application of Adsorption for Removal of Emerging Pollutants from Drinking Water (Doctoral dissertation, University of Saskatchewan).

Kunin, R. 1976. The use of macroreticular polymeric adsorbents for the treatment of waste effluents. Pure and Applied Chemistry, 46(2-4), 205-211.

Kyzas, G. Z., Deliyanni, E. A., Bikiaris, D. N. & Mitropoulos, A. C. 2018. Graphene composites as dye adsorbents: Review. *Chemical Engineering Research and Design,* 129**,** 75-88.

Le, X., Dong, Z., Zhang, W., Li, X. & MA, J. 2014. Fibrous nano-silica containing immobilized Ni@Au core-shell nanoparticles: A highly active and reusable catalyst for the reduction of 4-nitrophenol and 2-nitroaniline. *Journal of Molecular Catalysis A: Chemical,* 395**,** 58-65.

Lefebvre, O. & Moletta, R. 2006. Treatment of organic pollution in industrial saline wastewater: A literature review. *Water Research,* 40**,** 3671-3682.

Leo, L., Loong, C., Ho, X. L., Raman, M. F. B., Suan, M. Y. T. & Loke, W. M. 2018. Occurrence of azo food dyes and their effects on cellular inflammatory responses. *Nutrition,* 46**,** 36-40.

Li, K., Zheng, Z., Feng, J., Zhang, J., Luo, X., Zhao, G. & Huang, X. 2009. Adsorption of p-nitroaniline from aqueous solutions onto activated carbon fiber prepared from cotton stalk. *Journal of Hazardous Materials,* 166**,** 1180-1185.

Luo, J., Huang, K., Zhou, X. & Xu, Y. 2020. Hybrid films based on holistic celery nanocellulose and lignin/hemicellulose with enhanced mechanical properties and dye removal. *International Journal of Biological Macromolecules,* 147**,** 699-705.

Ma, M., Liu, Z., Hui, L., Shang, Z., Yuan, S., Dai, L., Liu, P., Liu, X. & Ni, Y. 2019. Lignin-containing cellulose nanocrystals/sodium alginate beads as highly effective adsorbents for cationic organic dyes. *International Journal of Biological Macromolecules,* 139**,** 640-646.

Maté, C., Ryan, A. J. & Wright, S. E. 1967. Metabolism of some 4-nitroaniline derivatives in the rat. *Food and Cosmetics Toxicology,* 5**,** 657-663.

Mathur, A. M., Moorjani, S. K. & Scranton, A. B. 1996. Methods for synthesis of hydrogel networks: A review. *Journal of Macromolecular Science, Part C: Polymer Reviews,* 36**,** 405-430.

Morales, A., Labidi, J. & Gullón, P. 2020. Effect of the formulation parameters on the absorption capacity of smart lignin-hydrogels. *European Polymer Journal,* 129**,** 109631.

Muhi Mohammed, F. 2011. Modelling and design of water treatment processes using adsorption and electrochemical regeneration*.* Doctor of Philosophy thesis, University of Manchester.

Narimani, F. & Mansour Lakouraj, M. 2015. Synthesis and characterization of super dye adsorbent hydrogels based on acrylic acid and acryloyl tetrasodium thiacalix[4]arene tetrasulfonate. 64**,** 1482-1490.

Naseem, K., Begum, R. and Farooqi, Z.H. 2017. Catalytic reduction of 2-nitroaniline: a review. Environmental Science and Pollution Research, 24(7), 6446-6460.

Nasrollahzadeh, M., Bidgoli, N. S. S., Issaabadi, Z., Ghavamifar, Z., Baran, T. & Luque, R. 2020. Hibiscus Rosasinensis L. aqueous extract-assisted valorization of lignin: Preparation of magnetically reusable Pd NPs@Fe_3O_4 lignin for Cr(VI) reduction and Suzuki-Miyaura reaction in eco-friendly media. *International Journal of Biological Macromolecules,* 148**,** 265-275.

NG, C., Losso, J. N., Marshall, W. E. & Rao, R. M. 2002. Freundlich adsorption isotherms of agricultural by-product-based powdered activated carbons in a geosmin–water system. *Bioresource technology,* 85**,** 131-135.

NGA, N. K., Thuy chau, N. T. & Viet, P. H. 2020. Preparation and characterization of a chitosan/MgO composite for the effective removal of reactive blue 19 dye from aqueous solution. *Journal of Science: Advanced Materials and Devices,* 5**,** 65-72.

Wahid, Z. A., Mohd Rawi, S. N., Nasrullah, M. and Wahidatul, A. Z. 2016. Pretreatment of reactive dye from textile wastewater by coagulation technology. Int. Res J Eng Tech, 3(12), 56-72.

Nyankson, E., Agyei-tuffour, B., Annan, E., Yaya, A., Mensah, B., Onwona-agyeman, B., Amedalor, R., Kwaku-frimpong, B. & Efavi, J. K. 2019. Ag_2CO_3-halloysite nanotubes composite with enhanced removal efficiency for water soluble dyes. *Heliyon,* 5**,** e01969.

Pan, B., Du, W., Zhang, W., Zhang, X., Z, Q., Pan, B., Lv, L., Zhang, Q. & Chen, J. 2007. Improved adsorption of 4-nitrophenol onto a novel hyper-cross-linked polymer. *Environmental science & technology,* 41**,** 5057-5062.

Pan, B., Pan, B., Zhang, W., Lv, L., Zhang, Q. & Zheng, S. 2009. Development of polymeric and polymer-based hybrid adsorbents for pollutants removal from waters. *Chemical Engineering Journal,* 151**,** 19-29.

Pan, B., Zhang, Q., Meng, F., Li, X., Zhang, X., Zheng, J., Zhang, W., Pan, B. & Chen, J. 2005. Sorption enhancement of aromatic sulfonates onto an aminated hyper-cross-linked polymer. *Environmental science & technology,* 39**,** 3308-3313.

Panda, H. 2013. A concise guide on textile dyes, pigments and dye intermediates with textile printing technology, Niir Project Consultancy Services.

Pandian, B., Arunachalam, R., Easwaramoorthi, S. & Rao, J. R. 2020. Tuning of renewable biomass lignin into high value-added product: Development of light resistant azo-lignin colorant for coating application. *Journal of Cleaner Production,* 256**,** 120455.

Qin, Y., Yuan, M., Hu, Y., Lu, Y., Lin, W., Ma, Y., Lin, X. & Wang, T. 2020. Preparation and interaction mechanism of Nano disperse dye using hydroxypropyl sulfonated lignin. *International Journal of Biological Macromolecules,* 152**,** 280-287.

Raghunath, S., Anand, K., Gengan, R. M., Nayunigari, M. K. & Maity, A. 2016. Sorption isotherms, kinetic and optimization process of amino acid proline based polymer

nanocomposite for the removal of selected textile dyes from industrial wastewater. *Journal of Photochemistry and Photobiology B: Biology,* 165**,** 189-201.

Rajasulochana, P. & Preethy, V. 2016. Comparison on efficiency of various techniques in treatment of waste and sewage water – A comprehensive review. *Resource-Efficient Technologies,* 2**,** 175-184.

Naseem, R. and Tahir, S. S., 2001. Removal of Pb (II) from aqueous/acidic solutions by using bentonite as an adsorbent. *Water Research*, 35(16), 3982-3986.

Ravishankar, K., Venkatesan, M., Desingh, R. P., Mahalingam, A., Sadhasivam, B., Subramaniyam, R. & Dhamodharan, R. 2019. Biocompatible hydrogels of chitosan-alkali lignin for potential wound healing applications. *Materials Science and Engineering: C,* 102**,** 447-457.

Sahiner, N., Karakoyun, N., Alpaslan, D. and Aktas, N., 2013. Biochar-embedded soft hydrogel and their use in Ag nanoparticle preparation and reduction of 4-nitro phenol. International *Journal of Polymeric Materials and Polymeric Biomaterials,* 62(11), 590-595.

Salam, M. A. 2015. Adsorption of nitroaniline onto high surface area nanographene. *Journal of Industrial and Engineering Chemistry,* 28**,** 67-72.

Sanyang, L., Ghani, W.A.W.A.K. and Zainudin, R., 2013. Sorption of Phenol from Wastewater by Hydrogel-biochar Composite. *International Journal of Engineering and Technology,* 10(1), 38-49.

Schwierz, F. 2010. Graphene transistors. *Nature Nanotechnology,* 5**,** 487-496.

Clark, M. 2011. Fundamental principles of dyeing. Handbook of Textile and Industrial Dyeing; *Woodhead Publishing: Cambridge, UK,* 1, 1-27.

Şenlik, K., Gezici, O., Guven, I. & Pekacar, A. I. 2017. Adsorption of nitroaniline positional isomers on humic acid-incorporated monolithic cryogel discs: Application of ligand-exchange concept. *Journal of Environmental Chemical Engineering,* 5**,** 2836-2844.

Shi, L., Yu, Q., Mao, Y., Huang, H., Huang, H., Ye, Z. & Peng, X. 2012. High catalytic performance of gold nanoparticle-gelatin mesoporous composite thin films. *Journal of Materials Chemistry,* 22**,** 21117-21124.

Singh, C., GoyaL, A. & Singhal, S. 2014. Nickel-doped cobalt ferrite nanoparticles: efficient catalysts for the reduction of nitroaromatic compounds and photo-oxidative degradation of toxic dyes. *Nanoscale,* 6**,** 7959-7970.

Sparks, D. L. 2003. 5 - Sorption Phenomena on Soils. *In:* SPARKS, D. L. (ed.) *Environmental Soil Chemistry (Second Edition).* Burlington: Academic Press.

Steve, K., Erika, T., Reynold, T. & Paul, M. 1998. Activated carbon: a unit operations and processes of activated carbon. *Environmental Engineering,* 25**,** 350-749.

Subramaniam, M. N., Goh, P.-S., Lau, W.-J., NG, B.-C. & Ismail, A. F. 2019. Chapter 3 - Development of nanomaterial-based photocatalytic membrane for organic pollutants removal. *In:* Lau, W. J., Ismail, A. F., Isloor, A. & AL-Ahmed, A. (eds.) *Advanced Nanomaterials for Membrane Synthesis and its Applications.* Elsevier.

Tan, L., Jain, K. & Rozaini, C. 2010. Adsorption of textile dye from aqueous solution on pretreated mangrove bark, an agricultural waste: equilibrium and kinetic studies. *Journal of applied sciences in environmental sanitation,* 5(3).

Tang, C.-Y., Yu, P., Tang, L.-S., Wang, Q.-Y., Bao, R.-Y., Liu, Z.-Y., Yang, M.-B. & Yang, W. 2018. Tannic acid functionalized graphene hydrogel for organic dye adsorption. *Ecotoxicology and Environmental Safety,* 165**,** 299-306.

Todd, J. 2018. History of Composites. ThoughtCo.

Vankar, P. S. 2000. Chemistry of natural dyes. *Resonance,* 5**,** 73-80.

Wan, W.-X., Chen, Y., Zhang, J., Shen, F., Luo, L., Deng, S.-H., Xiao, H., Zhou, W., Deng, O.-P., Yang, H., Xiao, Y.-L., Huang, C.-R., Tian, D., He, J.-S. & Wang, Y.-J. 2019. Mechanism-based structure-activity relationship (SAR) analysis of aromatic amines and nitroaromatics carcinogenicity via statistical analyses based on CPDB. *Toxicology in Vitro,* 58**,** 13-25.

Wang, B., Huang, J., Deng, S., Yang, X. & Yu, G. 2012. Addressing the environmental risk of persistent organic pollutants in China. *Frontiers of Environmental Science & Engineering,* 6**,** 2-16.

Wang, S., Sun, H., Ang, H. M. & Tadé, M. O. 2013. Adsorptive remediation of environmental pollutants using novel graphene-based nanomaterials. *Chemical Engineering Journal,* 226**,** 336-347.

Wang, W., Lu, T., Chen, Y., Tian, G., Sharma, V. K., Zhu, Y., Zong, L. & Wang, A. 2019. Mesoporous silicate/carbon composites derived from dye-loaded palygorskite clay waste for efficient removal of organic contaminants. *Science of The Total Environment,* 696**,** 133955.

Wang, X., Jiang, C., Hou, B., Wang, Y., Hao, C. & Wu, J. 2018. Carbon composite lignin-based adsorbents for the adsorption of dyes. *Chemosphere,* 206**,** 587-596.

Wei, R., Xiang, D., Long, H., Xu, C. & Li, J. 2020. Reduction of iron oxide by lignin: Characteristics, kinetics and superiority. *Energy,* 197**,** 117203.

Williamson, K. L. & Masters, K. M. 2016. *Macroscale and Microscale Organic Experiments*, Cengage Learning.

Wong, Y., Ranjini, K. & Wan-nurdiyana, W. 2014. Removal of Congo Red and Acid Yellow 36 Dye Using Orange Peel and Rice Husk as Absorbent. *Oriental Journal of Chemistry,* 30**,** 529-539.

Wongcharee, S., Aravinthan, V. & Erdei, L. 2019. Mesoporous activated carbon-zeolite composite prepared from waste macadamia nut shell and synthetic faujasite. *Chinese Journal of Chemical Engineering,* 27**,** 226-236.

Wu, Y., Gao, M., Chen, W., Lü, Z., Yu, S., Liu, M. & Gao, C. 2020. Efficient removal of anionic dye by constructing thin-film composite membrane with high perm-selectivity and improved anti-dye-deposition property. *Desalination,* 476**,** 114228.

Yang, W. C., Shim, W. G., Lee, J. W. & Moon, H. 2003. Adsorption and desorption dynamics of amino acids in a nonionic polymeric sorbent XAD-16 column. *Korean Journal of Chemical Engineering,* 20**,** 922-929.

Yu, F., Yang, C., Zhu, Z., Bai, X. & Ma, J. 2019. Adsorption behavior of organic pollutants and metals on micro/nanoplastics in the aquatic environment. *Science of The Total Environment,* 694**,** 133643.

Zeng, L., Lou, X., Zhang, J., Wu, C., Liu, J. & Jia, C. 2019. Carbonaceous mudstone and lignin-derived activated carbon and its application for supercapacitor electrode. *Surface and Coatings Technology,* 357**,** 580-586.

Zeng, T., Ma, Y.-R., Niu, H.-Y. & Cai, Y.-Q. 2012. A novel Fe_3O_4 graphene Au multifunctional nanocomposite: green synthesis and catalytic application. *Journal of Materials Chemistry,* 22**,** 18658-18663.

Zhang, G. & Ma, Y. 2013. Mechanistic and conformational studies on the interaction of food dye amaranth with human serum albumin by multispectroscopic methods. *Food chemistry,* 136**,** 442-449.

Zhang, X., Li, A., Jiang, Z. & Zhang, Q. 2006. Adsorption of dyes and phenol from water on resin adsorbents: effect of adsorbate size and pore size distribution. *Journal of hazardous materials,* 137**,** 1115-1122.

Zhang, X., Zhang, P., Wu, Z., Zhang, L., Zeng, G. & Zhou, C. 2013. Adsorption of methylene blue onto humic acid-coated Fe_3O_4 nanoparticles. *Colloids and Surfaces A: Physicochemical and Engineering Aspects,* 435**,** 85-90.

Zhaoyi, X., Quanxing, Z., Changlong, W. & Liansheng, W. 1997. Adsorption of naphthalene derivatives on different macroporous polymeric adsorbents. *Chemosphere,* 35**,** 2269-2276.

Zhu, Y., Li, Z. and Chen, J., 2019. Applications of lignin-derived catalysts for green synthesis. *Green Energy & Environment,* 4(3), 210-244.

Zhu, Z., Liu, D., Cai, S., Tan, Y., Liao, J. & Fang, Y. 2020. Dyes removal by composite membrane of sepiolite impregnated polysulfone coated by chemical deposition of tea polyphenols. *Chemical Engineering Research and Design,* 156**,** 289-299.

Chapter Three: Experimental

3.1 Materials

Sodium lignosulphonate was obtained from ABA Tech CC in Kwa-Zulu-Natal, South Africa, without any prior processing. Mondi Richard Bay provided different variants of black liquor. Humic acid, sulphuric acid, sodium hydroxide, sodium borohydride, dimethyl sulfoxide (DMSO), triethylamine, azoisobutyronitrile, acrylonitrile, maleic anhydride, acryloyl chloride were purchased from Merck and Sigma Aldrich. The dyes used, viz., Reactive Blue 222, Reactive Red 195 and Reactive Yellow 145, Congo Red and Methylene Blue were purchased from Colchem Chemicals and Dyes South Africa. Double deionized was used to prepare solutions and was obtained from a MilliQ Millipore system. Whatman filter paper no 1 was used for all filtrations. All the glassware was thoroughly washed using double deionized water. For the pH studies, the adjustments were made using either 0.1 M HCl or 0.1 M NaOH solutions. All the analyses were performed in triplicate, and the mean was used for the calculations.

3.2 Instrumentation

The Perkin Elmer Spectrum 100 FT-IR Spectrometer, CPU 32 main with a Universal ATR (attenuated total reflection), was used to determine the functional groups present. The samples were analyzed in the scanning range of 4000 cm^{-1} to 380 cm^{-1}, with a resolution of 1 cm^{-1}. The ZEISS EVO 15 Environmental Scanning Electron Microscope analyzer coupled with the Energy Dispersive X-ray Diffractometer D8 Advance from Bruker functioned in a nonstop 9-9 scan in sealed coupled mode with Cu-K radiation was used for the surface morphology analysis. HR-TEM JOEL JEM 2000EXII transmission electron microscope was used to determine the diffraction and lattice fringe images. A Brunauer-Emmet-Teller (BET) surface analyzer- Micromeretics Tristar II was used. A Mettler Toledo TGA system and a Differential Scanning Calorimetry model 1

SF/1346 with STARe system software were used to determine the thermal stability of the developed adsorbents. A Shimadzu UV 1800 UV/Visible Spectrophotometer was used to determine the absorbance readings with quartz cuvettes. All the samples were scanned in the 800–200 nm region, at a scanning rate of 0.5 nm/s. The SPL 15 MP Labcon Platform Shaker was used for agitating the conical flasks at a speed of 150 rpm. The Hettich Universal II Centrifuge was used at speed at 4000 rpm. The Metrohm 691 pH meter was used for the pH measurements.

3.3 Experimental

3.3.1 The synthesis of humic acid-lignosulphonate composites (HLC)

11g HA and 26g LS were dissolved in 100 mL deionized water and then transferred into a round bottom flask. After that, an excess of sulphuric acid was added slowly, with stirring. The mixture was refluxed for 24 hr at 90 °C. The reaction was cooled to room temperature and poured into ice water. The contents were filtered, washed with water, and dried for 24 hours in an oven.

3.3.2 The synthesis of humic acid- lignosulphonate-maleic anhydride composites (HLMAC)

In a round bottom flask, 5g HLC and 10g maleic anhydride (MA) was dissolved in DMSO. Catalytic amounts of triethylamine were added, and the mixture was refluxed in an oil bath for 5 hr at 100 °C. The resultant product was washed with acetone to remove unreacted MA. The material was dried for 48 hr at 60 °C. Thereafter, 3 g of the material and 7 g of acrylonitrile were dissolved in 35 g of DMSO, followed by 0.1 g of azoisobutyronitrile (AIBN). The reaction was conducted under a nitrogen atmosphere at 60 °C for 22 hr. The product was filtered, washed, and dried at 60 °C for 24 hr.

3.3.3 Preparation of the humic-based kraft composite (HKLC)

A mixture of 10g of kraft lignin and humic acid was added to 50mL concentrated sulphuric acid for 24 hours. Thereafter, the solution was washed several times with deionized water and left to dry in an oven at 110 °C for 96 hr. It was then transferred into a furnace at 250 °C for 2 hr. The material was washed with deionized water several times and treated with aqueous KOH at a mass ratio of 1:3 mixed thoroughly for 24 hr till a high viscous liquid was obtained. It was washed with deionized water, dried in an oven for 48 hr at 100°C, cooled, and finally infused in concentrated HNO_3 at 75°C for 36 hr. The material was washed with deionized water and air-dried at 60°C for 24 hr.

3.3.4 Preparation of Sodium Borohydride Solution

A 0.01000 M of sodium borohydride solution was prepared by dissolving 3.784mg of $NaBH_4$ into a 10 mL volumetric flask and bringing the solution to mark with deionized water. For all reduction experiments, a freshly prepared $NaBH_4$ solution was used.

3.3.5 Method for the preparation of textile dye standard for the adsorption studies

A 1000.0 mg/L stock solution of mixed dye was prepared by weighing 0.5000 g of each reactive dye into a 500 mL volumetric flask. The dye standard mixture was dissolved in deionized water and the solution was accurately made up to 500 mL. An aliquot of 10 mL, 20 mL, 30 mL, 40 mL, 50 mL and 60 mL were quantitatively transferred separately into 100 mL volumetric flasks and each of the solutions was accurately diluted to 100 mL with deionized water to yield a 20, 40, 60, 80, 100 and 120 ppm solutions, respectively. These solutions were required to generate the calibration curves and kinetic and equilibrium studies. UV-Vis Spectroscopy determined the λ max of each dye solution and a calibration graph was plotted to find molar absorptivity constants.

3.3.6 Kinetic and Equilibrium Studies

3.3.6.1 The Adsorption of textile dyes - The Effect of Quantity HLMAC on Dye Adsorption

A fixed quantity of (0.5g – 2.0g) adsorbent was weighed and transferred into a separate 100 mL conical flask. The 60 mL of 80ppm mixed dye was added separately into each conical flask, and each flask was shaken in a shaking incubator at 180 rpm for the fixed time interval of 15 to 120 min. The mixture was transferred into a centrifuge tube and centrifuged for 10 min, decanted, and analyzed by UV-Visible spectroscopy.

3.3.6.2 Variation of parameters: batch adsorption method for the dyes.

The Effect of Initial Dye Concentration on Adsorption

1.500 g of HLMAC, presented in Table 3.1, was added to the eight conical flasks. After that 60 mL of 40ppm, 60 ppm, 80 ppm and 100ppm of mixed dye, were added to each flask and simultaneously shaken at 180 rpm for 15 to 120 min. Next, the mixture was transferred into a centrifuge tube and centrifuged for 10 min, decanted, and analyzed by UV-Visible spectroscopy.

The Effect of pH of the Dye Solution on Adsorption

An aliquot of 60 mL of an 80 ppm mixed dye was quantitatively transferred separately into eight individual 100 mL beakers. The pH was then adjusted by using 0.1 M HCl or 0.1 M NaOH solution. The pH of the studied dye solutions was 2.00, 5.0, 7.0, 8.0, 10 and 12. Once the desired pH had been reached, the dye solution was quantitatively added to the 100 mL conical flask. These eight solutions containing the respective adsorbents were simultaneously shaken at a fixed time interval of 120 min at 180 rpm. Next, the mixture was transferred into a centrifuge tube and centrifuged for 10 min, decanted, and analysed by UV-Visible spectroscopy. The UV-Visible results were documented to find the optimum pH that can be used for the adsorption process.

The different parameters, such as effects of dye concentrations, adsorbent dosage, and pH were varied. All analysis was done using the UV-visible spectrophotometer scanning at the 250 – 800 nm region. Lambda maximums were obtained for each dye. The experimental data were calculated to find the adsorption isotherm using the Langmuir and Freundlich models.

3.7 Reduction studies on nitroaromatics and dyes using humic-based kraft composite

Preparation of dye and nitroaromatic solution

The respective solutions (Table 3) were prepared accordingly. The solutions were prepared for each of the solutions used by dissolving the particular masses into a 100 mL volumetric flask using deionized water. The solutions were made up 100 mL with deionized water.

All solutions were diluted to give their respective concentrations of approximately 1.000 x 10^{-5} M.

Table *3.* Quantities of different dye and nitroaromatic solution used.

Solution used	Concentration /M	Mass/g
Congo red	0.0017	0.0544
Methylene blue	0.0001	0.0032
2-nitroaniline	0.007	0.1005
3-nitroaniline	0.0013	0.0180
4-Nitro-o-phenylenediamine NPDA	0.0001	0.0015

The UV-Visible spectroscopy analyzed each solution prepared in Table 3 to determine the starting peak prior to the reduction studies. 1.9 mL of the prepared solution (Table 3) were separately added into a quartz cuvette and a fixed quantity (between 50- 250 mg) of HKLC and then analyzed by UV-Visible spectroscopy. Thereafter, 0.10 mL of 0.01M NaBH4 was added to the cuvette, and this solution was analyzed at time intervals. In reducing NAs and dyes, the colored solution turned colorless, thus demonstrating a visual confirmation of the reduction process.

Chapter Four: Results, Discussion and Conclusion

In this study, we synthesized two composites viz., humic acid-lignosulphonate-maleic anhydride composites (HLMAC) which was utilized for the adsorption of three reactive dyes and humic-acid based kraft composite (HKLC) for the reduction of nitroanilines and five selected dyes.

PART A

In the first synthetic part of the study, we focused on the synthesis of HLMAC which was a two-step reaction. In the first step, humic acid was reacted with lignosulphonate in the presence of trace amounts of sulphuric acid which acted as the catalyst for dehydration. Hence, amongst other possible bonds, the ester bonds were formed between the two components. In the second step of the reaction, the new molecule was reacted with maleic anhydride followed by acrylonitrile and azoisobutyronitrile. It was evident that the maleic anhydride reacted with the phenolic hydroxy groups of the HLC molecule to form more ester linkages. In essence, a new polymer blend was obtained as HLMAC however this composite requires more characterization techniques such as ^{1}H-NMR, ^{13}C-NMR and MS-TOF to better understand the detailed structure.

A proposed reaction scheme (Figure 11) is presented for the final composite HLMAC.

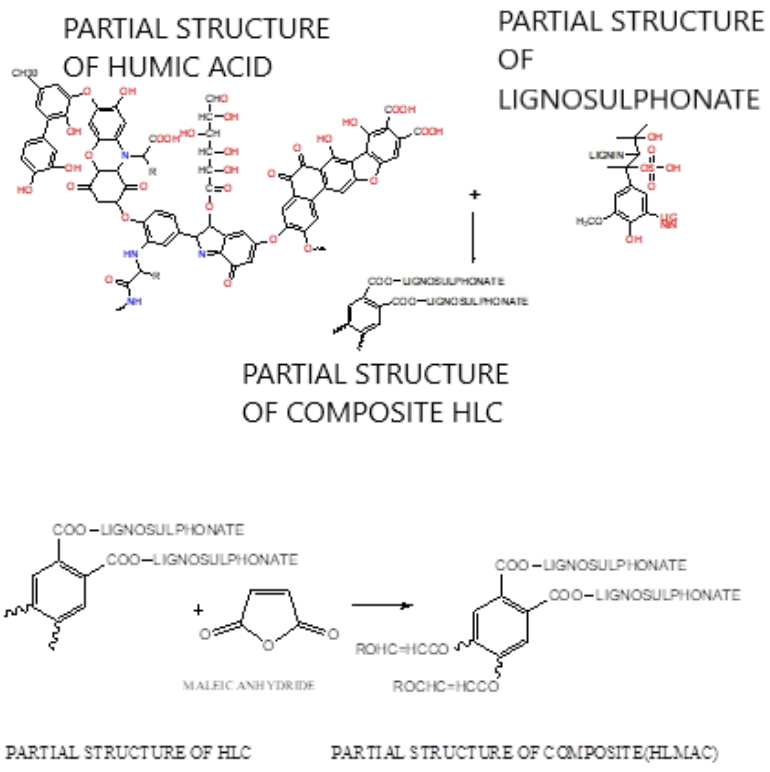

Figure 11. The synthesis of humic acid- lignosulphonate-maleic anhydride composite

4.1. Characterisation of humic acid- lignosulphonate-maleic anhydride composite

4.1.1. FTIR

The resulting synthesized composite HLMAC was initially analyzed by FTIR to confirm the functional groups which are present in the composite. The spectrum of FTIR shown in Fig. 12(a) exhibits the peaks at 3470, 3290, 2885, 1714, 1642, 1507, 1231, 1137, 1057, 823 and 566 cm^{-1} corresponding to stretching of H-bonded -OH, carboxyl -OH, aromatic C-H, -C=O, C=C, C-C, C-O, S=O and polyphenyl groups. And the another resulting synthesized humic lignosulphonate composite (HLC) was also analyzed by FTIR to confirm its functional groups which are present in the material. The obtained spectrum of FTIR shows in Fig. 12(b) which exhibits the peaks at

3340, 3220, 2865, 1718, 1612, 1517, 1271, 1127, 1067, 813 and 556 cm^{-1} corresponding to stretching of H-bonded -OH, carboxyl -OH, aromatic C-H, -C=O, C=C, C-C, C-O, S=O and polyphenyl groups. Generally humic acid contains the following functional groups as H-bonded -OH, -C-H, conjugated -C=O, aromatic -C-H bending vibration, C-C, C-O stretching and polyphenyl group stretching, that leads to show the relevant bands at 3388, 2937, 1623, 1383, 1246, 1137 and 623 cm^{-1}, respectively. Mostly, the prominent peaks of aromatic character could be obtained from humic acid. The primary chemical structures of both spectra contain very similar functional groups like -OH stretch, C=O, C-C, aromatic -C-H and polysaccharides as shown in Fig. 14(c). The emergence of alcoholic (-OH) and free phenolic groups may be seen in all individual and composite material at the wavelength in the range of 3600 to 3300 cm^{-1}. These bands are due to the complexation of chains in humic acid (Stevenson. *et. al.* 1994) as a result of the management strategy used with humic acids being more recalcitrant than lignosulphonates. There are broad bands that appeared in the range between 3400 to 3200 cm^{-1} in all humic and lignosulphonates which represent H bridges in stretching of -COOH and -OH of phenolic groups. In addition, multiple bands were observed in the fingerprint region (1900 to 800 cm^{-1}) with varying intensities. The stretching and widening could be related to the strength of intramolecular bonds, and the greater number of bridges with broader width is an indicator of the substantial acidity of the material (Dias. *et. al*. 2009). Usually, the aromatic characters for all humic and their composite materials were obtained at around 1507 cm^{-1}. The band at 1623 cm^{-1} occuring in the HA spectrum with low intensity, corresponds to conjugated C=O stretching groups and this was turned up to 1714 cm^{-1}. The highlights of the above spectra reveal that the conjugated carboxyl group converted to the carbonyl group which is probably the ester linkage. Furthermore, the lignosulphonate also holds most of the functional groups observed in HA. Fig. 12(d) illustrates the FTIR spectrum of

lignosulphonate located at 3365, 2930, 1592, 1510, 1416, 1169, 1034, 650, 516 cm^{-1} can be assigned to -OH, -C-H, -C=C, aromatic -C-H bending vibrations, -C-C, -C-O, -S=O stretching and polysaccharides stretching. (Shen.*et. al*. 2008) The S-O stretching vibration group in sulfonic groups generated by the interaction of sodium sulfite with the secondary -OH of the aliphatic side chain of lignins are attributed to the band occurring at 620-650 cm^{-1}.

The symmetric carbonyl stretching peak for maleic anhydride is at 1853, while the asymmetric stretch is at 1780. For unsaturated cyclic anhydrides these two peaks typically fall from 1860 to 1840 and 1780 to 1760, respectively. For saturated cyclic anhydrides, such as succinic anhydride whose structure is seen in Figure 2, these peaks fall at 1870–1845 and 1800–1775.Note in Figure 12 that the high-wavenumber symmetric C=O stretching peak is weaker than the lower-wavenumber asymmetric C=O stretching peak. This pattern is opposite that for noncyclic anhydrides as seen above. Thus, the peak intensity ratio of the two anhydride C=O stretching peaks can be used to determine whether an anhydride is noncyclic or cyclic. For noncyclic anhydrides the higher-wavenumber symmetric C=O stretch is more intense, while for cyclic anhydrides the lower-wavenumber asymmetric stretch is more intense. Again, a double carbonyl stretch with one or both peaks at a relatively high wavenumber is a strong indication of an anhydride. If the lower-wavenumber peak is more intense it is cyclic. Then use the position of the two C=O stretches and Table II to determine whether the anhydride is cyclic saturated or cyclic unsaturated.

Like noncyclic anhydrides, cyclic anhydrides have a C-O bond and hence a C-O stretch. It falls anywhere from 1300 to 1000. In the spectrum of maleic anhydride in Figure 12 this peak fall at 1058 and is labeled C. Additionally, cyclic anhydrides have a strong C-C stretching peak from 960 to 880, in Figure 12 this peak fall at 894.

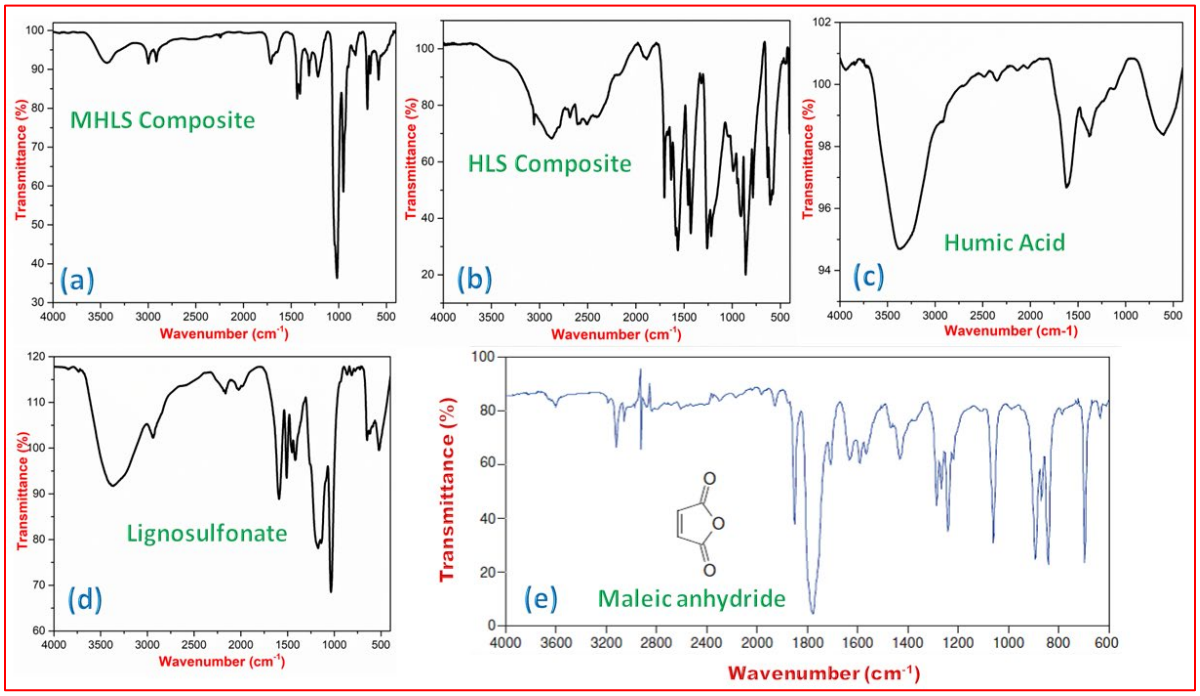

Figure 12. FTIR spectrum of (a) HLMAC (b) HLS (c) Humic acid and (d) Lignosulphonate

4.1.2. TGA-DSC

The pyrolysis behaviour of HLMAC and HLS materials were examined using TGA-DSC at for better understanding the carbonization process of the precursor as indicated in Fig. 13. This material has three prominent weight loss phases across the whole temperature range, implying a multi-decomposition process, according to the TGA curves. The loss of moisture along with easily decomposing chemically active functional groups like carboxyl and weakly bonded compounds makes a sudden initial loss, which is observed at 100 to 200 ºC. Next, the chemically active polar organic functional groups such as NH^{+}, SO_3^{-} interactions and oxygen linkages decomposed thermally at around 200-400 º C would be a second significant loss. The loss of lignosulphonate dopant is the third loss at temperature above 400 ºC. Most of the oxygen-containing groups and rearrangement of the carbonaceous material would decompose in this stage with aromatic

compounds namely phenol, guaiacol or syringol, alkyls such as methane, ethane, ethene, carbon dioxide and carbon monoxide (Zhang. *et. al*. 2015). Few small molecules which contain sulfur and sodium forms a primary carbonaceous structure. The TG profile of the composite is almost similar to the fractions of humic acid as shown in the Fig. 13. Furthermore, previously Campanella and Tomassetti (Campanella *et. al*. 1990) reported that the thermal degradation of humic acid with supporting of FTIR spectroscopy, reveals that there is a significant loss occurred at around 280 ^{o}C, due to the unsaturation and decarboxylation of organic molecules. In addition to that, the decomposition of carboxylic, phenolic, carbonyl and alcoholic groups was observed by Ioselis et al.(1985), at temperature near 300^{o}C. In this thermal analytical condition, there is a possibility to form a new cyclic structure from aromatic structural compounds. These cyclic structures could be obtained in the actual humic acid and its composite by cyclization of aliphatic chains through heat.

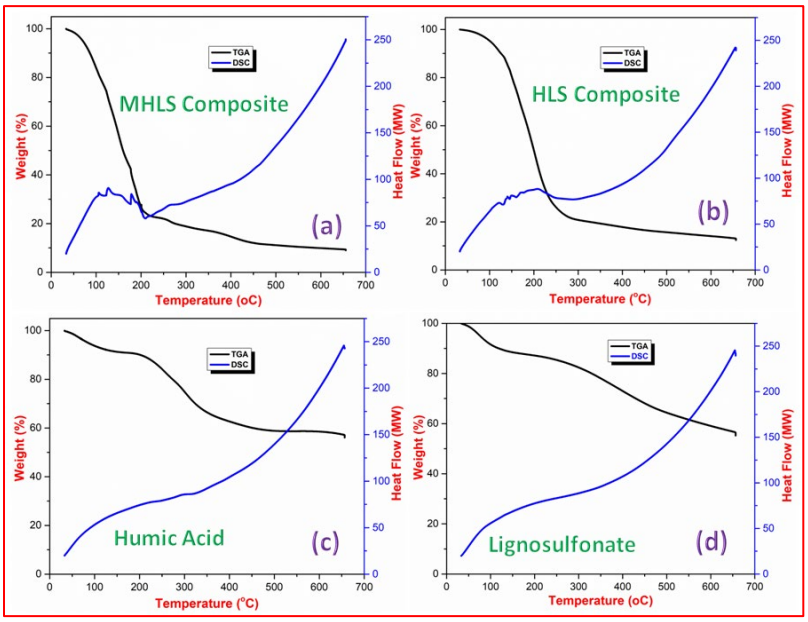

Figure 13. DSC-TGA for (a) HLMAC (b) HLS (c) Humic acid and (d) Lignosulphonate

4.1.3. XRD

XRD analysis of humic acid, lignosulphonate and HLMAC and presented in Fig. 14. In this case, HLMAC replicates mostly the crystalline structure of lignosulphonate's crystalline pattern. The humic lignosulphonate doesn't have any specific crystalline structure of its parent precursors. In the composite, the diffraction peaks found at 4.48, 3.35, 2.58, 2.46 and 1.82^{o} all corresponded to the humic acid as reported in the literature (Naidja. *et.al.* 2002). According to the XRD spectrum, humic acid-containing samples had a broad peak approximately at 22.35-22.70^{o} and several sharp peaks that can be attributed to crystal nature has been shown in Fig. 16. These peaks further confirm that the crystalline nature of humic acid was not disturbed in the newly synthesized composite.

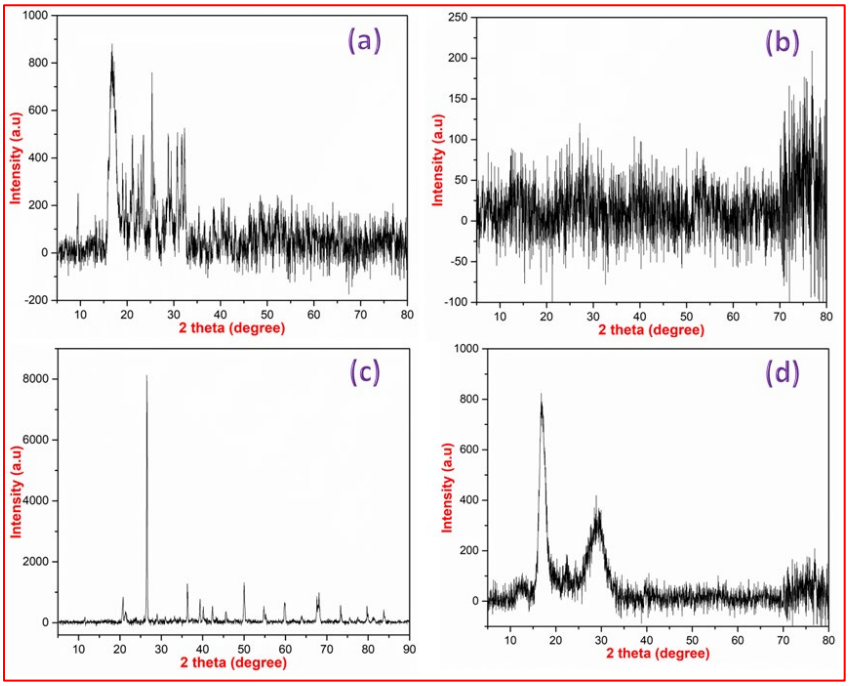

Figure 14. XRD spectrum of (a) HLMAC (b) HLS (c) Humic acid and (d) Lignosulphonate

4.1.4. SEM-EDS

Scanning electron microscopy-Energy dispersive spectroscopy (SEM-EDS) was used to determine the surface morphology and surface characterization of HLMAC as shown in Fig. 15a. It discloses the surface texture and porosity of the composite and features as a significant part in defining the surface accessibility for the adsorption of dyes on the composite. (Dandge *et al.,* 2016) Furthermore, it was noticed that the particles of lignosulphonate appeared as hollow and spherical shapes on the composite of SEM images. The SEM of humic acid shows that the particles were gritty and clumpy with uneven shapes. This indicated that the particles were denser due to the humic acid fractions. (Li *et al*., 2011) The SEM images of the composite show a hierarchical structure when compared to lignosulphonate. The surface area increased with the porosity which is good to increase the number of adsorption sites that improves its adsorption property. Furthermore, the existing macropores are irregularly distributed on its surface of composite which really helps to accommodates azo dye molecules in a way to get great adsorption properties. (Dandge *et al*. 2016, Wu. *et. al*. 2012) In this investigation, the SEM micrographs were recorded in two various magnifications ranges such as 1 micron and 500 nm (Fig. 15a) for getting better understating of surface morphology of the composite. The highlights of the above clearly show that the overall particle size improvement with subsequent densifications in the composite when compared to humic acid spectrum. This is due to the presence of lignosulphonate in the composite. According to the micrographs, it was seen that breakage and agglomeration observed at varying degrees during adsorption. The spherical particles have appeared close to the newly formed smaller particles agglomeration in the resulting composite powder.

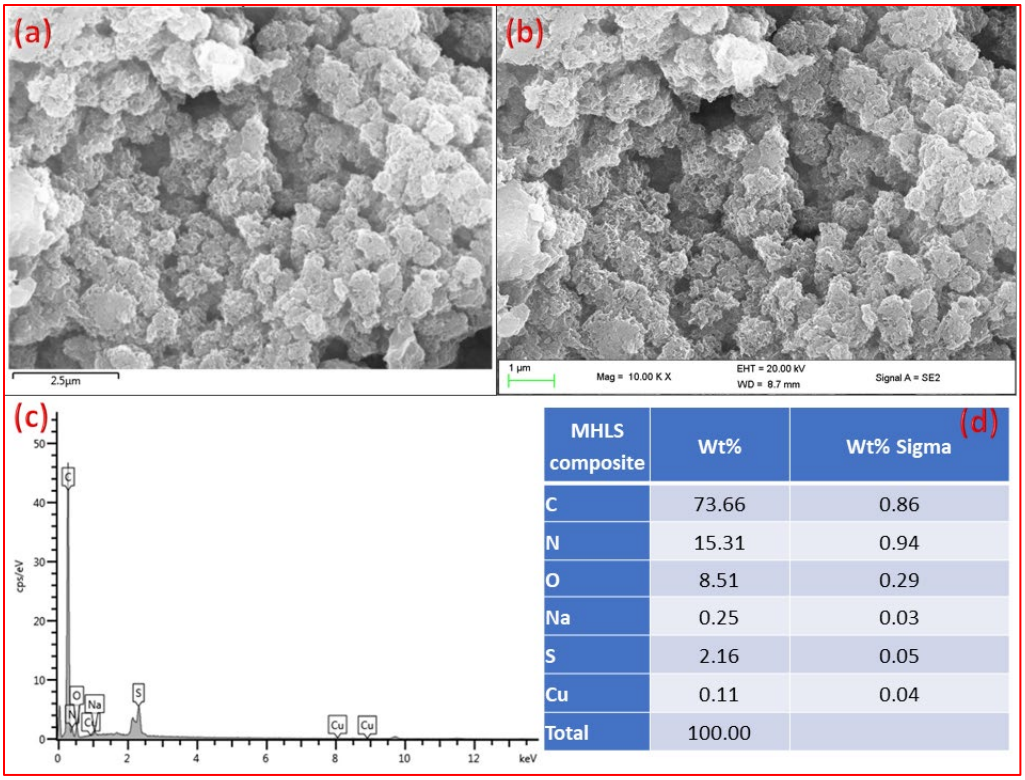

MHLS composite	Wt%	Wt% Sigma
C	73.66	0.86
N	15.31	0.94
O	8.51	0.29
Na	0.25	0.03
S	2.16	0.05
Cu	0.11	0.04
Total	100.00	

Figure 15. SEM morphological and EDS image of HLMAC

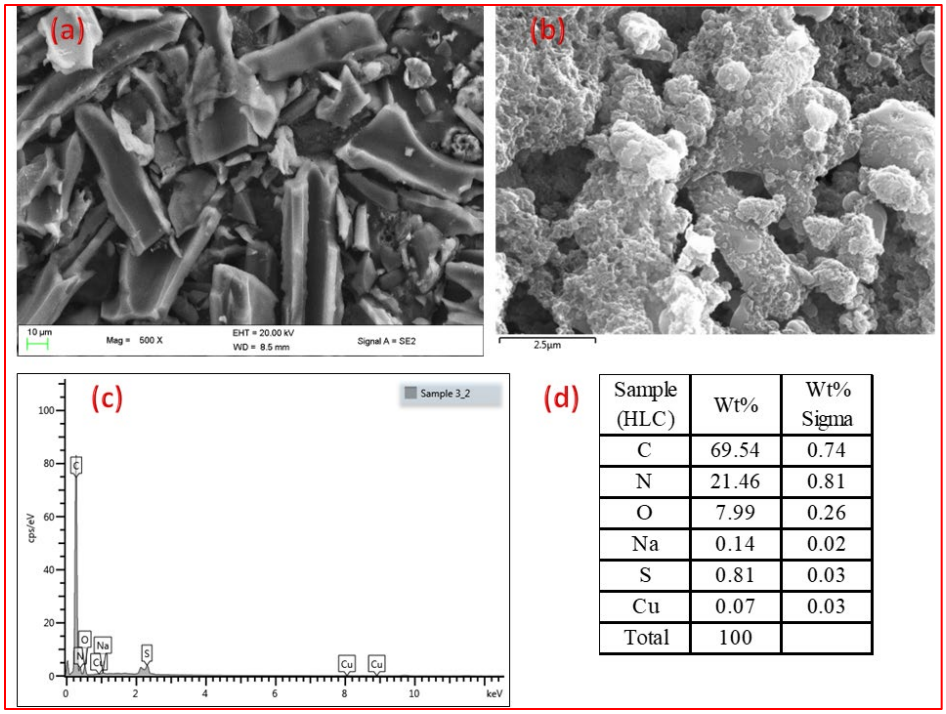

Sample (HLC)	Wt%	Wt% Sigma
C	69.54	0.74
N	21.46	0.81
O	7.99	0.26
Na	0.14	0.02
S	0.81	0.03
Cu	0.07	0.03
Total	100	

Figure 16. SEM morphological and EDS image of HLS composite

4.1.5. TEM

Figure 17 shows the deep morphological properties of prepared material by TEM analysis. After the addition of lignosulphonate to the humic acid, the smooth surface layer became rough and some thin flakes were noticed on the edge, as compared to the structure of pure humic acid (Fig. 17). The color of the final composite is different from the reactant materials color which further confirms the successfulness of the composite synthesis. In addition to that, analysis of EDS clearly explains the elemental presence on the composite as shown in Fig. 17.

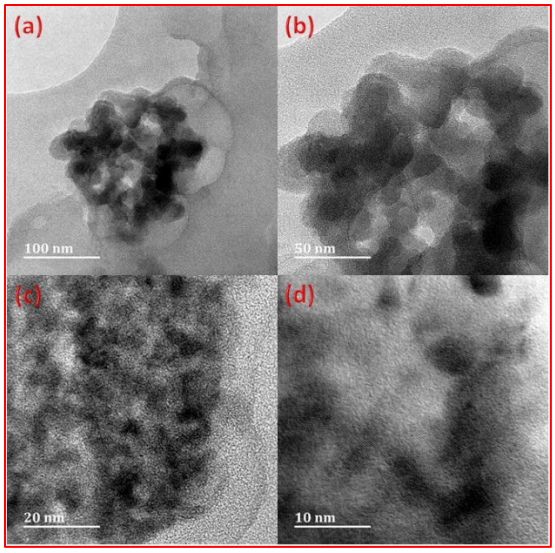

Figure 17. TEM image for HLMAC in various magnification

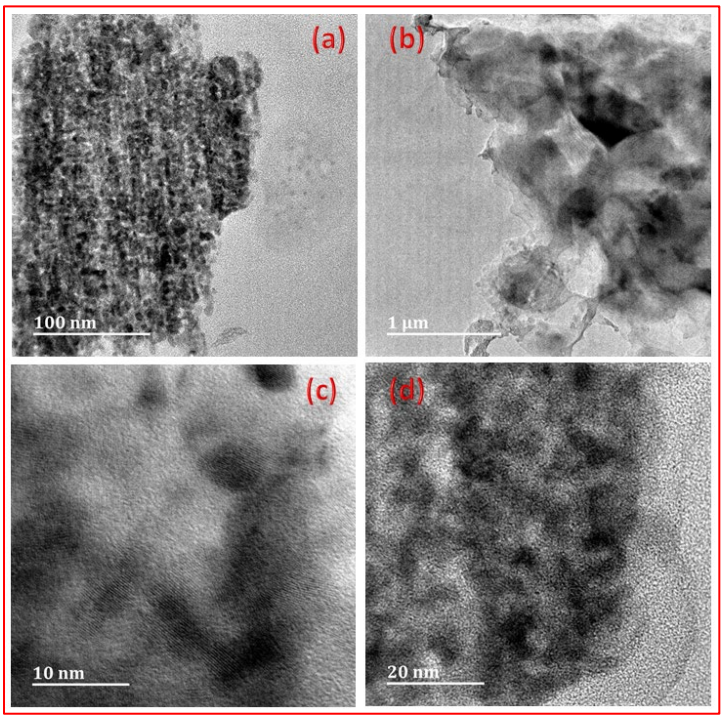

Figure 18. TEM image for HLS composite in different magnification

4.1.6. BET

Nitrogen adsorption-desorption isotherms of HA, LS and HLMAC samples were measured at 77 K using BET (Fig. 19). The resulting composite had a BET surface area of 16.233 m^2g which was greater than HA and LS materials. This suggests that the pollutant molecules may find it easier to reach the composite due to the larger surface area. The N_2 adsorption/desorption investigation reveals that the hybrid humic lignosulphonate material is primarily made up of mesopores with a few micropores and strong interconnectivity. The distribution of pore sizes is centred at 2.5 nm and 7.5 nm shown in figure 19. And the total pore volume is 2.62 cm^3/g. Previous research has demonstrated that lignosulphonate's structural characteristics, particularly its molecular weight and sulfonation degree, have a significant impact on its dispersion property and azo dye reduction effect (Dash. *et al.,* 2010).

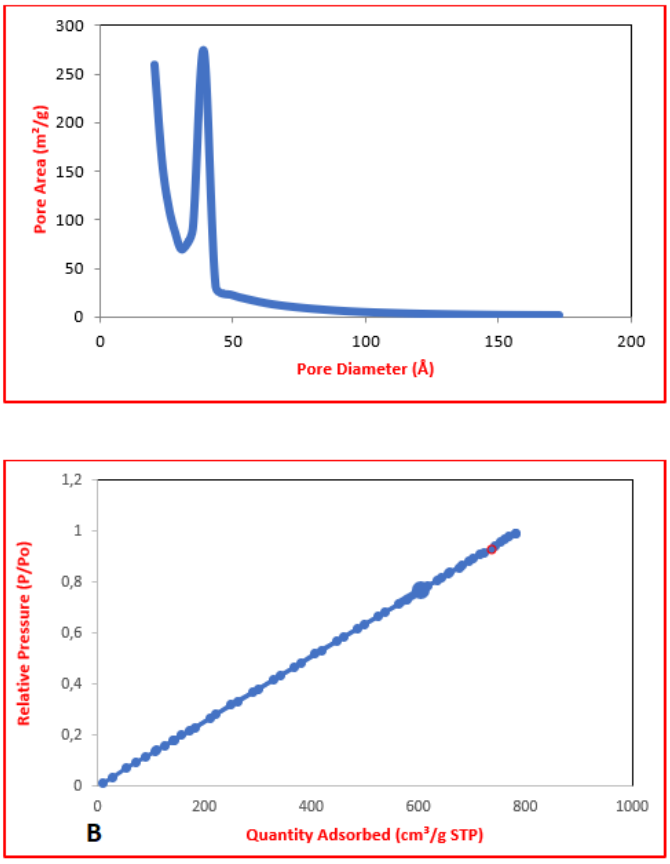

Figure 19. A: Pore size distribution of HLMAC B : Linear isotherm of HLMAC

4.1.7 The calibration curve for the mixed azo dyes

UV-vis spectrometer was used to measure the absorbance of various concentrations such as 20, 40, 60, 80, 100 and 120 ppm of dye solutions. A standard deviation (calibration) curve was plotted from the above as shown in Table 4 and Fig. 20. The equation of the graph was used to calculate the concentrations for the different absorbances.

Table 4. Calibration curve of the azo dues

Concentration (in ppm)	Absorbance		
	Reactive Blue 222	Reactive Red 195	Reactive Yellow 145
20	0.273	0.448	0.425
40	0.364	0.783	0.665
60	0.622	1.227	1.032
80	0.808	1.608	1.36
100	1.309	2.206	1.839
120	1.591	2.638	2.248
R^2	0.9646	0.9954	0.9953
Gradient	0.013	0.0185	0.0219
LOD/ppm	0.273	0.448	0.37
LOQ/ppm	1.591	2.638	2.248

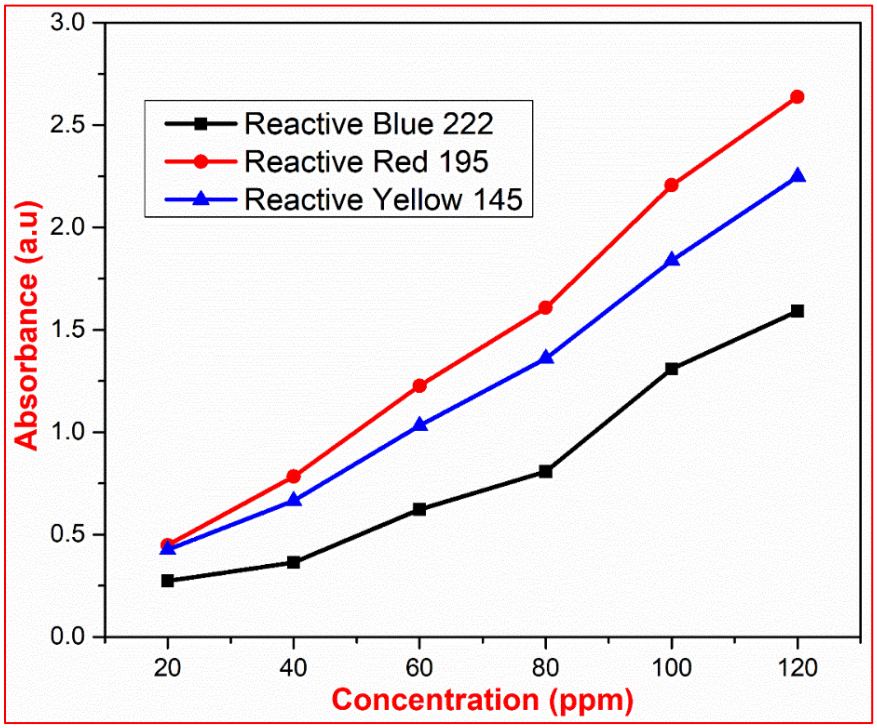

Figure 20. The calibration graph for Reactive Blue 222, Red 195 and Yellow 145

4.2. Effect of pH on adsorption

A study on the effect of pH for dye removal was demonstrated in this investigation. The buffer solution was used to make various pH's ranging from 3 to 11 for the dye solution. Particularly, this composite shows effective adsorption in basic medium specifically in the range from 8 to 11 as shown in Fig. 21-23. This behaviour could be attributed to the changes in the ionic characteristics of the lignosuphonate on the humic acid bulk molecule. The protonation or deprotonation was observed on the surface functional groups under varied pH conditions. Humic lignosulphonate (HLS) composite provide negative surface charge with numerous sulphate and carboxyl groups from lignin and humic acid that dropped, as the pH was lowered. The hydrogen ions in excess competed with methylene blue (MB) molecules (cationic dye) and invaded.

4.2.1. Influence of the various experimental limiting factors

4.2.1.1 Effect of the pH on the mixed azo dyes

Generally, a change in the pH of the solution leads to a change in the surface charge of an adsorbent. It is found that pH is one of the most critical parameters which impact the adsorption process. Six mixed dye solutions of 60 ml each were prepared in separate conical flasks with the dye concentration of 80 mg/L and the initial pH of the dye solution were determined. The series of pH values such as 2.0, 5.0, 7.0, 8.0, 10.0 and 12.0 were prepared using a 1 M solution of HCl or NaOH through a pH meter. The flasks were agitated for 120 min, and then their absorbances of dye were mesured by the UV-vis spectrophotometer. Thus, the amount of the final dye concentration in solutions was calculated and is indicated in Tables 5 to 10.

Table 5. Absorption studies of dye solution at pH 2

Time/minutes	Absorbance			Concentration/Ce (mg\L)			qt=(Co-Ce)/X (mg/g)		
	RR	RB	RY	RR	RB	RY	RR	RB	RY
15	1.375	0.747	1.139	64.61	62.93	63.64	15.39	17.07	16.36
30	1.291	0.728	1.108	60.79	61.5	61.95	19.21	18.5	18.05
45	1.245	0.714	1.084	58.67	60.45	60.7	21.33	19.55	19.3
60	1.132	0.691	1.045	53.53	58.64	58.56	26.47	21.36	21.44
75	1.098	0.686	1.037	51.98	58.27	58.12	28.02	21.73	21.88
90	1.048	0.667	1.004	49.71	56.78	56.36	30.29	23.22	23.64
115	1.011	0.611	0.91	48.02	52.49	51.29	31.98	27.51	28.71

120	0.934	0.577	0.853	44.49	49.88	48.2	35.51	30.12	31.8

Table 6. Absorption studies of dye solution at pH 5

Time/minutes	Absorbance			Concentration/Ce (mg\L)			qt=(Co-Ce)/X (mg/g)		
	RR	RB	RY	RR	RB	RY	RR	RB	RY
15	1.377	0.69	1.074	64.7	58.59	60.12	15.3	21.41	19.88
30	1.293	0.648	1.003	60.88	55.36	56.3	19.12	24.64	23.7
45	1.247	0.625	0.964	58.76	53.56	54.17	21.24	26.44	25.83
60	1.134	0.568	0.868	53.62	49.21	49.02	26.38	30.79	30.98
75	1.1	0.551	0.84	52.07	47.9	47.48	27.93	32.1	32.52
90	1.05	0.526	0.798	49.8	45.98	45.2	30.2	34.02	34.8
115	1.013	0.508	0.766	48.11	44.55	43.51	31.89	35.45	36.49
120	0.936	0.469	0.701	44.58	41.56	39.98	35.42	38.44	40.02

Table 7. Absorption studies of dye solution at pH 7

Time/minutes	Absorbance			Concentration/Ce (mg\L)			qt=(Co-Ce)/X (mg/g)		
	RR	RB	RY	RR	RB	RY	RR	RB	RY
15	1.018	0.508	0.843	48.31	44.59	47.62	31.69	35.41	32.38
30	0.964	0.481	0.797	45.84	42.5	45.15	34.16	37.5	34.85
45	0.939	0.468	0.776	44.69	41.53	44	35.31	38.47	36

60	0.835	0.416	0.688	39.97	37.53	39.27	40.03	42.47	40.73
75	0.73	0.364	0.599	35.18	33.47	34.47	44.82	46.53	45.53
90	0.685	0.341	0.561	33.11	31.72	32.41	46.89	48.28	47.59
115	0.639	0.318	0.523	31.03	29.97	30.33	48.97	50.03	49.67
120	0.407	0.201	0.326	20.42	20.98	19.7	59.58	59.02	60.3

Table 8. Absorption studies of dye solution at pH 8

Time/minutes	Absorbance			Concentration/Ce (mg\L)			qt= (Co-Ce)/X (mg/g)		
	RR	RB	RY	RR	RB	RY	RR	RB	RY
15	0.826	0.523	0.709	39.53	45.69	40.42	40.47	34.31	39.58
30	0.748	0.474	0.643	35.97	41.96	36.86	44.03	38.04	43.14
45	0.696	0.442	0.6	33.6	39.47	34.48	46.4	40.53	45.52
60	0.566	0.361	0.49	27.67	33.26	28.54	52.33	46.74	51.46
75	0.475	0.304	0.413	23.51	28.91	24.38	56.49	51.09	55.62
90	0.423	0.272	0.369	21.14	26.42	22.01	58.86	53.58	57.99
115	0.397	0.256	0.347	19.95	25.18	20.82	60.05	54.82	59.18
120	0.345	0.224	0.303	17.58	22.69	18.44	62.42	57.31	61.56

Table 9. Absorption studies of dye solution at pH 10

Time/minutes	Absorbance			Concentration/Ce (mg\L)			qt=(Co-Ce)/X (mg/g)		
	RR	RB	RY	RR	RB	RY	RR	RB	RY
15	1.055	0.531	0.855	50.01	46.35	48.3	29.99	33.65	31.7
30	1.037	0.522	0.84	49.2	45.67	47.5	30.8	34.33	32.5
45	0.992	0.5	0.802	47.15	43.93	45.44	32.85	36.07	34.56

60	0.88	0.443	0.707	42.01	39.57	40.29	37.99	40.43	39.71
75	0.756	0.381	0.602	36.36	34.79	34.63	43.64	45.21	45.37
90	0.606	0.306	0.476	29.53	29.01	27.79	50.47	50.99	52.21
115	0.323	0.163	0.236	16.6	18.07	14.86	63.4	61.93	65.14
120	0.229	0.116	0.156	12.27	14.4	10.52	67.73	65.6	69.48

Table 10. Absorption studies of dye solution at pH 12

Time/minutes	Absorbance			Concentration/Ce (mg\L)			qt=(Co-Ce)/X (mg/g)		
	RR	RB	RY	RR	RB	RY	RR	RB	RY
15	1.131	0.61	1.026	53.49	52.39	57.51	26.51	27.61	22.49
30	1.078	0.583	0.981	51.07	50.34	55.08	28.93	29.66	24.92
45	1.056	0.572	0.962	50.04	49.47	54.06	29.96	30.53	25.94
60	1.028	0.558	0.939	48.79	48.41	52.81	31.21	31.59	27.19
75	0.98	0.534	0.898	46.59	46.55	50.6	33.41	33.45	29.4
90	0.845	0.466	0.783	40.42	41.33	44.42	39.58	38.67	35.58
115	0.737	0.412	0.692	35.5	37.16	39.5	44.5	42.84	40.5
120	0.586	0.336	0.565	28.6	31.32	32.59	51.4	48.68	47.41

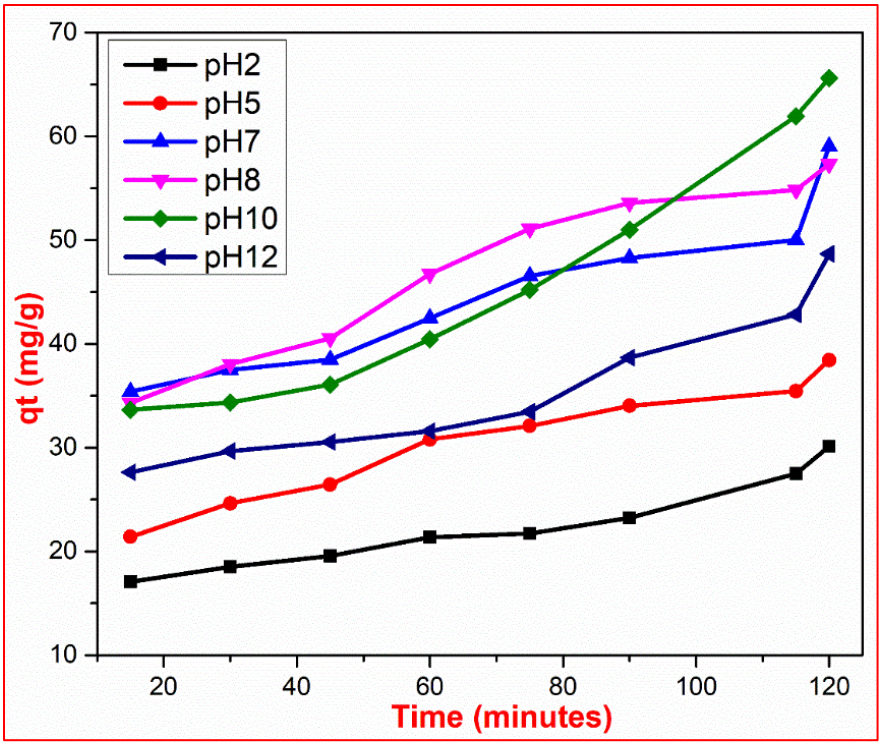

Figure 21. Adsorption studies of reactive blue at pH ranges from 2 to 12

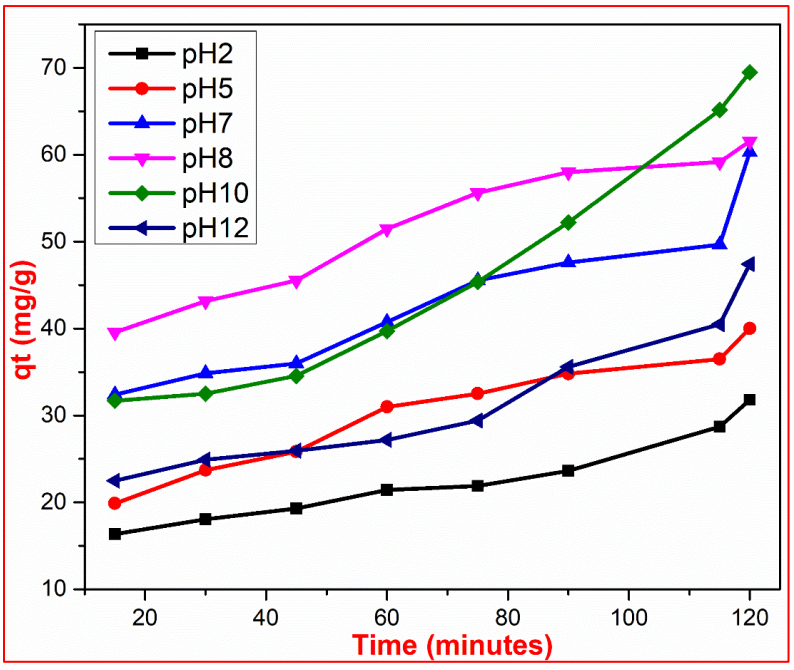

Figure 22. Adsorption studies of reactive yellow at various pH ranges

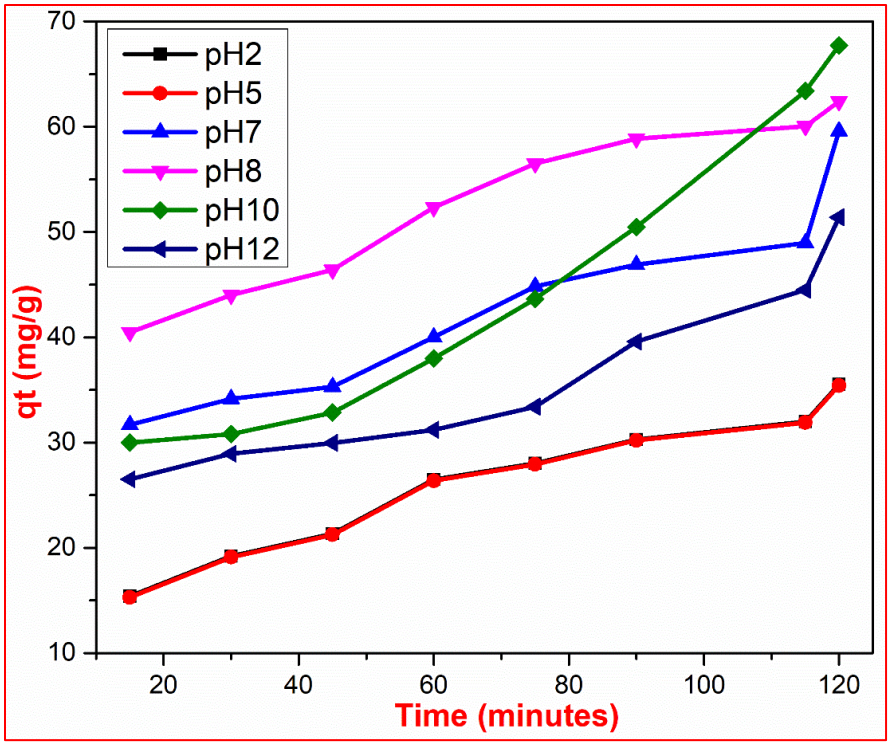

Figure 23. Adsorption studies of reactive red at various pH ranges

4.2.3.2. UV Studies

Removal of the reactive dyes from an aqueous solution using the adsorption process was monitored by UV-vis spectrophotometry at different pH levels. The dye removal efficiency was significantly affected by the pH of the solution, and it depends on the nature of the adsorbate and adsorbent. Several pH ranges including 2.0, 5.0, 7.0, 8.0, 10.0, and 12.0 were studied for azo dye mixtures. At pH 2.0, the dye removal was the lowest. Furthermore, the maximum adsorption was achieved at pH 8, as displayed in Figures 24, 25 and 26. Initially, adsorption increases with increasing pH of the solution until it attains it's maximum; thereafter, it decreases even while further increasing the pH. (Chen. *et. al.,* 2009). More surface charges on the MHLS composite are one of the main reasons for reactive dye molecule adsorption, which can be affected by the pH of the solution. (Anbia. *et. al.,* 201, Mahmoud. *et. al.,* 2012, Kim. *et.al.,* 2001) It was observed that these

investigated dyes appear to be stable in the pH range of 6-8, and the color changes are also obtained in the same pH range. It was also observed that the quantity of adsorption and adsorption capacity increased within the pH range of 7 and 8. Therefore, the charged functional groups on the composites required a pH from 7 to 8 to explore their maximum adsorption for investigated dyes. (Anbia. *et. al.,* 2001, Kim. et.al., 2001) By increasing the pH, more negatively charged functional groups appear on its surface, which helps remove dyes easily in the wastewater system (Shen.*et. al.* 2008). Particularly, hydroxyl and carbonyl functional groups on the surface of the composite play a vital role in the removal of dyes, as found in this study. At the same time, these functional groups get polarised in acidic conditions, which leads to generating electrostatic interactions and weak H-bonding and van der Walls interactions. Furthermore, the investigated combined azo dyes appear as positively charged molecules in acidic conditions; therefore, more electrostatic repulsion occurs, reflecting less adsorption in low pH.

4.2.3.3 Effect of contact time

In this case, the combined dye solution was prepared in the concentration of 80 ppm in a conical flask containing the required amount of composite. These flasks were introduced into the mechanical shaker for times of 15, 30, 45, 60, 75, 90, 105 and 120 minutes. After that, the absorbance through a vis-UV spectrophotometer was determined. The results are shown in Table 11. Fig. 24 shows the graphical representation of time vs qt.

$$qt = (C_o - C_e)/X$$

Where, qt illustrates the amount of dye adsorbed per unit mass of composite (mg/g), C_o is the initial concentration of dye solution and C_e is the final concentration.of dye solution.

Table 11. The effect of time on adsorption

Time/minutes	Absorbance			Concentration/Ce (mg\L)			qt=(Co-Ce)/X (mg/g)		
	RR	RB	RY	RR	RB	RY	RR	RB	RY
15	1.297	0.647	1.168	61.07	55.23	65.2	18.93	24.77	14.8
30	1.153	0.582	1.049	54.47	50.28	58.78	25.53	29.72	21.22
45	1.011	0.518	0.857	47.98	45.37	48.38	32.02	34.63	31.62
60	0.863	0.413	0.734	41.25	37.24	41.73	38.75	42.76	38.27
75	0.719	0.356	0.670	34.65	32.86	38.27	45.35	47.14	41.73
90	0.575	0.280	0.476	28.08	27.01	27.82	51.92	52.99	52.18
115	0.413	0.142	0.263	20.71	16.41	16.32	59.29	63.59	63.68
120	0.282	0.100	0.203	14.72	13.18	13.04	65.28	66.82	66.96

Fig. 24 shows the influence of time duration on the adsorption of dyes. In reactive red and yellow dyes, the early stage of the adsorption seems to be very fast and slowing down to reach their saturation. However, the dye concentration does not change after 120 minutes (Fig. 24). This reveals that either equilibrium was attained after 120 minutes, or all dye molecules have been adsorbed by composite.

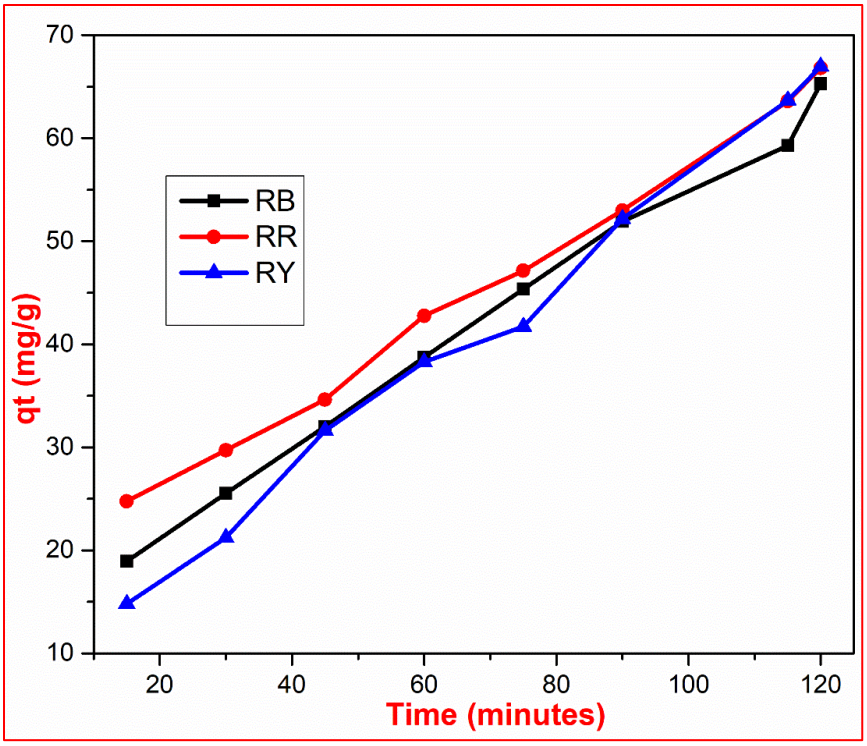

Figure 24. The effect of time on adsorption

4.2.3.4 Effect of concentration on adsorption

This study determines the adsorption capacity of MHLS composite at pH 8 and ambient temperature. It was observed (Fig. 25, 26 and 27) that the adsorption progression of reactive blue was affected by its initial concentration. A significant amount of dye has been adsorbed at high concentrations. In addition, a wide range of adsorption capacity was obtained amongst the three - dyes combined solutions. A concentration gradient has produced the layer near the interface of the adsorbent due to probably a concentration plunge at high concentration. This could have occurred due to the mass transfer of combined dyes to the HLMAC interface (Brigatti et.al., 2000).

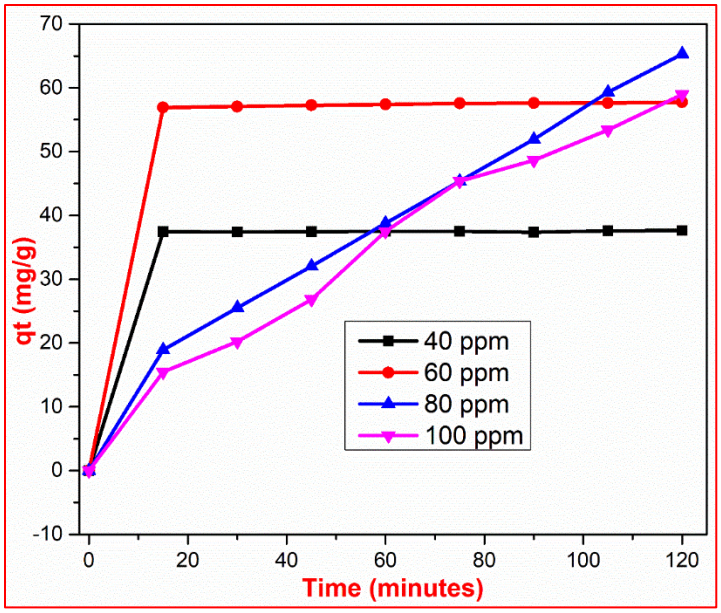

Figure 25. Adsorption of reactive red at various concentrations

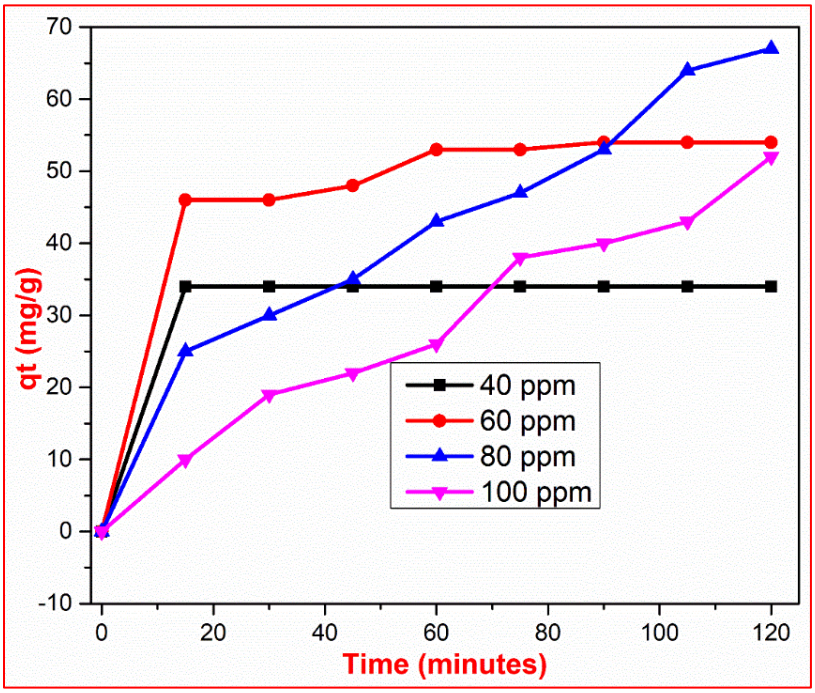

Figure 26. Adsorption of reactive blue at the concentration of 40, 60, 80 and 100 ppm.

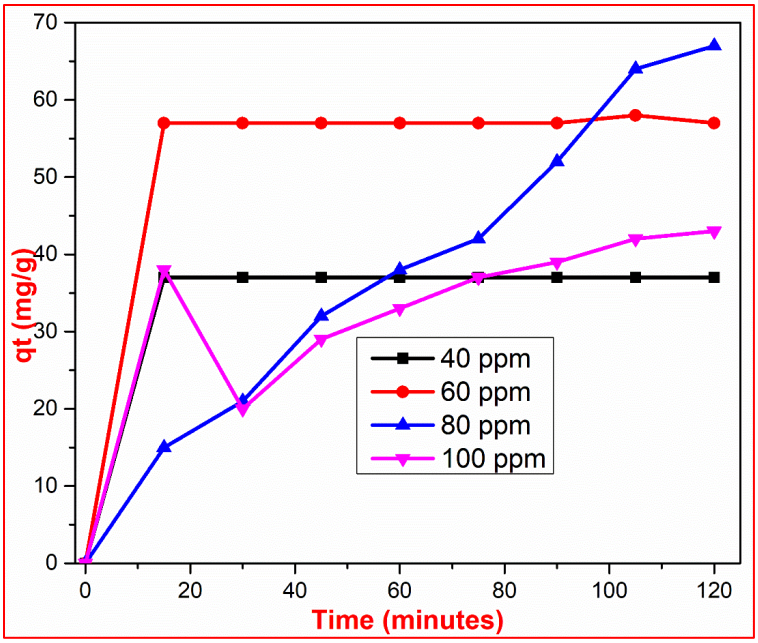

Figure 27. Adsorption of reactive yellow at the concentration of 40, 60, 80 and 100 ppm

4.2.3.5 The effect of dosage

The objective was to determine the optimum dosage of HLMAC required to adsorb 80.0 mg/L dye solution. A series of doses such as 0.5, 1.0, 1.5 and 2 g were used to optimize the quantity required. All these doses were applied to the dye solution at constant stirring for 2 hours, and thereafter their absorbance values were measured using UV-vis spectroscopy. Fig. 28-30 shows that higher dosages of HLMAC adsorb a more significant number of dye molecules. In this case, the dyes 195 reactive red and 145 reactive yellow were completely adsorbed at the dosage of 1.5 g and above of MHLS composite, while dye 222 reactive blue was adsorbed at an even lower dose due to its available adsorption sites being adequate. Adsorption is influenced by the availability and number of adsorption sites necessary to complete the adsorption process. Therefore, increasing the dosage of the composites leads to generating more available adsorption sites due to increasing the surface

area of the composite. From this study, the optimum dosage of adsorbent was 1.5 g for the adsorption of 80 ppm concentrated dye solution

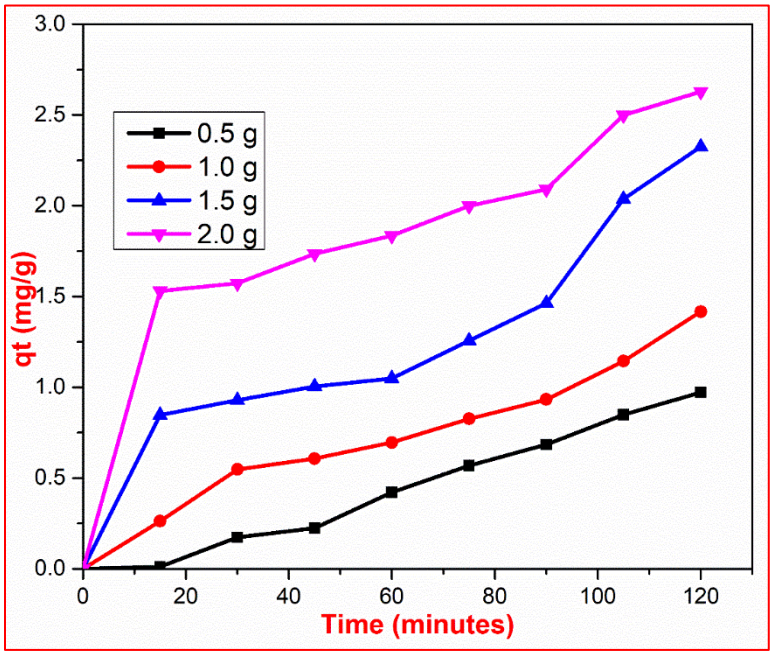

Figure 28. Adsorption of reactive red at various dosages of HLMAC

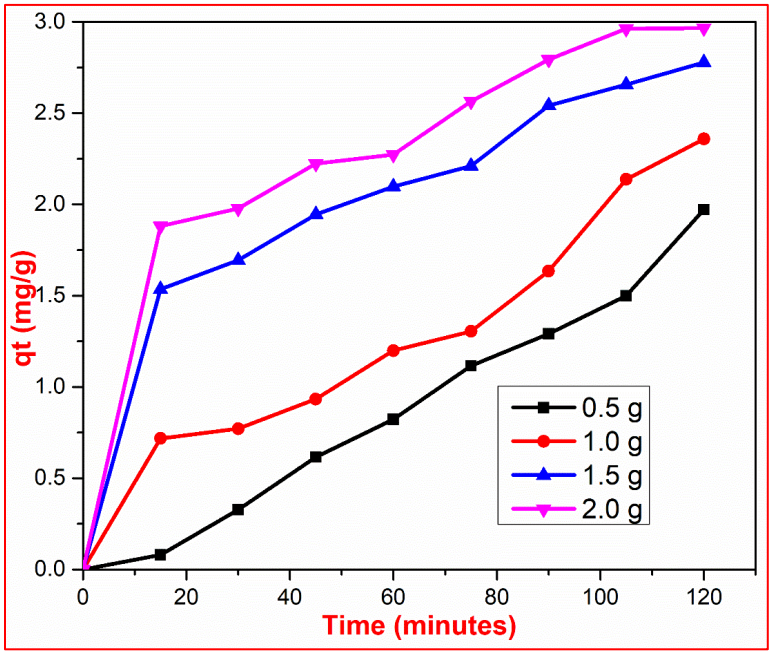

Figure 29. Adsorption of reactive blue at various dosages of HLMAC

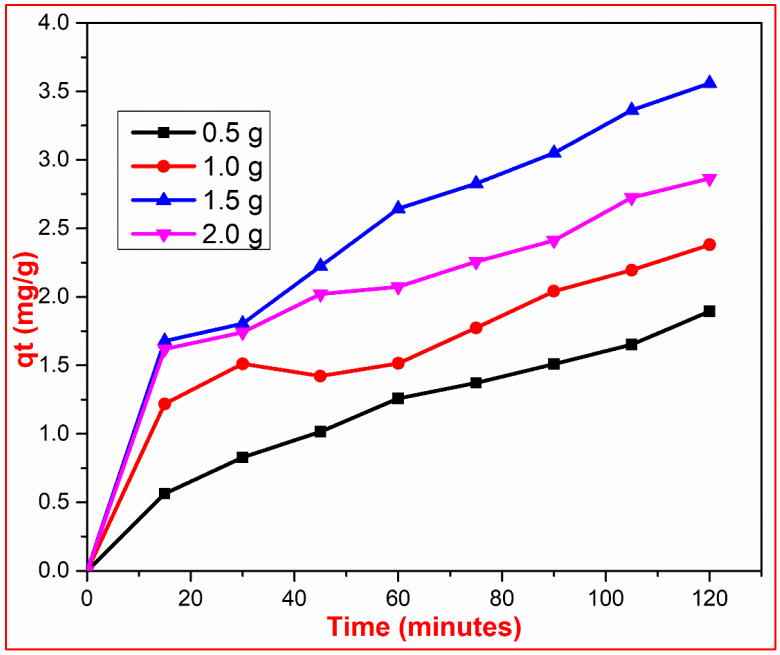

Figure 30. Adsorption of reactive yellow at various dosages of HLMAC

4.2.3.6 Adsorption kinetics

The degree of adsorption concerning contact time was monitored to study the kinetic behaviour of the adsorbent towards dyes and the time profiles as shown in Figure 28-30. Almost, all three dyes showed rapid adsorption; a 30 minute contact period provided around 73 percent adsorption, while equilibrium was reached in about 120 minutes. The number of dyes adsorbed didn't change appreciably over the time after this period. The quick adsorption of dyes onto HLMAC could imply that the majority of the adsorbent's reactive sites are open to dye interaction. The time that takes to reach equilibrium is unaffected by the initial concentrations. The dye adsorption time profile is a smooth, single and continuous curve that leads to saturation, implying probably monolayer adsorption of dyes on the surface of adsorbent.

Owing to the bulkier organic molecular network of composite and the swelling nature of humic acid consequently its network is adequately stretched to facilitate dyes diffusion. This enlarged

network of the adsorbent is more suitable for the interaction between the active functional sites and the highly promising adsorption sites of carboxylic groups on the adsorbent surfaces. The highlights of the above show that there is a complexation reaction observed between HA from the adsorbent surface and dye molecules because usually, these complexation reactions are very fast which would be shown by complexation studies of HA with metal ions.

4.2.3.7 Adsorption isotherm

The relationship between the concentration of reactive dyes and the adsorbed quantity at the interface as well as the adsorbed quantity is a measure of the adsorption processes equilibrium position, and it can be described using one or more isotherm models. The quantitative determination of the adsorption capacity or amount of adsorbent required for adsorption of reactive dyes from wastewater has been interpreted by only the adsorption data via theoretical or empirical equations. The adsorption of the dyes was dependent on the concentration of adsorbent. From adsorption data, the amount of Reactive Red, Reactive Blue and Reactive Yellow increased from 20 - 40, 15 - 45, and 30 - 78 ppm, respectively. Since adsorption is a surface phenomenon, the nature and strength of interactions between an adsorbate and an adsorbent is essential interaction an adsorbate functional groups and functional group on the surface of the adsorption. The adsorption mechanisms can be either chemisorption (covalent or ionic bond formation) or physisorption (hydrogen bonding or Van der Waal interaction, size exclusion etc). One of the scaffold common amongst the three dyes is the chlorotriazine group. The most likely possibility is that the dyes can form covalent bond through the chlorotriazine group with surface hydroxyl group on the adsorbent. However, repulsion interaction is also expected by sulphonate groups of the dyes and those on the adsorbents. The net interaction will therefore be a compromise among the reinforcing and competing forces. This study shows that the experimental data were satisfactorily

correlated by the non-linear forms of Freundlich and Dubinin-Readushkevich adsorption isotherm equations.

$$q_e = \frac{Q^0 b C_e}{1+bC_e} \quad (3)$$

$$q_e = K_F C_e^{1/n} \quad (4)$$

$$q_e = q_m(\varepsilon^2)^{-\beta} \quad (5)$$

Where q_e is the amount of reactive dye adsorbed at equilibrium over the mass of adsorbent material (mg g^{-1}) and C_e is the equilibrium concentration (mg L^{-1}) of the adsorbate. Langmuir constants related to the monolayer adsorption capacity (ma g^{-1}) and energy or intensity of adsorption (Lmg^{-1}) be consistent with units and the way you write them in the thesis was represented as Q_0 and b. The results are shown below in Figure 31, and all fit a straight with R approximately to 1. The adsorption curves are single smooth and continuous a plateau. The adsorption data fitted the Langmuir adsorption isotherm thereby illustrating that monolayer adsorption occurred. This adsorption linear isotherm predicts that adsorption of adsorbate on the adsorbent surface is a linearity function herweby the changing of dependent and independent variable is linear.

The non-linear optimization method was used to get the detailed analysis of correlations for these isotherms of reactive dyes. The three isotherm equations adequately describe the adsorption data but the best fit is to the Langmuir model, from which we can assume that adsorption of several reactive dyes would not take place beyond a monolayer coverage and all adsorption sites are equivalent with uniform energies of adsorption without any interaction between the adsorbed molecules. Also a comparison between the theoretical Langmuir, Freundlich and Dubinin-Readushkevich isotherms were made The resulting parameters for all three isotherms are tabulated in Table 2. As shown, Q_0 is indicative of adsorption capacity changes. Similar results are also reported by earlier workers. The Freundlich exponent 1/n indicates the favorability of adsorption.

Values of 1/n<1.0 represent favourable adsorption conditions. The values of 1/n obtained in the present study for all the three metal ions are less than unity, indicating the favourable adsorption of numerous dyes onto composites. The value of D-R constant is related to the adsorption free energy E (kJ mol^{-1}), which is defined as the free energy change required to transfer 1 mol of ions from the solution to the solid surface. From the equation E = (2ˇ)-1/2 can be used to calculate E. The class of adsorption reaction would be determined through the magnitude of E. The adsorption energy of physisorption and chemisorption processes are in the range of 1-8 kJ mol^{-1} and 20-40 kJ mol^{-1} respectively. In contrast, ion exchange can be used to explain adsorption, when the value of E would observe in between 8.0 and 16.0 kJ mol^{-1}. The derived values of E for investigated dyes onto humic lignosulphonate could be in the range between 7 to 8 kJ sol^{-1}. This indicates mainly an ion exchange reaction, which exposes that the adsorption of dyes onto the composite mostly proceeds by binding surface functional groups as stated earlier.

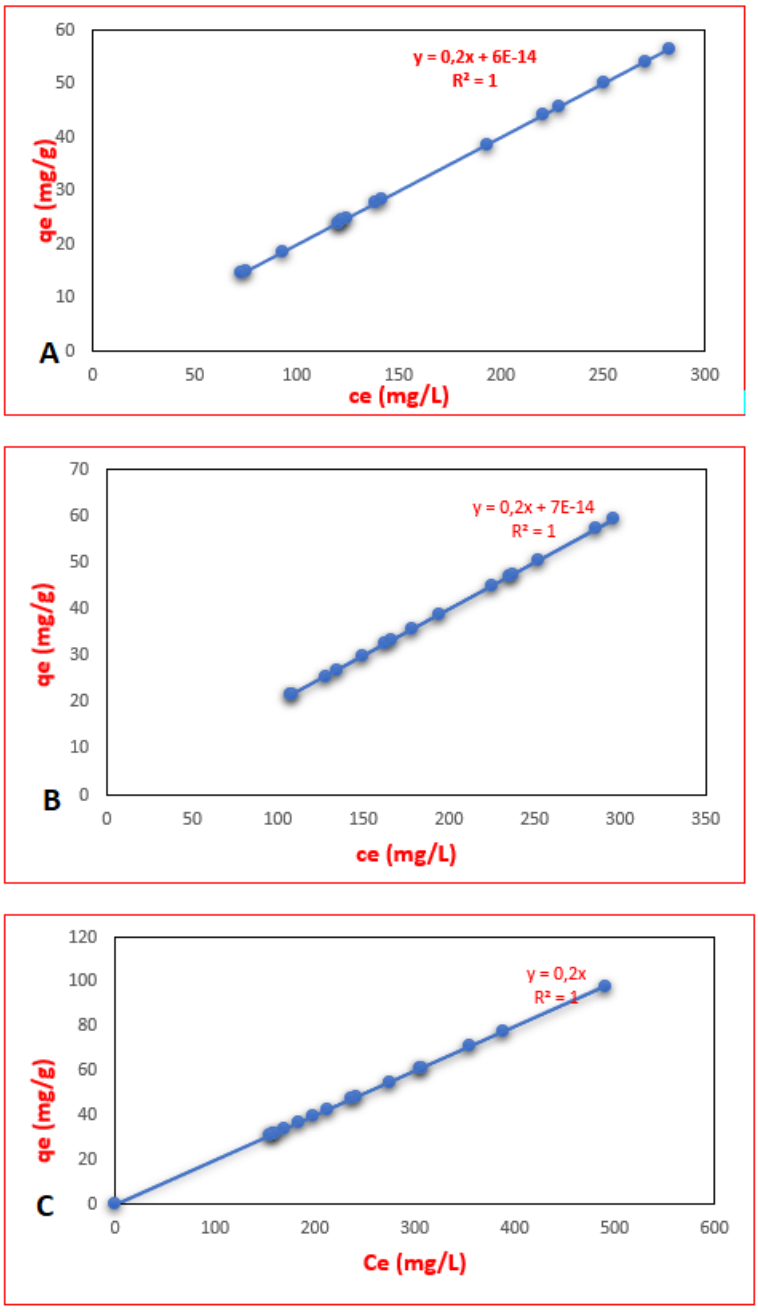

Figure 31. Fitting experimental data for A) 80ppm RR on MHLS on Langmuir model B) 80ppm RR on MHLS on Langmuir model C) 80ppm RR on MHLS on Langmuir model

PART B

In the second synthetic part of the study, we focused on the synthesis of humic acid -based kraft liquor composite (HKLC) which was a one-step reaction. Herein, we used kraft lignin (waste black material from the Kraft Process) and humic acid in the presence of sulphuric acid. One of the expected bonds was the ester linkage.

4.3. Characterization of humic acid -based kraft liquor composite

4.3.1. FTIR

FTIR analysis was used to identify the functional groups present in HKLC, as shown in Fig. 32. The broad absorption at 3452 cm^{-1} is the -OH stretching vibration of aromatic and aliphatic parts. The peak at 2940 cm^{-1} is the stretching vibration of C-H bands for aromatic or methylene groups of the side chains. The aromatic ring containing the -C=C- stretching vibration band is 1657 cm^{-1}. The peak at 1432 cm^{-1} is the symmetric bending -O-CH_3. In the HKLC spectrum, the linkages of α-O-4 and β-O-4 in the composite showed stretching of C-O-C at 1264 cm^{-1}. (Zhuang. et., al. 2000) The characteristic C-O stretching of carbohydrate material gives absorption at 1071 cm^{-1}. (Mija. et. al. 2017) The following functional groups correspond -OH (H-bonded), -C-H, conjugated -C=O, aromatic -C-H bending vibration C-C, C-O stretching, and polyphenyl group stretching to 3373, 2928, 1618, 1377, 1247, 1132 and 612 cm^{-1}, respectively. The majority of aromatic peaks might be obtained from the HA component. In comparing both spectra, similar functional groups like -OH stretch, C=O, C-C, aromatic and -C-H (Fig. 31). At 3600-3300 cm^{-1}, alcoholic (-OH) and free phenolic groups are observed in all HA, KL, and composite materials. Broadbands emerge in all humic and kraft liquor in 3400-3200 cm^{-1}, indicating H bridges stretching -COOH and -OH of phenolic groups. Several bands with various strengths were also present in the fingerprint area from (1900-800) cm^{-1}, indicating the new unique composite. In the spectrum of HA, there was a

low-intensity absorption at 1623 cm^{-1} corresponding to conjugated C=O stretch: it was observed in HKLC at 1714 cm^{-1}. This observation suggests that the carbonyl group might be from the conjugated carboxyl group.

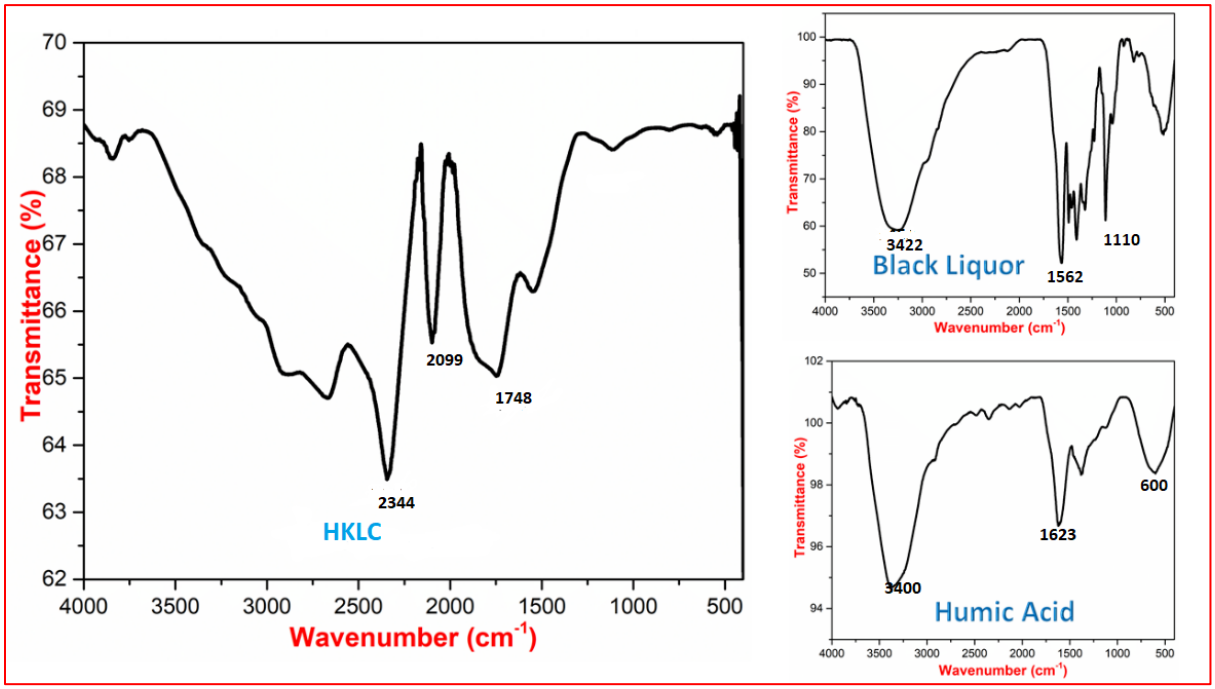

Figure 32. FTIR Spectrum of humic acid, kraft liquor and HKLC

4.3.2. XRD

The XRD pattern of HKLC is shown in Fig. 33, with reflection peaks indexed using Joint Committee on Powder Diffraction Standards (JCPDS) cards. According to JCPDS, the XRD profile showed sharp and intense peaks between 30 and 40 degrees, followed by additional less intense peaks, all attributable to humic acid with the monoclinic crystalline structure. Fig. 33 shows the results of the XRD analysis of humic acid and HKLC. Both humic acid and composites have nearly the same diffraction pattern, with no notable differences, indicating that their crystallinity has not changed. Diffraction peaks at 4.48, 3.35, 2.58, 2.46 and 1.82 were detected in the composite, all of which correlate to humic acid as reported in the literature.

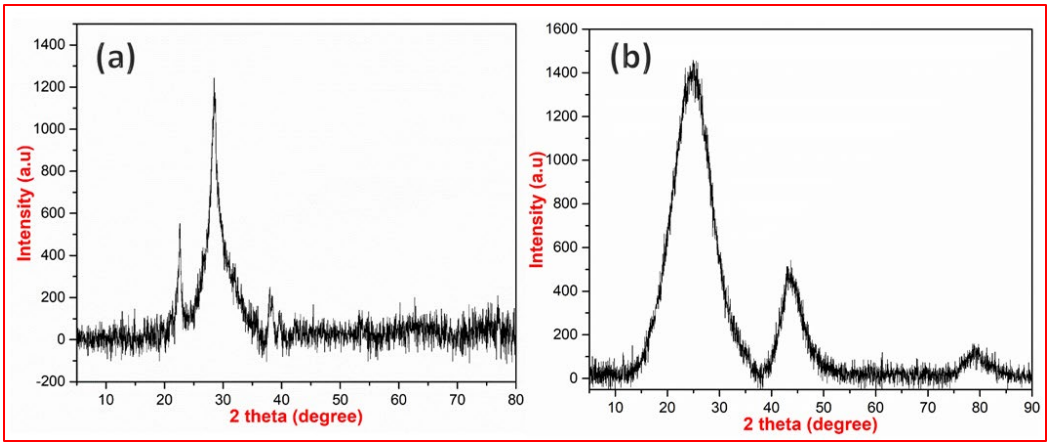

Figure 33. XRD for Kraft Lignin (a) and HKLC (b)

4.3.3. TGA-DSC

TGA and DSC of HKLC were used to gather more information about its thermal behavior and stability at high temperatures (Fig. 34). According to the TGA curves, this material shows three distinct weight loss phases across the temperature range implying a multi-decomposition process. Initially, around at 100ºC there is a slight dip due to water evaporation. The second substantial loss would be the thermal decomposition of chemically active polar organic functional groups such as NH^{+}, SO_3^{-} interactions, and oxygen linkages at roughly (200-400) ^{o} C. Finally, the third weight loss was observed at above 400 ^{o} C due to the loss of specific functional groups of lignin in kraft liquor. Also, weakly bonded compounds, including oxygenated groups and rearranged carbonaceous materials, would decompose into aromatic compounds such as phenol, guaiacol or syringol, alkyls such as methane, ethane, carbon dioxide and carbon monoxide.

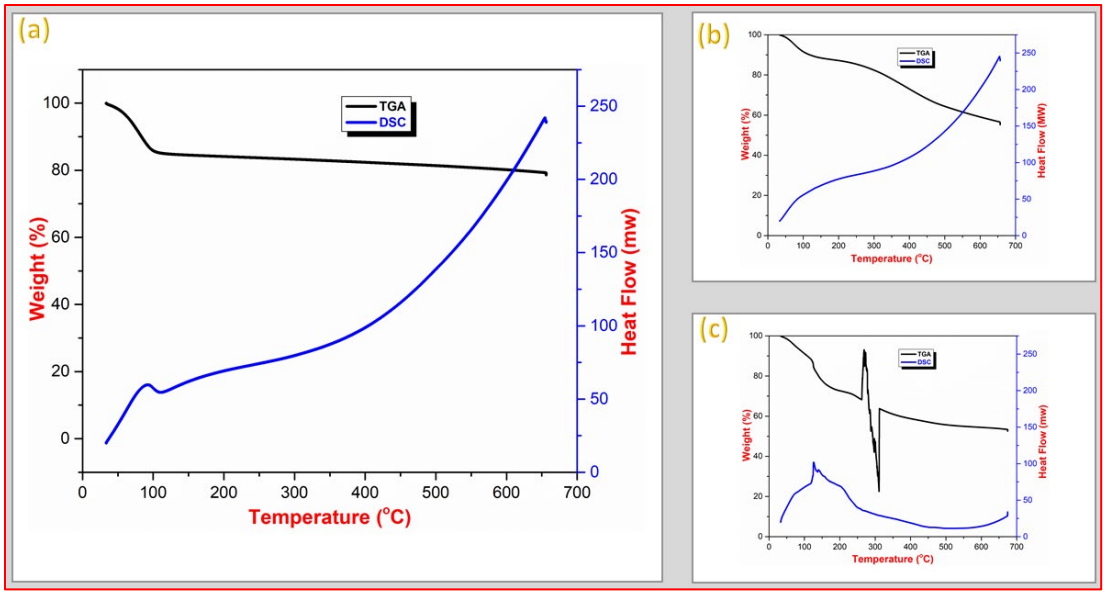

Figure 34. TGA and DSC for HKLC

4.3.4. SEM-EDS

SEM (Fig. 35) was used to determine the surface morphology and elements present on the surface. Particles of an average size of 20-35 nm are observed on the sample's surface. The porosity and surface texture of the composite is vital to understanding the surface accessibility of the composite for dye adsorption reported by Dandge et al (2016). SEM images shows that the humic acid particles were gritty and clumpy, with irregular appearances. Li et al. (2011) reported that the structured composite was denser due to humic acid's fraction. The improved surface area with consistent porosity helps increase the adsorption sites and overall properties of adsorption. Therefore, these adsorption sites easily accommodate the nitro molecules onto their surface micropores. This study has recorded SEM micrographs in two different magnification ranges, such as 1 micron and 500 nm, as shown in Fig. 35. The unshaped particles in HKLC appeared near the newly produced smaller agglomerated particle. Compared to the structure of raw humic acid, the smooth surface layer became rough, and some thin flakes were seen on the edge after the successful

addition of kraft lignin into humic acid, as shown in Fig. 35. Additionally, the EDS spectrum identifies the elements present on the composite.

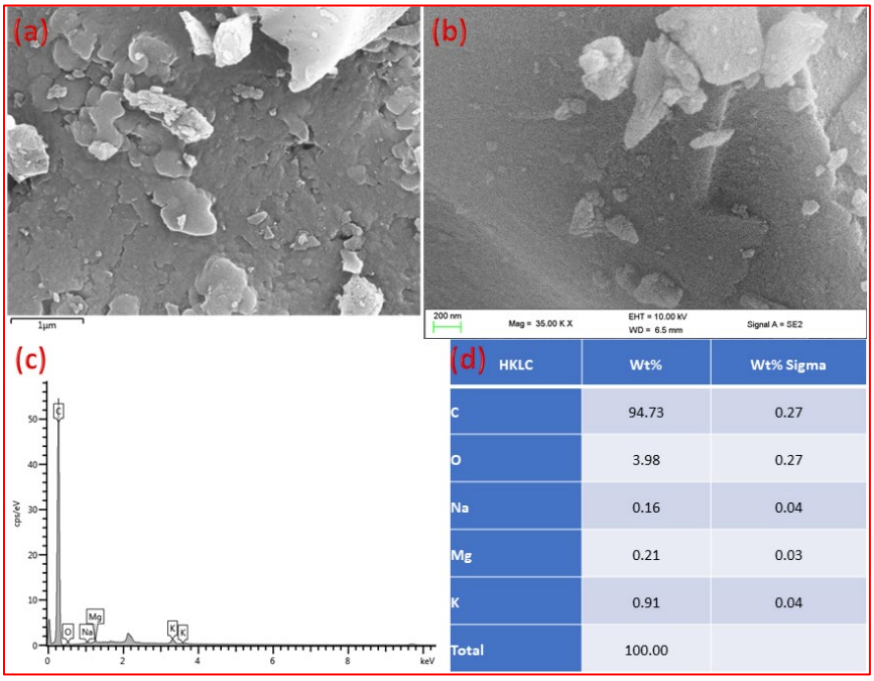

Figure 35. SEM and EDS for HKLC

4.3.5. TEM

The detailed morphology of the composite was illustrated by TEM analysis, as shown in Fig. 36. This composite looks like a resin due to the significant quantity of kraft liquor. Also, the addition of humic acid into kraft liquor makes the resin surface rougher. This is a different texture compared with the nature of humic acid. The color of the composite material is greyish black. The rough surface of the composite nature helps enhance the catalytic activity of the material.

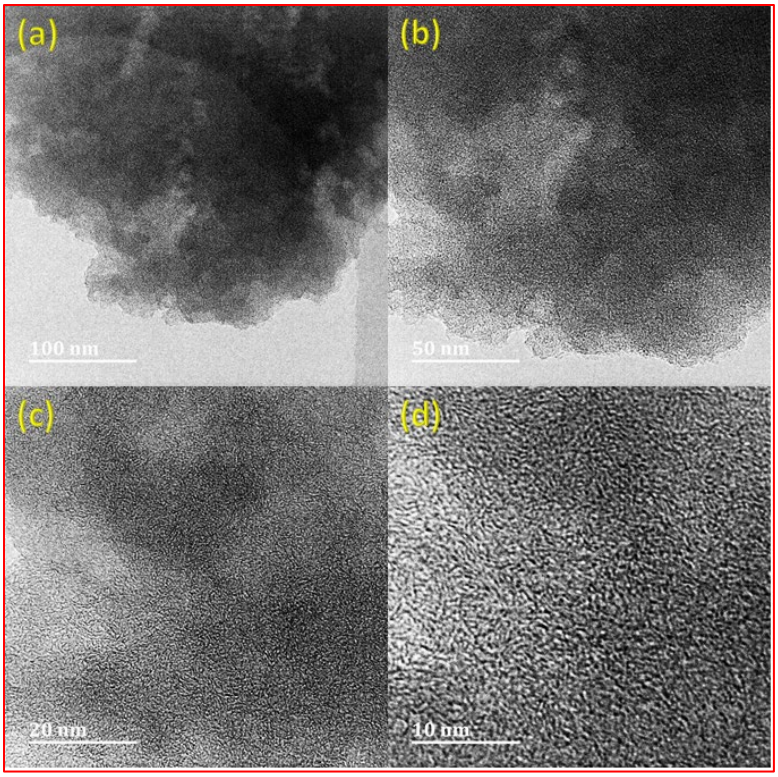

Figure 36. TEM analysis of HKLC

4.3.6. BET Surface area analysis

Nitrogen adsorption-desorption isotherms of HA, kraft liquor and HKLC were inspected at 77 K. The BET surface area of the resulting composite has a greater surface area (16.23 m^2/g) compared to humic acid and kraft liquor. Due to this large surface area, the nitroaromatics molecules may find it easier to reach the composite. The N_2 adsorption/desorption investigation reveals that HKLC material comprises mesopores with a few micropores and strong interconnectivity. The distribution of pore sizes is centered at 2.5 nm and 7.5 nm, while the total pore volume is 2.62 cm^3/g. Previous research has demonstrated that sulfonate's structural characteristics, specifically its molecular weight and sulfonation degree, significantly impact its dispersion property and dye reduction effect.

4.4. Reduction of nitro aniline compounds and dyes using kraft lignin composite

This study was conducted on various nitro anilines and some selected dyes. The objective was to ascertain the catalytic activity of HKLC in reducing some selected small molecules. Therefore, UV-visible spectroscopy coupled with visual observation was the technique of choice. In this study, several nitro anilines, namely 2-NA, 3-NA, 4-NA and 4-nitro-2, 3-diamine, and Methylene blue and Allura red, were investigated with catalytic amounts of HKLC. NaBH4 was used to initiate this reduction process; the new catalyst played an essential part in completing the reaction. Reactions were performed in an aqueous medium at room temperature.

The characteristic 2 absorption peaks for 2-NA, 3-NA, 4-NA and 4-nitro-2, 3-diamine were observed at λmax 410 nm and 240 nm, 360 nm and 300 nm, 380 nm and 240 nm, 410 nm and 240 nm, respectively. Also, the characteristic adsorption of Methylene Blue was observed at λmax 220, 280 and 310 nm while Congo red, Reactive Yellow and Allura Red showed absorption at 250 and 500 nm, 220 and 420 nm and 310 and 500 nm, respectively. Figures 37-44 show the absorption decrease when the reaction time was increased. This observation indicates the composite catalyzed the reduction of the nitro group to most probably the amino functional group. The research that was reported by Saloglua et., al. 2021 and Li. et., al. 2021 obtained a similar result. Alhaji. et., al. 2021 used FTIR to validate the reduction reaction: the absorption at 1400 and 1643 cm-1 for the nitro group disappeared, and the appearance of absorption at 3460 cm-1 suggested the amino group. Due to the high concentration of nitroaromatics, some UV spectrum was split at the top of the area, thus, it further explains the catalytic activity of the composite. The synthesized new nanocomposite was explained for the reduction process in terms of reduction of nitroarenes to amino compounds. Although the FTIR peaks at 1400 and 1643 cm^{-1} of the nitro compound were

reduced and the additional peak at 3460 cm^{-1} for the amino group was increased significantly, this has confirmed that the reduction reaction was done successfully. (Alhayali. et., al. 2021)

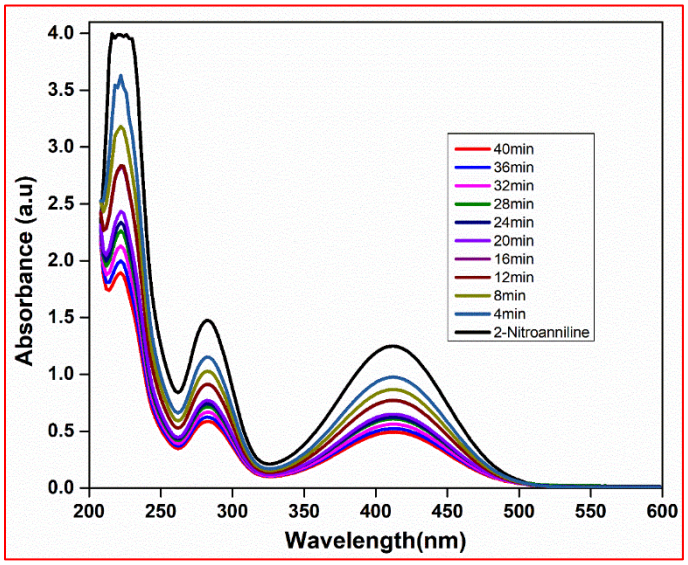

Figure 37. Reduction of 2-nitroaniline

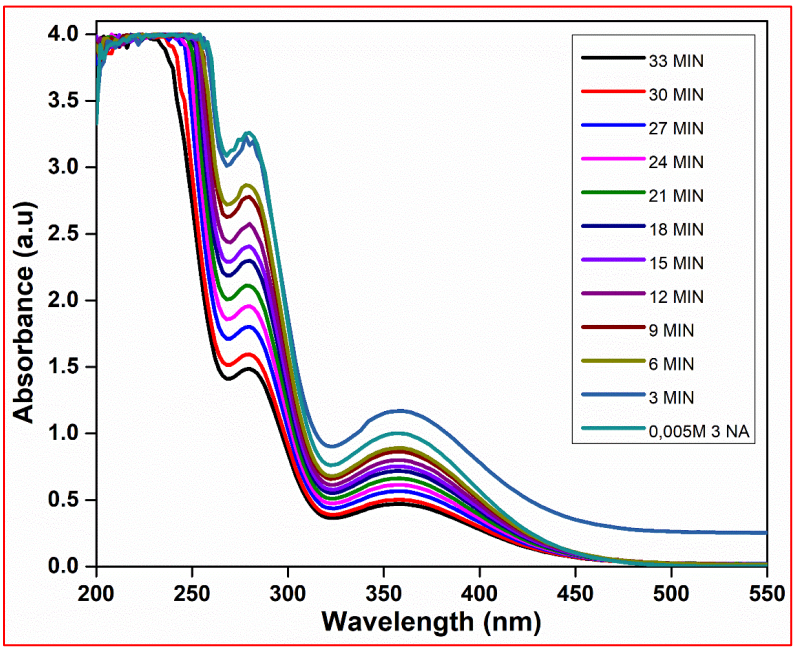

Figure 38. Reduction of 3-nitroaniline

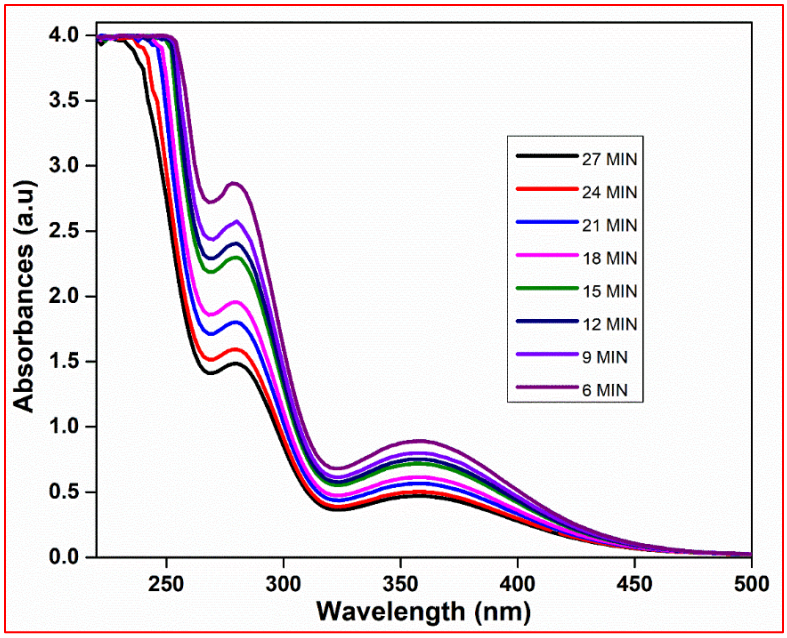

Figure 39. Reduction of 4-Nitroaniline

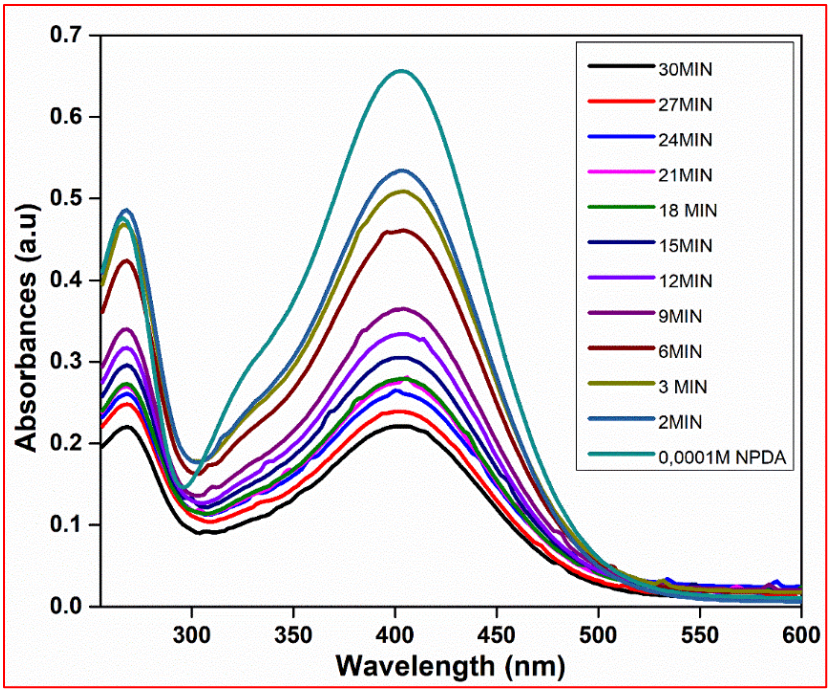

Figure 40. Reduction of NPDA

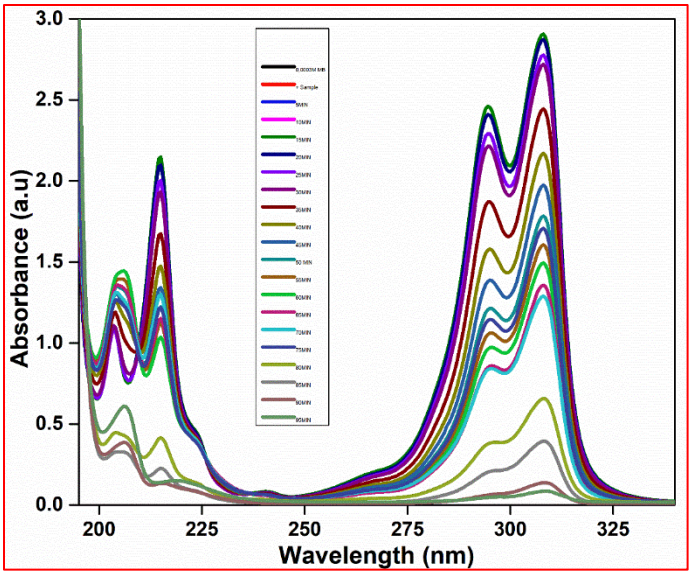

Figure 41. Reduction of Methylene Blue

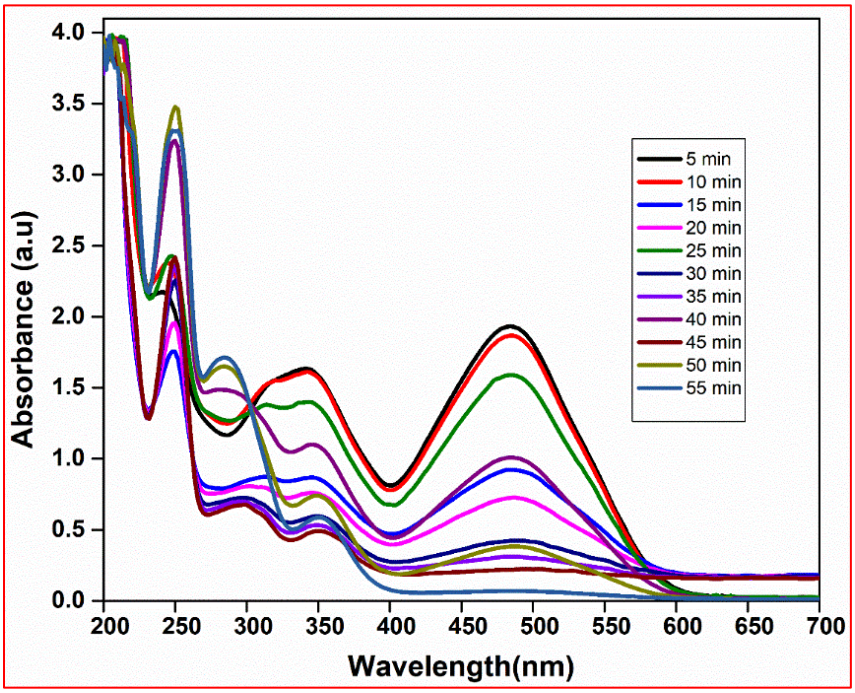

Figure 42. Reduction of Congo Red

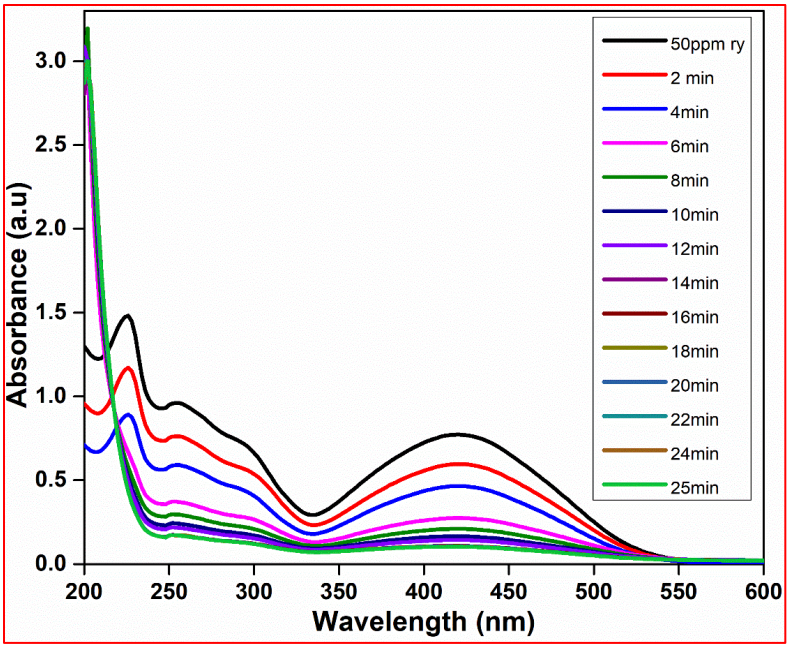

Figure 43. Reduction of Reactive Yellow

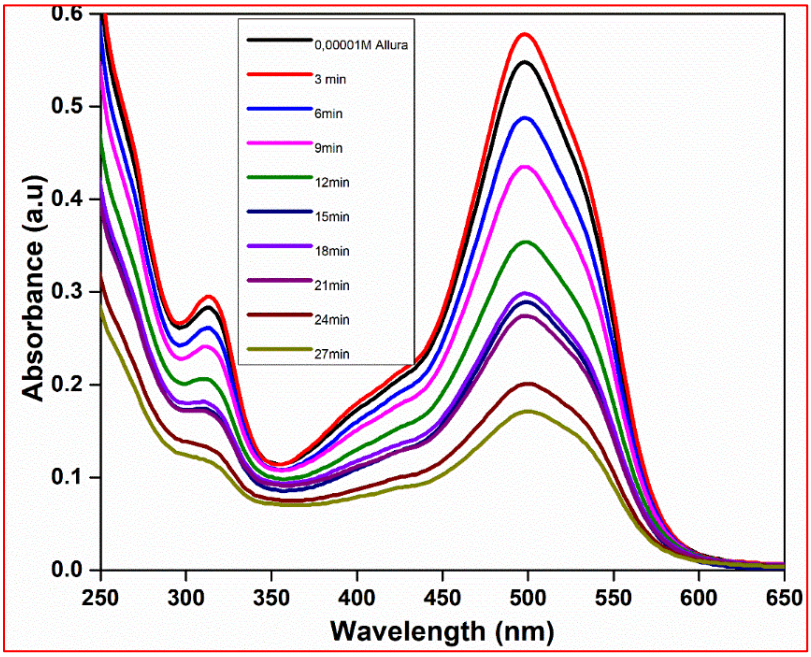

Figure 44. Reduction of Allura Red

Many research reports are available for catalytic reduction of nitroaromatics, mainly in the ortho or para isomers. However, meta nitrobenzene and nitro phenylene diamine were also selected in

this investigation. Generally, the meta substituted position is more rigorous, possibly for its resistance against the catalytic action. However, our composite could quickly reduce all NAs, implying its more substantial catalytic property. A plausible mechanism for reducing 4-nitroaniline to para phenylenediamine is shown in Fig. 44. The reaction is most probably initiated by hydride ions produced from $NaBH_4$, passing through lignin groups in the composite. The functional groups on the humic acid are firmly linked to the lignin groups of kraft liquor, which promotes electron transitions. Initially, NA might be absorbed by kraft humate because of strong Van der Walls interactions, and a high density of electrons promotes additional hydride ions to attack the nitro group. The development of a thin layered composite of the catalyst nanomaterial is thought to aid the reduction reaction by lowering the hole and electron recombination rate. In addition, there is easy release of hydride ions along with electrons from BH_4^-. Once the reduction reaction is completed, paraphenylenediamine desorption is likely to occur quickly, letting the cycle continue on the nanomaterial. The reduction reaction of nitro was promoted by the sequential loss of water which is shown in the mechanism.

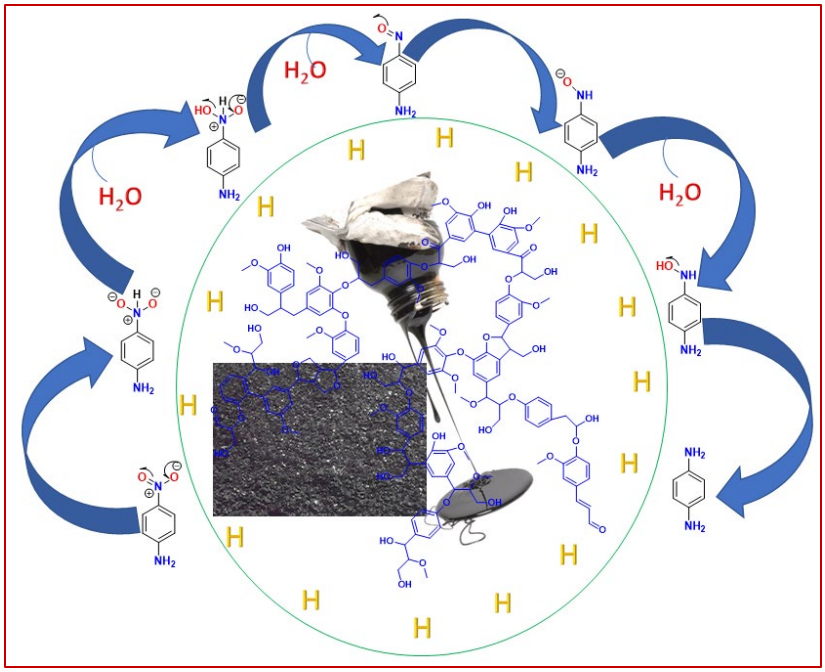

Figure 45. Reduction reaction mechanism for 4-nitroaniline to p-phenylenediamine

4.5. Conclusion

In conclusion, two composites HLMAC and HKLC were successfully synthesized and characterized by several techniques to reveal its physical and chemical properties. Infra-red spectroscopy clearly shows the functional groups present on the composites. The crystalline nature of the composites was the same as individual components like powdered nature. The composite morphology was determined by the SEM and TEM analysis, which showed homogeneous surfaces that further confirm the raw materials have reacted to form the homogeneous composite material. The highlight of the study is that the composites were successfully used to adsorb three Reactive dyes and reduce nitroanilines and five selected dyes. Low material cost, eco-friendly, easy to handle, and rapid reactions are the advantages of this study.

4.6 Recommendation

Although the HLMAC displayed good adsorption capacity to remove the three reactive dyes, it is recommended that the optimum dosage of the composite be further investigated. In addition, a fixed-bed column method could be compared against the batch method to ascertain the best methodology for dye removal. In the study on the reduction of nitro-aromatics by HKLC, it will be encouraging to determine the actual reduction product and the quantity produced.

References

Adyani, S. H. and Soleimani, E. 2019. Green synthesis of Ag/Fe_3O_4/RGO nanocomposites by Punica Granatum peel extract: Catalytic activity for reduction of organic pollutants. International Journal of Hydrogen Energy, 44(5), 2711-2730.

Alhayali, N. I., Özpozan, N. K., Dayan, S., Özdemir, N. A. L. A. N. and Yılmaz, B. S. 2021. Catalase/Fe_3O_4@Cu^{2+} hybrid biocatalytic nanoflowers fabrication and efficiency in the reduction of organic pollutants. *Polyhedron,* 194, 114888.

Anbia, M. and Ghaffari, A., 2011. Removal of malachite green from dye wastewater using mesoporous carbon adsorbent. *Journal of the Iranian chemical society,* 8(1), S67-S76.

Brigatti, M. F., Lugli, C. and Poppi, L. 2000. Kinetics of heavy-metal removal and recovery in sepiolite. *Applied Clay Science,* 16(1-2), 45-57.

Campanella, L., Tomassetti, M. and Piccolo, A. 1990. Thermogravimetric and IR analysis of different extracts of humic substances. *Thermochimica acta,* 170, 67-80.

Chen, H. and Zhao, J. 2009. Adsorption study for removal of Congo red anionic dye using organo-attapulgite. *Adsorption,* 15(4), 381-389.

Dandge, R., Ubale, M., Farooqui, M. and Rathod, S. 2016. Adsorption study for the removal of hazardous dye Congo red by biowaste materials as adsorbents. *International Journal of Application or Innovation in Engineering & Management,* 5(11), 9-16.

Daems, N., Wouters, J., Van Goethem, C., Baert, K., Poleunis, C., Delcorte, A., Hubin, A., Vankelecom, I. F. and Pescarmona, P. P. 2018. Selective reduction of nitrobenzene to aniline over electrocatalysts based on nitrogen-doped carbons containing non-noble metals. Applied Catalysis B: Environmental, 226, 509-522.

Dash, B. 2010. Competitive Adsorption of dyes (congo red, methylene blue, malachite green) on Activated Carbon.

Dias, B. D. O., Silva, C. A., Soares, E. M. B., Bettiol, W., Guerreiro, M. C. and Belizário, M. H. 2009. Infravermelho na caracterização de ácidos húmicos de Latossolo sob efeito de uso contínuo de lodo de esgoto. 33, 885-894.

El-Eswed, B. and Khalili, F. 2006. Adsorption of Cu (II) and Ni (II) on solid humic acid from the Azraq area, Jordan. *Journal of colloid and interface science,* 299(2), 497-503.

Ioselis, P., Rubinsztain, Y., Ikan, R., Aizenshtat, Z. and Frenkel, M. 1985. Thermal characterization of natural and synthetic humic substances. *Organic geochemistry,* 8(1), 95-101.

Kim, E. K. and Walker, H. W. 2001. Effect of cationic polymer additives on the adsorption of humic acid onto iron oxide particles. *Colloids and Surfaces A: Physicochemical and Engineering Aspects,* 194(1-3), 123-131.

Kumar, R., Umar, A., Kumar, R., Chauhan, M.S. and Al-Hadeethi, Y., 2021. ZnO-SnO_2 nanocubes for fluorescence sensing and dye degradation applications. *Ceramics International,* 47(5), 6201-6210.

Li, X., Xing, M., Yang, J. and Huang, Z. 2011. Compositional and functional features of humic acid-like fractions from vermicomposting of sewage sludge and cow dung. *Journal of hazardous materials, 185(2-3),* 740-748.

Li, D., Hua, T., Yuan, J. and Xu, F., 2021. Methylene blue adsorption from an aqueous solution by a magnetic graphene oxide/humic acid composite. *Colloids and Surfaces A: Physicochemical and Engineering Aspects,* 627, 127171.

Liu, Y., Liu, Y., Ji, C., Zhang, Y., Wang, Y., Qu, R. and Niu, Y., 2022. Fabrication of attapulgite/C3N4 hybridized metal organic framework nanocomposites by different strategies and study on adsorption properties for alizarin yellow GG. *Powder Technology,* 117113.

Mahmoud, D. K., Salleh, M. A. M., Karim, W. A., Idris, A. and Abidin, Z. Z. 2012. Batch adsorption of basic dye using acid treated kenaf fibre char: equilibrium, kinetic and thermodynamic studies. *Chemical Engineering Journal,* 181, 449-457.

Mija, A., van der Waal, J.C., Pin, J.M., Guigo, N. and de Jong, E., 2017. Humins as promising material for producing sustainable carbohydrate-derived building materials. *Construction and Building Materials*, *139*, 594-601.

Naidja, A., Huang, P. M., Anderson, D. W. and Van Kessel, C. 2002. Fourier transform infrared, UV-visible, and X-ray diffraction analyses of organic matter in humin, humic acid, and fulvic acid fractions in soil exposed to elevated CO_2 and N fertilization. *Applied spectroscopy,* 56(3), 318-324.

Rieman, W. and Walton, H. F. 2013. Ion exchange in analytical chemistry: international series of monographs in analytical chemistry. Elsevier.

Saloglua, D. and Sahinb, O. I. 2021. Removal of azo dyes-tartrazine, carmoisine, and Allura Red-from wastewater using Spirulina biomass-immobilized alginate beads: equilibrium, kinetics, thermodynamics, desorption, and reusability. *Desalination and Water Treatment,* 220, 431-445.

Seo, Y. S., Ahn, E. Y., Park, J., Kim, T. Y., Hong, J. E., Kim, K., Park, Y. and Park, Y. 2017. Catalytic reduction of 4-nitrophenol with gold nanoparticles synthesized by caffeic acid. *Nanoscale research letters,* 12(1), 1-11.

Song, Y., Xie, W., Yang, C., Wei, D., Su, X., Li, L., Wang, L. and Wang, J. 2020. Humic acid-assisted synthesis of Ag/Ag_2MoO_4 and Ag/Ag_2WO_4 and their highly catalytic reduction of nitro-and azo-aromatics. *Journal of Materials Research and Technology,* 9(3), 5774-5783.

Stevenson, F.J., 1994. Humus chemistry: genesis, composition, reactions. John Wiley & Sons.

Shen, Q., Zhang, T. and Zhu, M. F. 2008. A comparison of the surface properties of lignin and sulfonated lignins by FTIR spectroscopy and wicking technique. *Colloids and Surfaces A: Physicochemical and Engineering Aspects,* 320(1-3), 57-60.

Teacă, C.A., Bodîrlău, R.U.X.A.N.D.A. and Spiridon, I., 2014. Maleic anhydride treatment of softwood-effect on wood structure and properties. Cellul Chem Technol, 48, 863-868.

Qin, L., Zeng, G., Lai, C., Huang, D., Zhang, C., Cheng, M., Yi, H., Liu, X., Zhou, C., Xiong, W. and Huang, F. 2019. Synthetic strategies and application of gold-based nanocatalysts for nitroaromatics reduction. *Science of the Total Environment,* 652, 93-116.

Wu, H., Chen, F., Feng, Q. and Yue, X. 2012. Oxidation and sulfomethylation of alkali-extracted lignin from corn stalk. *BioResources,* 7(3), 2742-2751.

Zhang, W., Zhao, M., Liu, R., Wang, X. and Lin, H. 2015. Hierarchical porous carbon derived from lignin for high performance supercapacitor. *Colloids and Surfaces A: Physicochemical and Engineering Aspects,* 484, 518-527.

Zhuang, J., Li, M., Pu, Y., Ragauskas, A.J. and Yoo, C.G. 2020. Observation of potential contaminants in processed biomass using fourier transform infrared spectroscopy. *Applied Sciences*, *10*(12), 4345.